NUREG/CR-6789
ANL-01/31

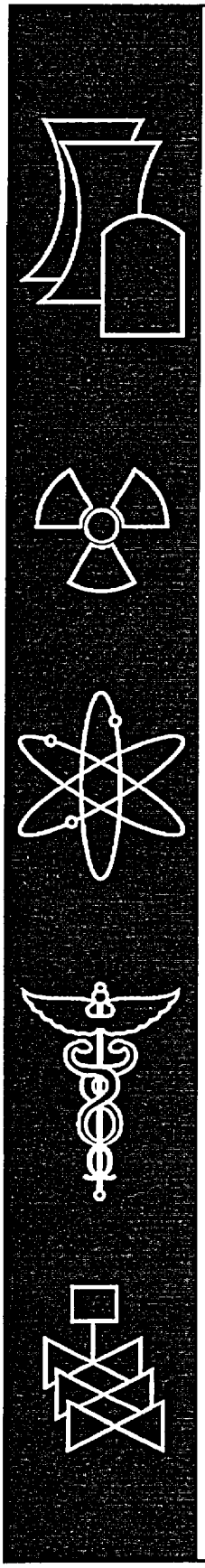

Results From Pressure and Leak-Rate Testing of Laboratory-Degraded Steam Generator Tubes

Argonne National Laboratory

U.S. Nuclear Regulatory Commission
Office of Nuclear Regulatory Research
Washington, DC 20555-0001

AVAILABILITY OF REFERENCE MATERIALS IN NRC PUBLICATIONS

NRC Reference Material

As of November 1999, you may electronically access NUREG-series publications and other NRC records at NRC's Public Electronic Reading Room at http://www.nrc.gov/reading-rm.html. Publicly released records include, to name a few, NUREG-series publications; *Federal Register* notices; applicant, licensee, and vendor documents and correspondence; NRC correspondence and internal memoranda; bulletins and information notices; inspection and investigative reports; licensee event reports; and Commission papers and their attachments.

NRC publications in the NUREG series, NRC regulations, and *Title 10, Energy*, in the Code of *Federal Regulations* may also be purchased from one of these two sources.

1. The Superintendent of Documents
   U.S. Government Printing Office
   Mail Stop SSOP
   Washington, DC 20402–0001
   Internet: bookstore.gpo.gov
   Telephone: 202-512-1800
   Fax: 202-512-2250
2. The National Technical Information Service
   Springfield, VA 22161–0002
   www.ntis.gov
   1–800–553–6847 or, locally, 703–605–6000

A single copy of each NRC draft report for comment is available free, to the extent of supply, upon written request as follows:

Address: Office of the Chief Information Officer,
Reproduction and Distribution
Services Section
U.S. Nuclear Regulatory Commission
Washington, DC 20555-0001
E-mail: DISTRIBUTION@nrc.gov
Facsimile: 301–415–2289

Some publications in the NUREG series that are posted at NRC's Web site address http://www.nrc.gov/reading-rm/doc-collections/nuregs are updated periodically and may differ from the last printed version. Although references to material found on a Web site bear the date the material was accessed, the material available on the date cited may subsequently be removed from the site.

Non-NRC Reference Material

Documents available from public and special technical libraries include all open literature items, such as books, journal articles, and transactions, *Federal Register* notices, Federal and State legislation, and congressional reports. Such documents as theses, dissertations, foreign reports and translations, and non-NRC conference proceedings may be purchased from their sponsoring organization.

Copies of industry codes and standards used in a substantive manner in the NRC regulatory process are maintained at—

The NRC Technical Library
Two White Flint North
11545 Rockville Pike
Rockville, MD 20852–2738

These standards are available in the library for reference use by the public. Codes and standards are usually copyrighted and may be purchased from the originating organization or, if they are American National Standards, from—

American National Standards Institute
11 West 42nd Street
New York, NY 10036–8002
www.ansi.org
212–642–4900

Legally binding regulatory requirements are stated only in laws; NRC regulations; licenses, including technical specifications; or orders, not in NUREG-series publications. The views expressed in contractor-prepared publications in this series are not necessarily those of the NRC.

The NUREG series comprises (1) technical and administrative reports and books prepared by the staff (NUREG–XXXX) or agency contractors (NUREG/CR–XXXX), (2) proceedings of conferences (NUREG/CP–XXXX), (3) reports resulting from international agreements (NUREG/IA–XXXX), (4) brochures (NUREG/BR–XXXX), and (5) compilations of legal decisions and orders of the Commission and Atomic and Safety Licensing Boards and of Directors' decisions under Section 2.206 of NRC's regulations (NUREG–0750).

NUREG/CR-6789
ANL-01/31

Results From Pressure and Leak-Rate Testing of Laboratory-Degraded Steam Generator Tubes

Manuscript Completed: November 2001
Date Published: November 2002

Prepared by
K. Kasza, S. Majumdar, J. Park,
J. Franklin

Argonne National Laboratory
9700 South Cass Avenue
Argonne, IL 60439

J. Davis, NRC Project Manager

Prepared for
Division of Engineering Technology
Office of Nuclear Regulatory Research
U.S. Nuclear Regulatory Commission
Washington, DC 20555-0001
NRC Job Code W6487

NUREG/CR-6789, has been reproduced from the best available copy.

Abstract

This report presents experimental results obtained from the pressure and leak-rate testing on laboratory-degraded steam generator (SG) tubes. This work is part of the NRC-sponsored Steam Generator Tube Integrity Program. Two tube test facilities were built to carry out the tests. One is the High-Temperature Pressure and Leak-Rate Test Facility (temperatures up to 343°C [650°F], pressures of up to 21 MPa [3000 psi], and pressurized-water flow rates up to 1520 L/min [400 gpm]) for conducting tube failure and leak-rate tests under prototypic SG operating conditions. The other is the Room-Temperature High-Pressure Facility (pressures up to 52 MPa [7,500 psi] and flow rates up to 48.4 L/min [12.8 gpm]) capable of testing at pressures associated with overpressure safety margins. The report includes information on flawed-tube testing protocols for tests with or without internal bladders, the validity of simple orifice flow models for the prediction of flow rates from flaws, and a large data base containing failure pressures and leak rates for machined and stress corrosion cracking (SCC) flaws produced in the laboratory.

Contents

Figures

Tables

Executive Summary

This report presents experimental results obtained from the pressure and leak-rate testing of laboratory-degraded steam generator (SG) tubes. This work is part of the NRC-sponsored Steam Generator Tube Integrity Program. This work is part of a task on Research on Degradation Modes and Integrity which is addressing the structural integrity of flawed SG tubes under normal operating, design-basis accident, and severe-accident conditions. This report describes results from tests under operating and design-basis accident conditions. Studies under severe-accident conditions have been reported in NUREG/CR-6575.

Two facilities capable of testing SG tubes under the needed conditions were built as part of the program. One of these is the High-Temperature Pressure and Leak-Rate Test Facility (temperatures up to 343°C [650°F], pressures of up to 21 MPa [3000 psi], and pressurized-water flow rates up to 1520 L/min [400 gpm]) for conducting tube failure and leak-rate tests under prototypical SG operating conditions. The other is the Room-Temperature High-Pressure Facility (pressures up to 52 MPa [7,500 psi] and flow rates up to 48.4 L/min [12.8 gpm]) for testing at high pressures to determine the structural margins associated with flawed tubes.

This report presents experimental results from the leak and failure pressure tests. The structural analysis models being developed to describe the behavior of flawed tubes are presented in an earlier report (NUREG/CR-6664).

Circular Orifice Tests

Initial leak tests were performed on tubes with circular orifices, which have a simple, precisely defined geometry. A simple orifice model incorporating a sharp-edged inlet with an orifice coefficient of 0.6 and incompressible flow was able to accurately predict flows through the orifices for both room-temperature and high-temperature tests with zero and nonzero back pressure. For the orifice sizes and stagnation conditions tested, the flow behaves like a single-phase incompressible flow with low frictional effects. Even at elevated temperatures, choked flow was not observed. This indicates that no flashing of water to steam is occurring in the orifices. Additional tests with smaller orifices down to 0.025 mm (0.001 in.) diameter and with tight flaws will be performed in the next phase of this program. For these more restrictive geometries, frictional effects are expected to become more important, and the potential for flashing and choked flow will increase.

Machined Notch Tests

Tests on electrodischarge machined (EDM) axial notches were conducted in both the High-Temperature Pressure and Leak-Rate Test Facility and the Room-Temperature High-Pressure Test Facility. A large series of tests on more complex flaw geometries, which were produced by laser-cutting, was also performed in the High-Pressure Facility. The tests conducted in the High-Temperature Pressure and Leak-Rate Test Facility did not use bladders because of it provides high flows at pressures up to those corresponding to design-basis main steam line break (MSLB) conditions. Tests in the High-Pressure Test Facility required bladders/foils for certain types of flaws and certain test objectives because of its more limited flow capacity (48.5 L/min [12.8 gpm]). Tests were performed to assess the impact of testing with bladders/foils and the influence of pressurization rate on the results.

SCC Flaw Testing

Tests on laboratory-grown SCC flaws were conducted in both the High-Temperature Pressure and Leak-Rate Test Facility and the Room-Temperature High-Pressure Test Facility. The tests have shown that that part-throughwall axial cracks in which the remaining ligament has a very nonuniform thickness may undergo increases in leak rate during constant-pressure hold times at both room temperature and 300°C (572°F). The increasing leak rate appears to be a consequence of progressive through-thickness rupture of the remaining crack tip ligament. The ligament failure continues until the remaining ligament thickness is large enough that time dependent deformation no longer occurs. In flawed specimens with nonuniform ligament thickness, initial leakage occurs at pressures significantly lower than those predicted based on an average ligament thickness.

Acknowledgments

The authors acknowledge the contributions of W. Lawrence, B. Fisher, E. R. Koehl, L. Knoblich, R. Clark, C. F. Konicek, D. R. Perkins, and C. W. Vulyak to the experimental work described in this report. The contributions of D. R. Diercks and W. J. Shack (Argonne National Laboratory), and of Dr. J. Muscara (Office of Nuclear Regulatory Research, U.S. Nuclear Regulatory Commission), to the development and guidance of the program are also gratefully acknowledged.

1 Introduction

This report presents experimental results obtained from the pressure and leak-rate testing of laboratory-degraded steam generator (SG) tubes. This work is part of the NRC-sponsored Steam Generator Tube Integrity Program. This work is part of a task on Research on Degradation Modes and Integrity, which addresses the structural integrity of flawed SG tubes under normal operating, design-basis accident, and severe-accident conditions. This report presents experimental results from the leak and failure pressure tests. The structural analysis models developed to describe the behavior of flawed tubes have been presented in Ref. 1. In addition, this report is limited to results from tests under operating and design-basis accident conditions. Studies under severe-accident conditions have been reported in Ref. 2.

Two facilities capable of testing SG tubes under the needed conditions were built as part of the program. One of these is the High-Temperature Pressure and Leak-Rate Test Facility (temperatures up to 343°C [650°F], pressures of up to 21 MPa [3000 psi], and pressurized-water flow rates up to 1520 L/min [400 gpm]) for conducting tube failure and leak-rate tests under prototypical SG operating conditions. The other is the Room-Temperature High-Pressure Test Facility (pressures up to 52 MPa [7,500 psi] and flow rates up to 48.4 L/min [12.8 gpm]) for testing at high pressures to determine the structural margins associated with flawed tubes.

These test facilities are described in Section 2. Section 3 describes the flawed-tube characterization procedures and test protocols developed and used in this program. Sections 4 and 5 describe test results from the various types of flaws tested, comprising 132 specimen tubes. Section 4 presents results for machined flaws, which include EDM circular holes and rectangular notches and laser-cut notches. Section 5 reports results from testing laboratory=produced SCC flaws.

Table 1 summarizes, by report section, the various objectives of the tests conducted, flaw geometries tested, and the number of flawed tubes in each category.

Table 1. Summary of tests performed

Report Section	Test Objectives	Flaw Geometry	No. of tubes
4.1 EDM circular holes	Data for evaluating simple orifice flow model; preparation for erosion tests; checkout of facilities; influence of high temperature	Sharp-edged circular holes; sizes 0.39-6.35 mm (1/64–1/4 in.) in diameter	16
4.2 EDM axial notches	Room- and elevated-temperature effects; leak-rate and predictability using orifice model; multiple flaw interaction and ligament size effect; influence of bladders/foils and pressurization rate; special flaw openings	Axial OD notches; single and two interacting; of lengths 6.35-38.1 mm (0.25–1.5 in.) and 60-100% throughwall (TW); initial width 0.19 mm (0.0075 in.)	42
4.3 Laser-cut notches	Evaluate behavior of single and very complex multiple axial and circumferential flaws; compare behavior with EDM notches; gain insight into complex SCC flaw behavior	Ten generic flaw geometries	24
5 SCC flaws	Test SCC flaws at room and elevated temperature for evaluating ability to predict flaw leak and structural behavior from pretest characterization; compare behavior with that of machined flaws	Axial and circumferential flaws of 100% and part TW; mainly OD but some ID; lengths of from 6.35-25.4 mm (0.25-1.0 in.); some roll transition flaws	50

2 Description/Capabilities of Test Facilities

In this section, the design and operation of the two test facilities are described. The facilities allow flawed tube testing under controlled and quantifiable conditions over a wide range of temperatures and pressures relevant to normal and faulted operation of steam generators.

2.1 High-Temperature Pressure and Leak-Rate Test Facility

The ANL High-Temperature Pressure and Leak-Rate Test Facility is used to obtain data on failure pressures, failure modes, and leak rates of flawed tubing at temperatures up to 343°C (650°F), pressures of up to 21 MPa (3000 psi), and pressurized-water flow rates up to 1520 L/min (400 gpm). This facility was designed to maintain pressures up to those expected in design-basis accidents for flow rates approaching 1000 L/min (250 gpm).

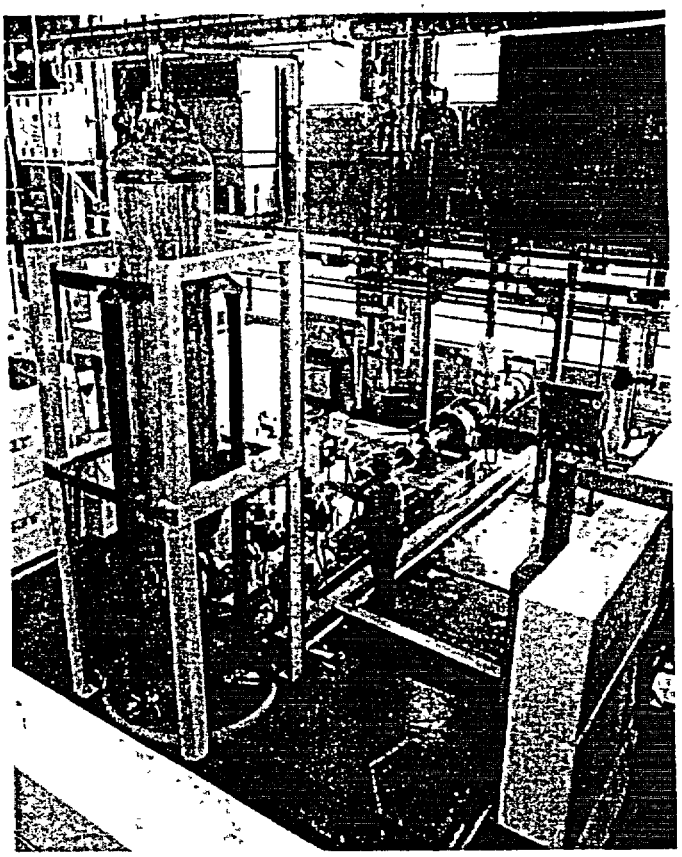

Figure 1.
ANL Pressure and Leak-Rate Test Facility.

The facility has (a) a large heated blowdown vessel with a water inventory of ≈760 L (200 gal), which provides high flow rates; (b) piping and valves sized to minimize pressure drop in the supply line to the flawed tube; (c) nitrogen cover-gas pressurization in the blowdown vessel with computer feedback control to maintain pressure even at high flow rates; (d) a downstream back-pressure regulator valve to control tube pressure differential, thereby minimizing non-prototypical two-phase flow from entering the tube and permitting rapid pressure control; and (e) a containment vessel for the tube test module. This test module can hold tubes of ≈0.15-1.0 m (6-40 in.) in length and can also be fitted with support stings to simulate support plate constraints on flawed tubes. A photograph of the facility is shown in Fig. 1.

A detailed schematic diagram of the facility is shown in Fig. 2, and a floor plan is shown in Fig. 3. The pressurized and heated blowdown vessel provides adequate water inventory for increasing the pressure differential (P1-P2) and testing tube specimens that contain preexisting throughwall flaws.

The tube specimen is housed in the test module containment vessel (Figs. 4 and 5). Tube pressure differential ramp-up is produced through a back-pressure regulator valve (V6) located downstream from the test module containment vessel. Pressure differential can also be ramped up by increasing the gas overpressure in the blowdown vessel. Both modes of operation can be carried out under manual or computer control. In the computer-controlled mode, the pressure can be programmed to simulate a prototypical transient-pressure history. The blowdown vessel is maintained at a constant pressure (P3) up to 21 MPa (3000 psi) during

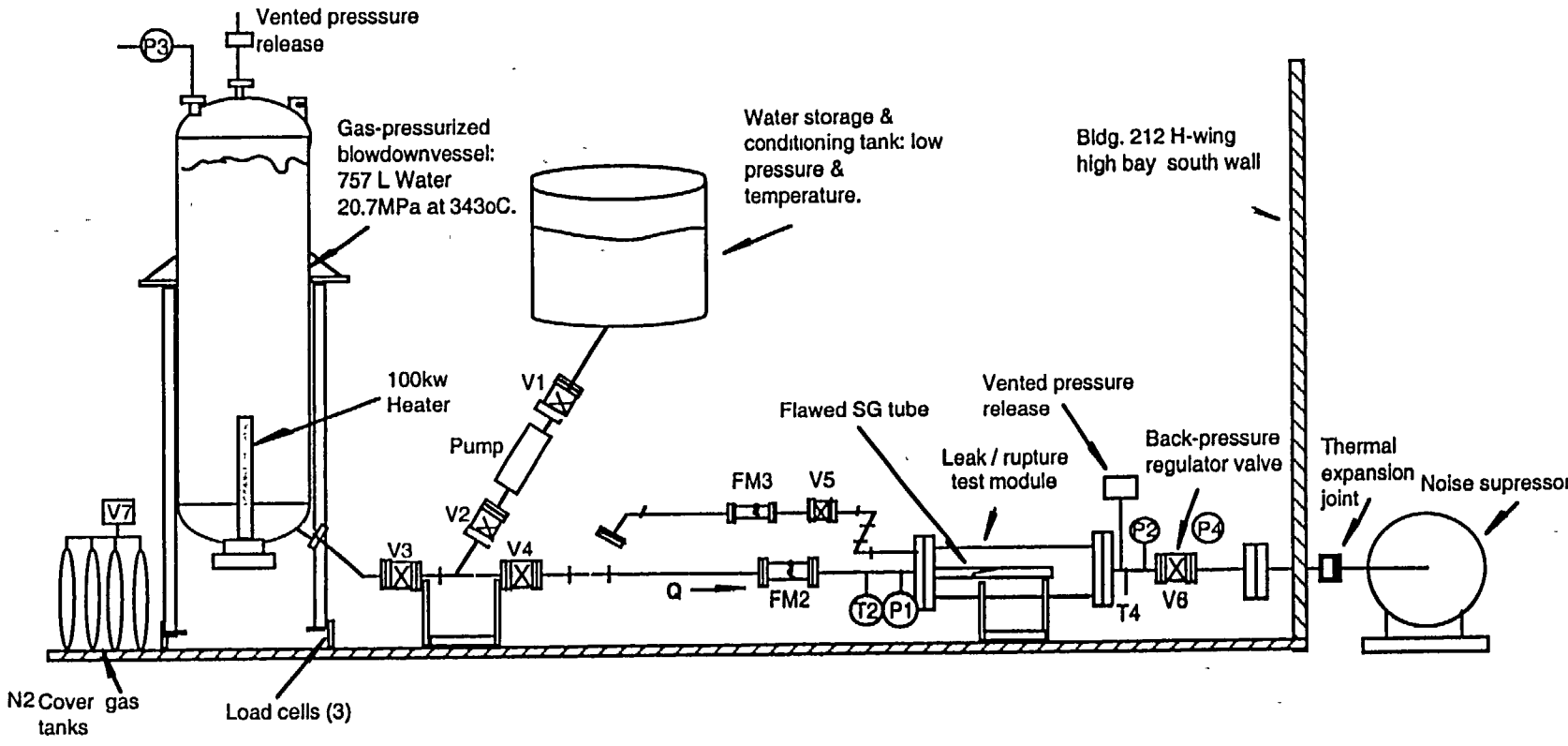

Fig. 2. Pressure and Leak-Rate Test Facility.

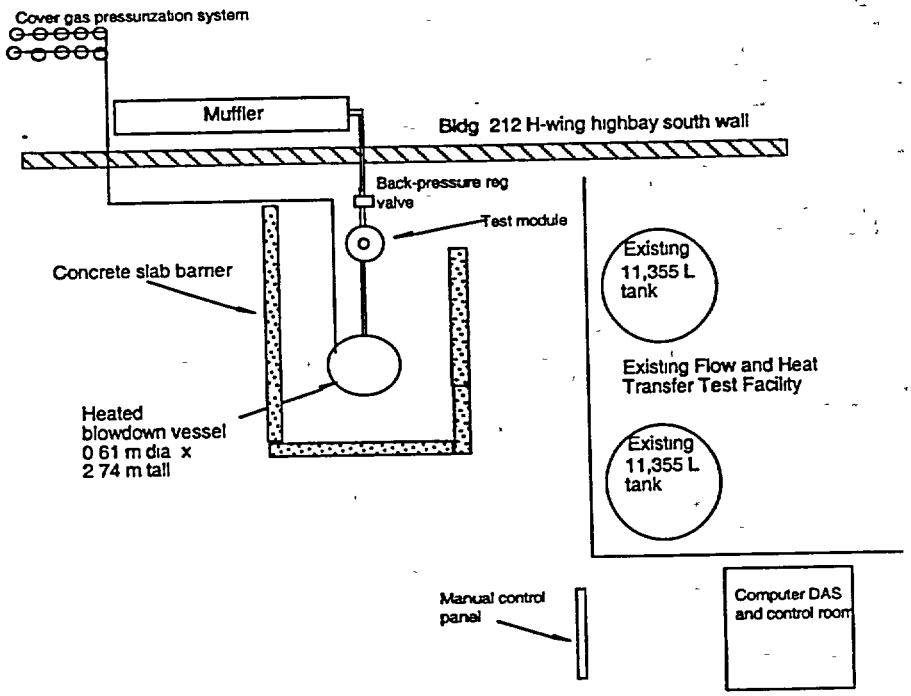

Figure 3. Floor layout of Pressure and Leak-Rate Test Facility.

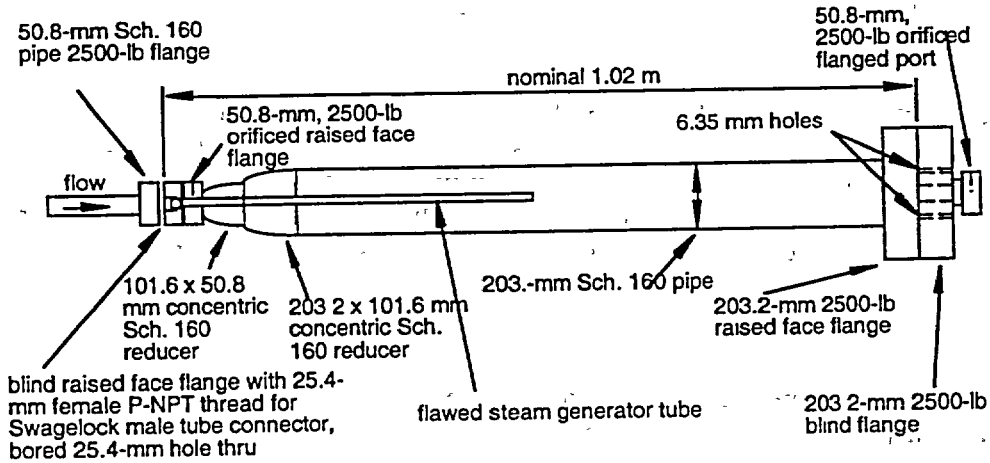

Figure 4. Tube test module for Pressure and Leak-Rate Test Facility.

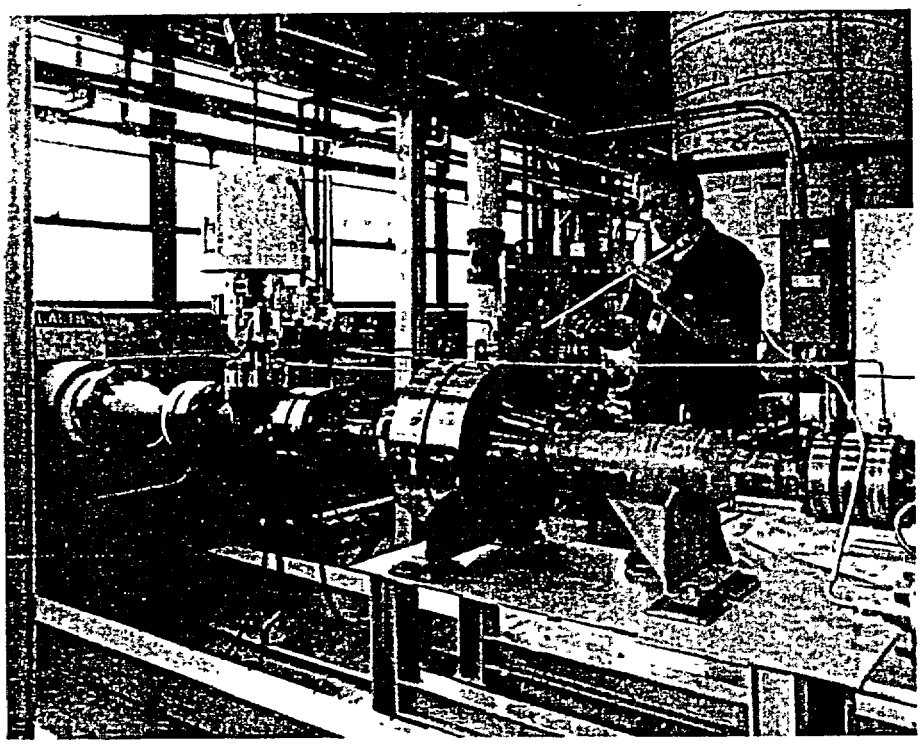

Figure 5.
Test module and typical tube specimen

a test by use of regulated nitrogen cover-gas pressurization from a 30-MPa (4400-psi) tank system of 0.9659 ML (34,110 standard ft^3) capacity. The differential pressure P1-P2 across the specimen wall is ramped up in a series of quasi-steady plateau increases through feedback control of valve V6, which controls pressure P2. The pressure P2 can also be increased linearly with time at differing rates. The flow rate Q, the pressure differential P1-P2, and the temperature are recorded as a function of time.

A turbine flow meter (FM2) is located immediately upstream of the test module to monitor the leak rate. Load cells in the support legs of the blowdown vessel are used to monitor the mass of the water in the blowdown vessel as a function of time, thereby providing a backup to and cross-check of the flow meter. Any flow through a flaw is routed outdoors through a large pipe to minimize back pressure and is discharged into a large muffler for noise suppression.

2.1.1 Facility Description

The internal diameter of the blowdown vessel (see Figs. 6 and 7) is 0.61 m (2 ft), and its length is 3.7 m (12 ft). The blowdown vessel walls are 64 mm [2.5 in.] thick. The internal diameter of the test module vessel (see Figs. 4 and 5) is 0.20 m (8 in.), and its length is 1 m (40 in.). Both vessels are constructed of welded Type 316 SS and are ASME Section VIII, Div. 1 Code designed and stamped for 21 MPa (3000 psi) at 343°C (650°F). The system has overpressurization protection vented to the outside. The pressurized components are shielded by stacked concrete slabs on three sides of the blowdown and test chamber vessels and associated piping. When the test system is at temperature and pressure, personnel are not permitted inside this barrier.

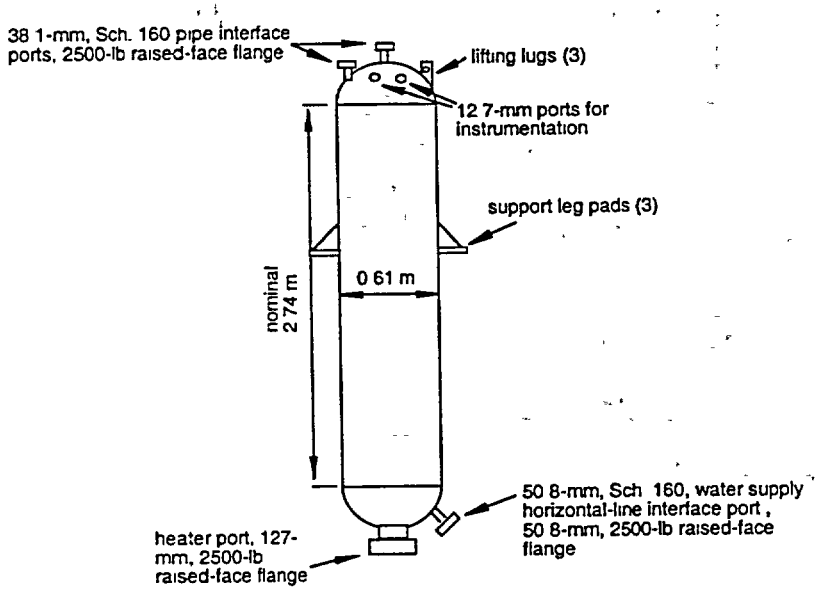

Figure 6. Blowdown vessel for Pressure and Leak-Rate Test Facility.

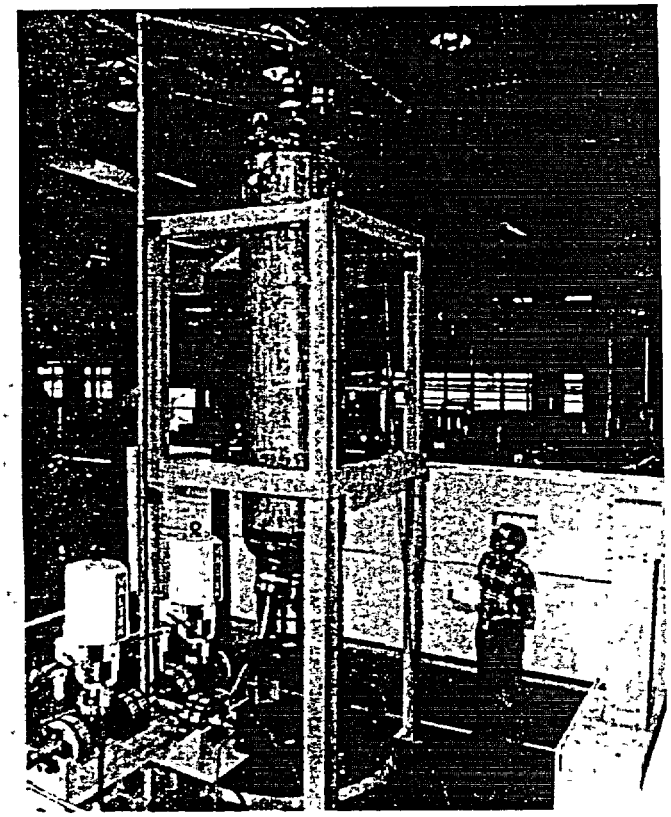

Figure 7.
Blowdown vessel and flow control valves V3 and V4.

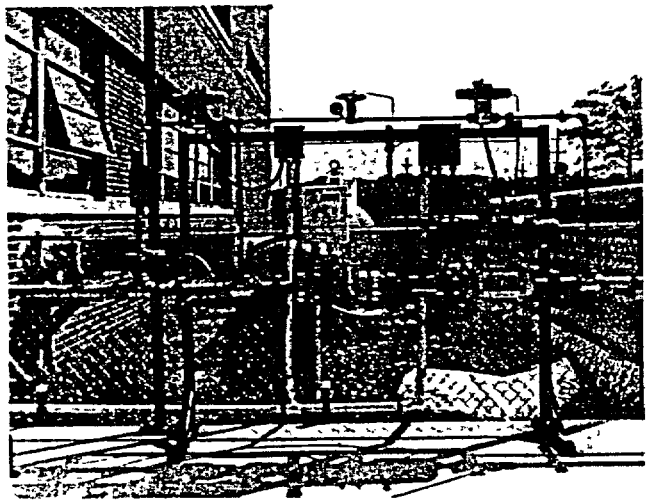

Figure 8.
Nitrogen gas pressurization system.

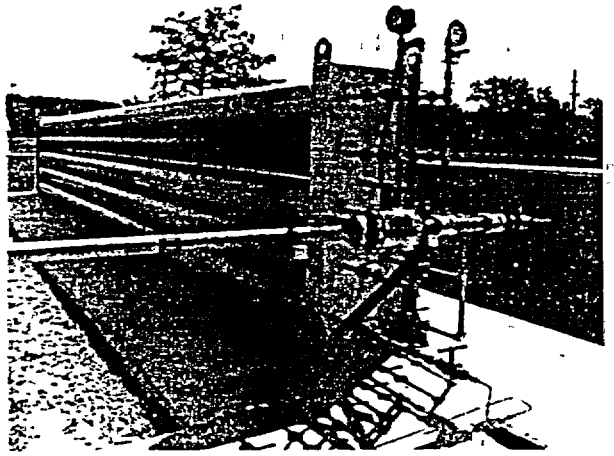

Figure 9.
High-pressure nitrogen gas storage tanks (10).

The blowdown vessel is pressurized by a nitrogen cover-gas pressurization system (see Figs. 8 and 9), which consists of 10 manifold-connected tanks, with a total capacity of 0.9659 ML (34,110 standard ft^3), located outside the laboratory room. Before each test, these tanks are pressurized with nitrogen gas to up to 30 MPa (4400 psi) by a four-stage compressor. The compressor is fed from an existing low-pressure bulk liquid nitrogen source tank.

Full pressurization for a test can be achieved in <6 h. The gas is piped in by a 50-mm (2-in.) supply line into the blowdown vessel through a flanged port on the top of the vessel. The water flow rate out of the blowdown vessel during a test can start at a few liters per minute or less and then suddenly increase to more than 760 L/min (200 gpm). The pressurization system is designed to maintain a constant cover-gas driving pressure over this wide range in flow conditions. The variation of the cover gas pressure from the desired set point is controlled to less than the 1% maximum variation from the desired set point over the full pressure range.

The high-pressure and high-temperature hardware of the facility is designed to operate under repeated cycling between ambient conditions and prototypical steam generator operating conditions. A 100-kW electrical flanged heater mounted in the bottom of the blowdown vessel is used to heat the water. Trace heating is installed on the piping connecting the blowdown vessel to the test module. Without the trace heating, the heated water from the blowdown vessel would be cooled considerably as it flows through the massive cooler connecting piping, particularly at low flow rates. Thermal expansion of components along the main flow path (up to 1.5 cm or 0.6 in.) is accommodated by a thermal expansion joint located in front of the noise suppressor, in the low-pressure zone.

The piping that connects the blowdown vessel to the test module is 50-mm (2-in.) Schedule 160, flanged Type 316 SS, to minimize pressure drop under flow conditions of 760 L/min (200 gpm). The 50-mm (2-in.) valves V3 and V4 (see Figs. 2 and 7) in the main flow path that connects the blowdown and test module vessels are also sized to pass the 760 L/min (200 gpm) flow with little pressure drop. The piping downstream of the test module is likewise large enough to minimize back pressure on the test module to ensure that the backpressure can be controlled by valve V6. Downstream of valve V6, the piping size is increased to 0.25 m (10 in.) to improve valve control and permit interfacing with the inlet of the noise suppressor.

The 75-mm (3-in.) back-pressure regulator valve V6, located downstream of the flawed-tube test module (see Figs. 2 and 10), is used to control and vary the pressure differential across a flawed tube that is being tested. For tests in which no throughwall flaw is initially present, water from the pressurized blowdown tank is routed into the test module through a small line under control of valve V5 at 4-8 L/min (1-2 gpm) to preheat the test assembly. Valve V6 operates on this flow to regulate P2. When the flawed tube begins to leak in response to increasing P1-P2, valve V6 maintains the desired pressure P2. When the tube leak becomes several times larger than the bleed flow from the blowdown vessel, the bleed flow can be turned off with valve V5.

Valve V6 operates under changing fluid conditions during a test. Initially, when P1-P2 is small, the pressure P2 in the test module will be above the saturation pressure of the water in the blowdown vessel, and a flawed tube will leak pressurized water into the test module. However, when P2 is reduced below the saturation pressure, the water leaking from the crack will flash to steam, and valve V6 will be controlling a steam flow. The facility is designed to accommodate tube leak rates as high as 760 L/min (200 gpm) of water, which corresponds to 12.6 kg/s (100,000 lb/h) of steam.

A turbine flow meter (FM2) is located just upstream of the test module to monitor the leak rate. The low end reading is ≈11 L/min (3 gpm), below which the turbine stops turning. An alternative method of leak rate measurement is provided by load cells in each of the three support legs of the vessel (see Fig. 11), which are used to measure the weight of the water in the vessel as a function of time. The load cells can detect water inventory changes of 1 kg (0.5 lb), thus permitting flow rate measurements down to tenths of a liter per minute.

The muffled noise suppressor outside the south wall of the laboratory space is designed to handle the maximum anticipated steam flow from the test module, 12.6-kg/s (100,000 lb/h), as well as possible overpressurization steam releases. The unit is 0.91 m (3 ft) in diameter and 5.2 m (17 ft) long and is capable of a 45-dB noise reduction.

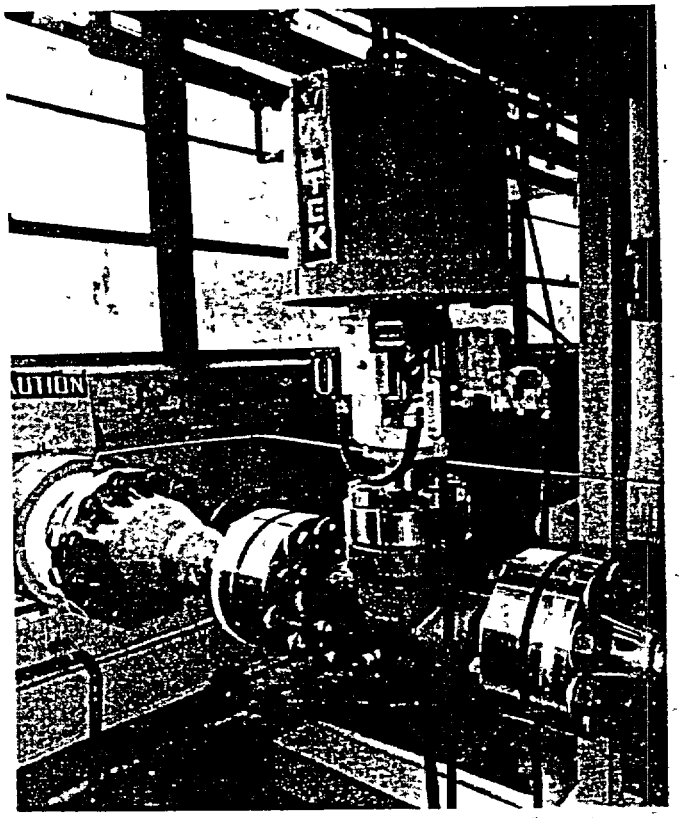

Figure 10.
Back-pressure regulator valve V6

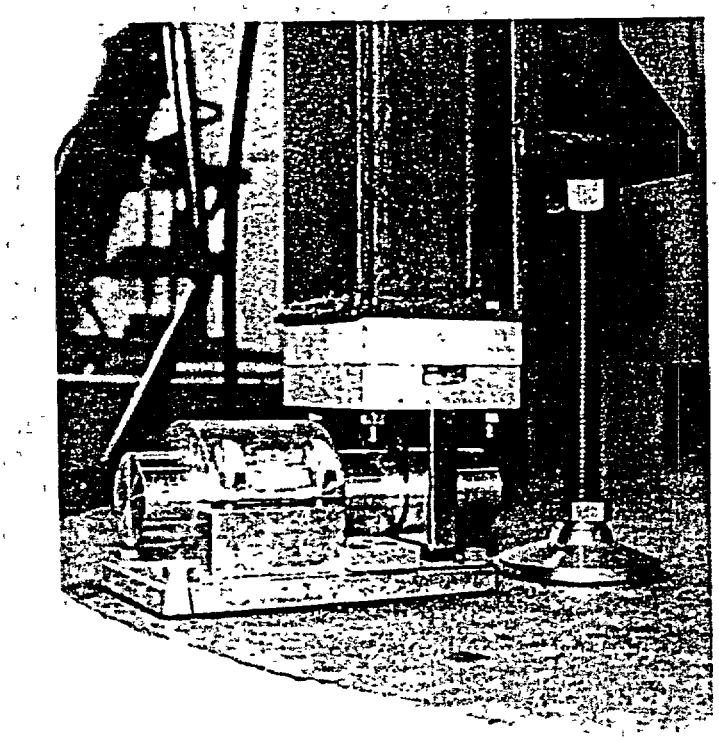

Figure 11.
Blowdown vessel leg load cell (one of three).

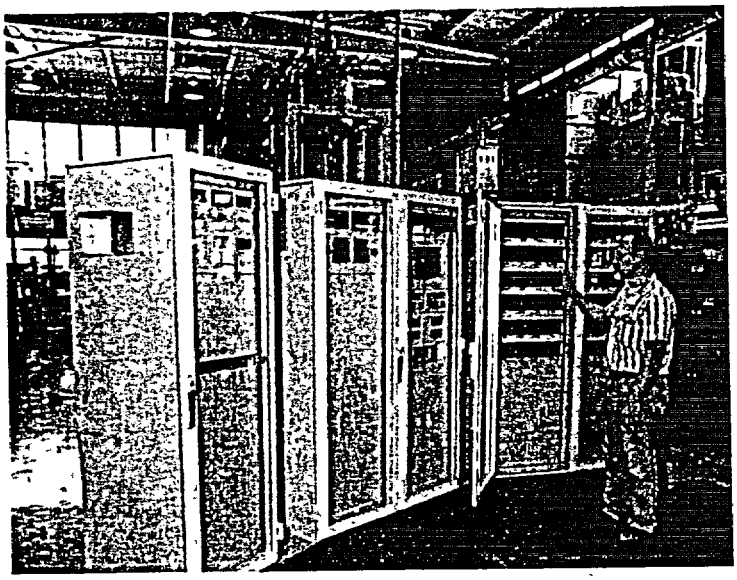

Figure 12.
Facility control cabinets

All signals for pressure, temperature, flow rate, electric power for the heaters (for the blowdown vessel and trace heaters on various components), and control valve actuation status are displayed on the master control panel (see Fig.12). Measurement and control signals are also logged into a computerized data acquisition and control system.

2.1.2 Facility Operation

The general philosophy of facility operation is to utilize manual control when bringing the facility to steady-state conditions for the beginning of a test and computer control for actual testing.

System setup under manual control includes configuring the facility for a particular test, attaining steady-state conditions associated with time zero of the test, and verifying that the computer software is properly configured for the transient portion of the test. It takes 5-6 h to heat up to 282°C (540°F). After the steady-state conditions are verified by the operator, the test is switched to computer control, and the transient portion of the test is initiated under computer control after a short stabilization period to eliminate any switching transients. Once under computer control, a test can terminate in several ways. The first of these is normal termination, in which the flawed tube progresses through stages of increasing leakage to crack instability and tube rupture, with a corresponding rapid increase in leak rate. However, it may be necessary to terminate a test before specimen rupture because the blowdown vessel is low on water, the back-pressure regulator valve fails to stabilize as it is changed under computer control, or the desired ramping of the pressure differential across the cracked tube cannot be achieved for any reason. Finally, the operator can manually override and terminate the test at any time because of safety concerns or any other reason. After a test is completed, overnight cooldown is required before the specimen can be removed from the test module. Specimen change requires 4 h for opening and reclosing the high-pressure, bolted, crushable, metal gasketed flanges on the heavy piping upstream of the test module and reinstallation of the insulation and instrumentation.

2.2 Room-Temperature High-Pressure Test Facility

The Room-Temperature High-Pressure Test Facility can produce pressures up to 51.7 MPa (7500 psi) and is being used to investigate the actual design margin associated with flawed tubes. Because the facility has a 48.4 L/min (12.8 gpm) flow capability at 51.7 MPa (7500 psi), tubes with small throughwall flaws can be tested without the use of a bladder. For somewhat larger cracks for which bladders and foils are required in order to maintain pressure, the small leaks that may occur during tube pressurization are less likely to result in an aborted test and perhaps a wasted tube specimen.

This facility can also be used for very-long-duration tests of crack stability and for long-duration crack jet-impingement erosion tests on adjacent tubes, since water can be continuously supplied from an outside source during a test. The apparatus is also capable of measuring very low flow rates (considerably less than the 0.04 L/min [0.01 gpm] lower limit for the Pressure and Leak-Rate Test Facility) through the use of flaw leak collection and timed measurement of water mass. Additionally, real-time, ultra-high-speed video recording (2000-12,000 frames per second) of crack and jet dynamic behavior can be done during testing.

2.2.1 Facility Description

A schematic diagram of the facility is shown in Fig. 13 and a photograph of the facility is shown in Fig. 14. Pressure is provided by a constant-rpm, single-acting triplex constant-displacement pump driven by a 60-hp electric motor (see Fig. 15) that provides a constant 48.4 L/min (12.8 gpm) flow of water at up to 51.7 MPa (7500 psi). Pump–generated pressure pulsation is <0.34 MPa (<50 psi). The pump has two safety relief valves for overpressurization protection, one located on the pump, and the other on the 139-L (40-gal) water accumulator suction tank. The lever-operated hydro-diverter control valve originally supplied with the pressurizer was modified to work in series with a screw unloader valve that allows more positive, finer control of pressurization. The pressurizer water pump system was also modified to operate with a continuous supply of water from the building water system by installing a pressure-regulating valve on the water line supplying the pump accumulator suction tank.

The tube pressurization rate can be varied from quasi-steady-state (<0.7 MPa/s or <100 psi/s) to 7-21 MPa/s (1000-3000 psi/s), which encompasses the rates given in Electric Power Research Institute (EPRI) guidelines for burst testing, to 70 MPa/s (10,000 psi/s). Pressurization over the full range of the system, 0-52 MPa (0-7500 psi), is possible at all of these pressurization rates.

The test module is shown in Fig. 16. It consists of a 0.46-m (18–in.)-diameter x 1.02-m (40-in.)-long stainless steel pipe with transparent Lexan™ plates at the ends of the module to confine the water jet spray produced by a leaking tube. A ultra-high-speed video camera and light source for illuminating the test tube are also shown in Fig. 16.

The tube support fixture, which is shown in Fig . 17, provides single- or two-point lateral support. It consists of two collars that fit around the tube and can be located anywhere along its length. The ability to vary tube lateral support conditions is important in testing tubes with circumferential flaws, where flaw behavior is sensitive to tube constraint. The two-point support also prevents axially flawed tubes from undergoing significant bending as a result of jet thrust upon failure.

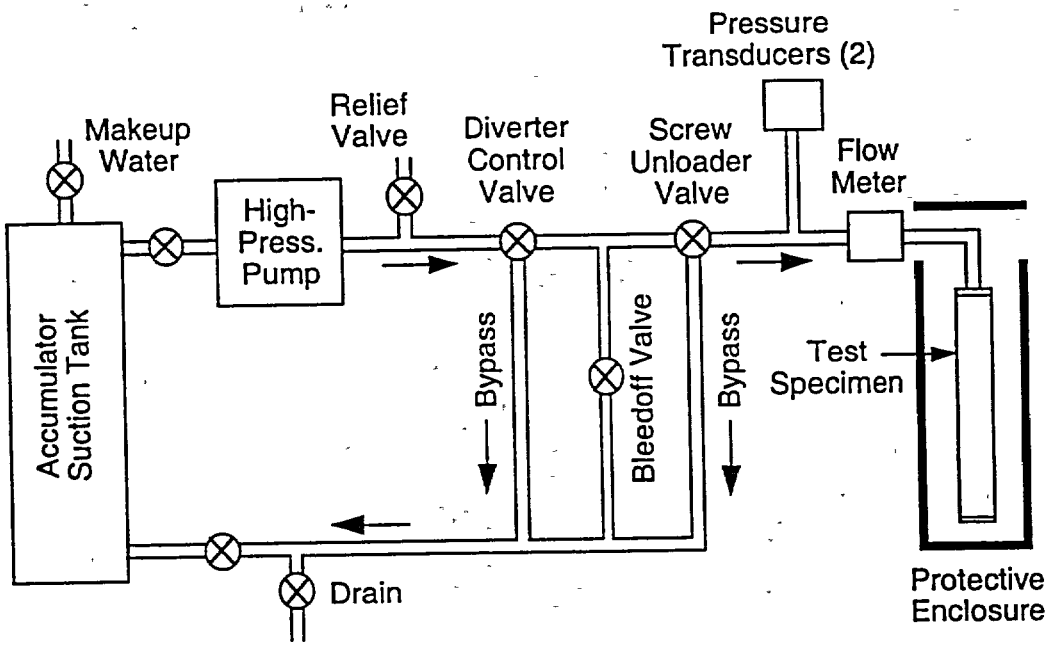

Figure 13. Schematic diagram of pressurizer and associated components in High-Pressure Test Facility.

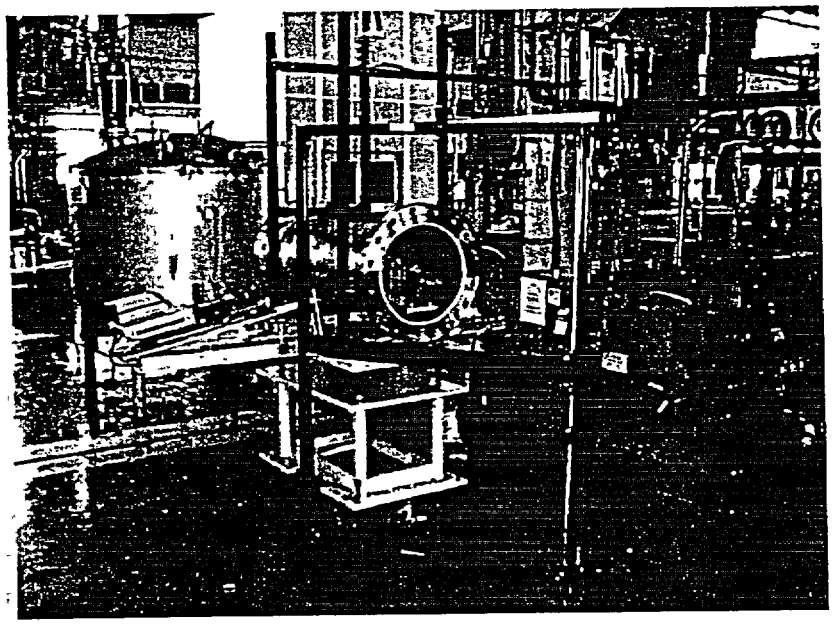

Figure 14. Overall view of major components of High-Pressure Test Facility: water pump pressurizer, test module, tube support, video system, and 3000-L (800-gal) tank for conducting tests on field-pulled tubes. Also shown is Lexan™ personnel-protection barrier

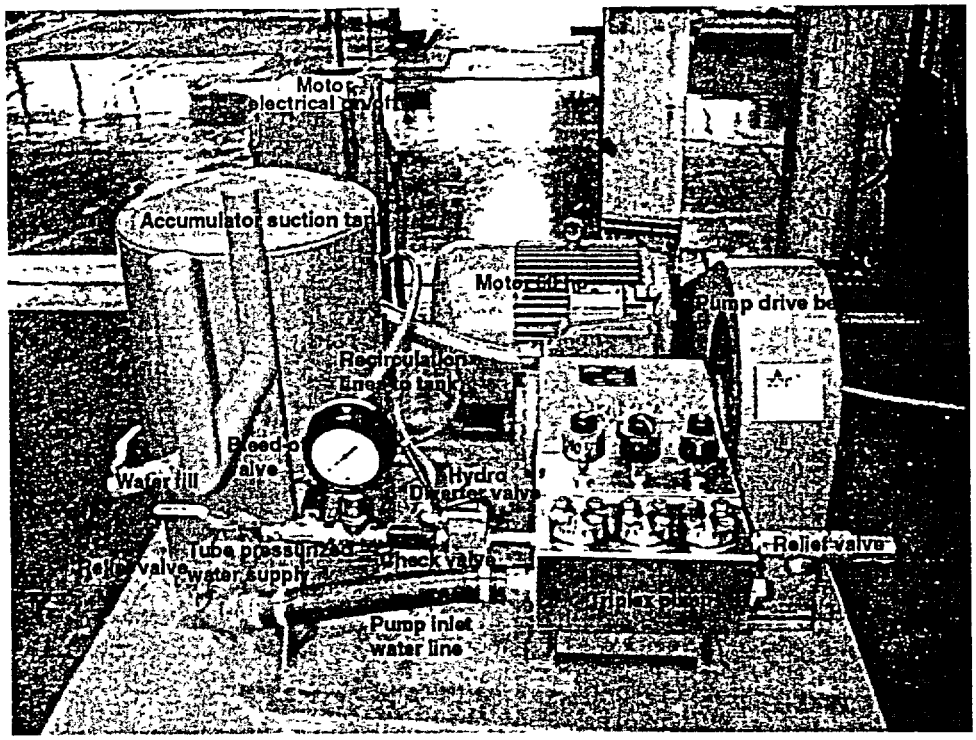

Figure 15. Water pump pressurizer.

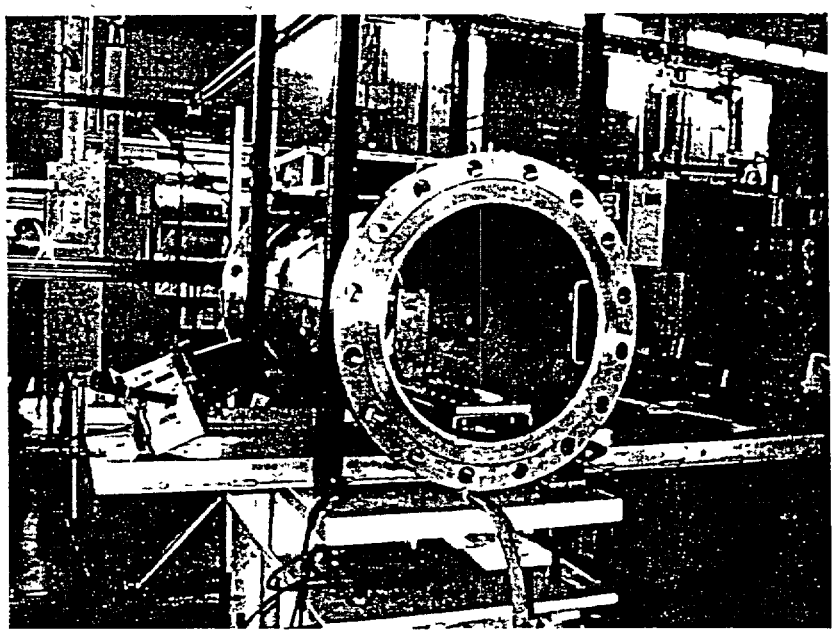

Figure 16 Test module and high-speed video camera and high-intensity light source mounted on test module support table.

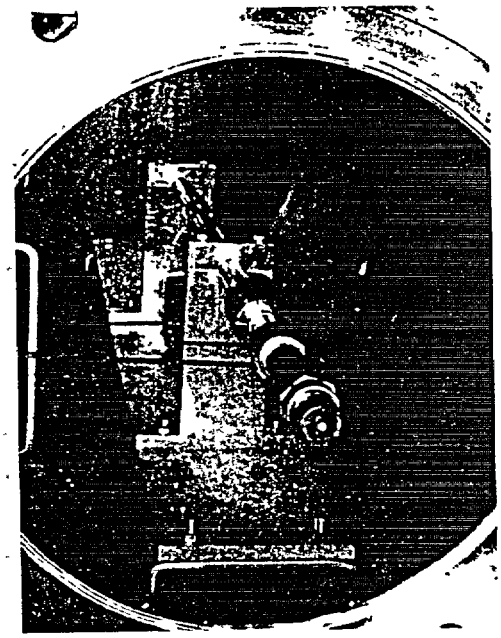

Figure 17.
Tube support system.

2.2.2 Facility Operation

The tube to be tested is mounted in the test module and fastened to the supply pipe that feeds water from the high-pressure pump. The pressure is controlled by the high-pressure bleedoff valve, diverter control valve, and screw unloader valve. The bleedoff valve can be used to rapidly depressurize the system, e.g., after the completion of test. The diverter control valve allows the pressure to be established at any value in the range from 0 to 51.7 MPa (0 to 7500 psi). Downstream and in series with the diverter valve is a spring-loaded screw unloader valve, which is used for more precise control of pressure.

Tube pressure is read on an analog pressure gauge and is also measured and recorded by two redundant pressure transducers. The flow is measured by both timed direct collection and weighing of water from the test module and by a flow meter immediately upstream of the tube. All data are recorded on both a multi-channel strip chart recorder and a computer data acquisition system.

3 Characterization/Test Protocols for Flawed Tubes

In this section, the procedures used to characterize a flaw before and after testing are described. These procedures are, in general, the same whether the flaw is a machined or a laboratory-grown SCC and regardless of which test facility is used. The test protocols for each facility are described. The protocols were established through testing to investigate the influence of the pressurization rate, bladder and foil characteristics, and facility operation procedures on flaw behavior and on the quality of the data. The studies supporting the adoption of the test protocols/procedures are discussed in Sections 4 and 5. In some areas such as the influence of pressurization rate and hold times, there is still more to be learned, and additional tests are planned.

3.1 Flawed-Tube Characterization

In general, the EDM and laser-cut flaws tested (comprising circular orifices and notches) are relatively easy to characterize, but the characterization of the SCC flaws is much more difficult. Each tube specimen is given an engraved alphanumeric identifier that enables it to be tracked through all phases of fabrication and testing. A detailed table has been developed for keeping track of the tube type, material type, source, pretest flaw characterization, test conditions, facility mode of operation, computer data records, posttest tube characterization, leak/rupture data analysis results, and any comments on testing pertinent to interpretation of data.

Bobbin coil and rotating pancake coil eddy current inspections are performed for all SCC specimens. Dye penetrant techniques are also used to estimate crack length and morphology. Low-pressure (0.28 MPa or 40 psi) air-bubble tests in a water bath are performed to identify regions of throughwall penetration. In these tests, a low-magnification optical microscope is used to detect any gas bubble leaks along the crack. Based on this information, the behavior expected during the pressure test is determined.

Posttest characterization includes digital photography to record and measure the final crack opening geometry and detailed metallography to assess the accuracy of the nondestructive evaluation (NDE) estimates of crack geometry.

3.2 Protocols for Room-Temperature High-Pressure Test Facility

Whenever possible, tests are performed without bladders or reinforcing foils and use quasi-steady pressurization rates to avoid complications in interpreting data and to maximize the data on flaw behavior. Short, deep, part-throughwall flaws can undergo considerable ligament tearing at pressures lower than that at which unstable burst occurs. To obtain information on the flaw opening resulting from ligament tearing and the associated leak rate before unstable burst occurs, the specimen is pressurized in pressure increments of 0.34-1.38 MPa (50 to 200 psi) with a 5 s to several minute hold at each pressure plateau.

At each plateau, a visual check is made through the viewing ports for any signs of leakage, and the pressure at first leak is recorded. The initial leakage may manifest itself as individual drops forming over a period of several minutes, and a continuous water jet typically will not develop until the pressure is further increased. Even SCC that exhibited throughwall leakage in the air bubble test at 0.3 MPa (40 psi) will often exhibit no leakage until relatively high pressures are applied in the water test. The test is continued under increasing pressure until the flaw is open enough that the flow rate exceeds the 48.4 L/min (12.8 gpm) limit of the facility or the flaw fails unstably.

If the flaw did not fail unstably in the initial test, a bladder and possibly a backup foil are inserted in the tube to permit continuation of the test. The most commonly used bladder is hard Tygon tubing with a 3.2-mm (1/8-in.) wall thickness. The tubing is just slightly smaller than the inside diameter of the specimen and is slipped inside the flawed tube and sealed in each end with a Teflon plug (see Section 4.2 for details). For cracks longer than 12.7 mm (1/2 in.), Stage II tests usually also require a 0.13-mm (0.005-in.)-thick brass foil that is inserted between the inner wall of the SG tube and the outer surface of the bladder. This foil is sized so that it extends 6.3 mm (0.25 in.) beyond the extremities of the flaw. The foil and bladder are

lubricated with a multipurpose spray lubricant to reduce friction between the foil and the SG tubing. To avoid extrusion of the bladder/foil through the flaw, the tube is pressurized at 3.5–7 MPa/s (500–1000 psi/s). The effects of pressurization rate on failure presssures are discussed in Section 4.2.2.

3.3 Protocols for High-temperature Pressure and Leak-Rate Test Facility

Tests in this facility do not use bladders. The flow capacity is adequate to test axial flaws as large as 25-38 mm (1.0-1.5 in.) in overall length and to drive them open by increasing the pressure. The differential pressure across the specimen is controlled by changing the back pressure on the tube, as discussed in Section 2.1. The pressure in the blowdown vessel during a test is always maintained sufficiently above the saturation pressure associated with the desired water temperature to prevent water flashing to steam in the water supply piping upstream of the test specimen. For flaws that don't leak initially or leak at a very low rate, the pressure difference across the specimen is raised in 0.34-1.38 MPa (50-200 psi) increments with a 5-10 s hold at each pressure plateau. If the flow rate begins to increase more quickly, the pressurization rate is correspondingly increased. In general, the pressurization rate will not exceed 0.69 or 1.38 MPa/s (100 or 200 psi/s). If major ligament tearing occurs for a large flaw with a sudden jump in flow rate to 380 L/min (100 gpm) or more, the test pressure is then set to a constant value. The actual pressure will initially vary, but through feedback control of the computerized gas pressurization valves, a steady-state pressure and corresponding flow rate will be obtained. The test will be automatically shut down when the vessel water inventory drops to a minimum level.

Another type of test is conducted to determine whether flaws will exhibit time-dependent opening under constant temperature and pressures associated with normal and main steamline break (MSLB) conditions. In this test, a 8.3 MPa (1200 psi) pressure differential is held from an hour to several hours (depending on leak rate and water inventory), and the flaw is monitored for signs of leak initiation or increased flow rate. After this hold period, the tube pressure differential is increased in 0.69 or 1.38 MPa (100 or 200 psi) increments up to MSLB pressure. At each step, the pressure is held constant for a period of a few seconds to several minutes, depending upon the flow rate. After the MSLB pressure is reached, the pressure is held for an extended time (dictated by remaining water inventory), and the leak rate monitored.

4 Test Results for Machined Flaws

All machined flaws were fabricated from 22.2-mm (7/8-in.)-diameter Alloy 600 SG tubing. EDM and laser cutting were used to fabricate single notches (both axial and circumferential), circular holes, and multiple flaw geometries of various types. Laser cutting was used because it could generate tighter flaws than could be achieved with EDM. The flaws were of various lengths and degrees of throughwall penetration. Most were of uniform depth, but variable depth flaws have also been used. In the initial testing, two or more identical specimens of each flaw type were tested to verify reproducibility of leak rate/failure data.

The flawed tubes were all 0.56 m (22 in.) long, with the flaw centered at 0.15 m (6 in.) from the end of the tube fitted with a welded plug. The unplugged end of the tube was held in place in the test module vessel of the High-Temperature Pressure and Leak-Rate Test Facility or the High-Pressure Test Facility by a Swagelok fitting mounted on a blind flange with a hole that permits flow to enter the flawed tube.

The analytical models and correlations used to predict the failure of tubes with throughwall and part throughwall notches are discussed in Refs. 1–3.

4.1 EDM Circular Holes

A series of tests was conducted on 22.2-mm (7/8-in.)-diameter steam generator tubes having EDM sharp-edged, circular throughwall holes using room- and high-temperature water in the Pressure and Leak-Rate Test Facility. Testing to date has covered hole sizes ranging from 0.40 to 6.35-mm (1/64 to 1/4-in.) in diameter. These test were initially used as a way of checking out the facility in bringing it online. The flow of a single-phase incompressible fluid through thin plate sharp-edged-entrance hole is known to be well predicted using a simple circular-orifice flow correlation.

Leakage from steam generator tubes occurs over a wide range of ratios of crack length (L) to crack opening widths (h), as shown in Fig. 18. Most of the data used in formulating and validating the current multiphase models for crack leak rate are based on tests simulating flow through stress corrosion cracks in thick-wall piping. In these cases, L/h is typically >100. As shown in Fig. 18, under MSLB conditions for cracks in steam generator tubes longer than about 6 mm (0.25 in.), L/h is <100, i.e., these cracks are more open than stress corrosion cracks in piping. The work of Amos and Schrock[4] and others has shown that L/h strongly influences whether choking can occur and also strongly influences the importance of friction and roughness effects. In addition, as discussed by Amos and Schrock, flashing of a metastable liquid depends on a relaxation time, which implies that the actual wall thickness as well as L/h may be important in determining when flashing occurs within the crack. For flows through a relatively large orifice such as a 0.79-mm (1/32-in.)-diameter hole at 17.2 MPa (2500 psi), the mean velocity of the jet is ≈120 m/s (≈400 ft/s). Thus, the flow through the tube wall requires $\approx 1 \times 10^{-5}$ s. The time to travel across the 6.35 mm (0.25 in.) gap to the adjacent tube is $\approx 5.2 \times 10^{-5}$ s. Because these times are short, in some cases, flashing may not occur within the crack or possibly not even completely in the gap between tubes.

The first set of orifices tested during facility checkout involved hole diameters of 6.35 mm (1/4 in.) (specimen T5EOTWX.250D), 3.175-mm (1/8 in.) (specimen T4EOTWX.125D), and 0.794 mm (1/32 in.) (specimen T6EOTWX.031D). The specimens were held fixed only on the inlet end.

Each orifice was checked for circularity, size, and sharpness of the entrance and exit edges. Depending on the entrance contours and the importance of roughness, the orifice coefficient can range from near unity to as low as 0.5. The EDM orifices show quite sharp edges, indicating that a coefficient in the lower end of this range should be appropriate. The EDM process was also found to leave a pebbly rough pattern on the walls of the orifice. Following testing, the orifices were checked for evidence of erosion.

During the tests, the pressure gradient across the tube wall for the three tubes was varied from 0 to 19 MPa (0 to 2800 psi) in several steps. All the tubes were tested at room temperature water, and the 3.175-mm (1/8-in.)-diameter hole was also tested at 282°C (540°F) with zero back pressure. No structural distortion or erosion of the hole was detected under these conditions in posttest examination.

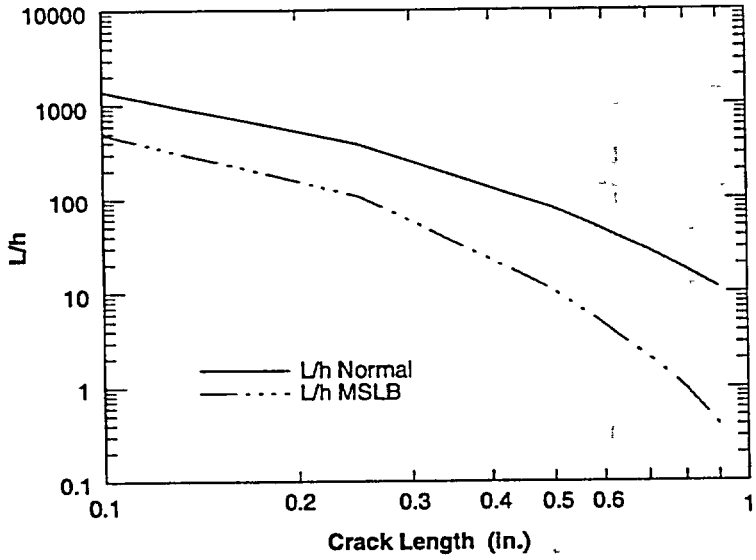

Figure 18.
Variation of the ratio of flow path length to the crack opening width with crack length for normal operating and main steam line break (MSLB) conditions.

Figures 19 and 20 show the pressure difference across the tube and the blowdown vessel weight, respectively, as a function of time for a room-temperature test on the 0.794-mm ($1/32$-in.)-diameter orifice. The tube was subjected to seven increasing pressure plateaus. The flow rate was determined by the measured change in blowdown vessel weight. For each pressure plateau of Fig. 19, the weight curve exhibits a straight-line segment. The slope of this segment, after applying a correction for increasing weight of the cover gas in the tank, is the water leak rate in kg/s.

The flow rates for the 0.794-, 3.175-, and 6.35-mm ($1/32$-, $1/8$- and $1/4$-in.)-diameter orifices at the nominal differential pressure of 17.2 MPa (2500 psi) were 2.76, 56.0, and 216 L/min (0.73, 14.8, and 57.0 gpm), respectively. The average jet velocity through the 3.175-mm ($1/8$-in.)-diameter orifice at 17.2 MPa (2500 psi) was 112 m/s (366 ft/s). Such jet velocities can produce significant lateral thrust, and the specimen with a 6.35-mm ($1/4$-in.)-diameter orifice was bent ≈10° from its axis as a result of this thrust (Fig. 21). No bending was observed for the specimens with smaller orifices.

The standard correlation for incompressible flow through a sharp-edged circular orifice is,

$$Q = C \cdot A \cdot \left(\frac{\Delta p}{\rho}\right)^{1/2}, \qquad (1)$$

where Q is the flow rate, C is the orifice discharge coefficient, A is the cross-sectional flow area, Δp is the pressure difference across the orifice, and ρ is the density of the fluid. Room-temperature flow rates were predicted quite well using a value of 0.6 for C. The orifice model predicts a temperature effect on flow rate through the dependence of fluid density on temperature. The density of water at 21 and 282°C (70 and 540°F) is 1.00 and 0.745 g/cm^3 (62.3 and 46.51 lb/ft^3), respectively. In two separate tests, the same tube tested at a pressure differential of 8.72 MPa (1265 psi) and a temperature of 282°C (540°F) exhibited a flow rate of 3.03 L/min (11.45 gpm). With C = 0.6, Eq. 1 predicts a flow rate of 3.04 L/min (11.51 gpm), in very good agreement with the experimental value. The orifice correlation predicts a flow rate of

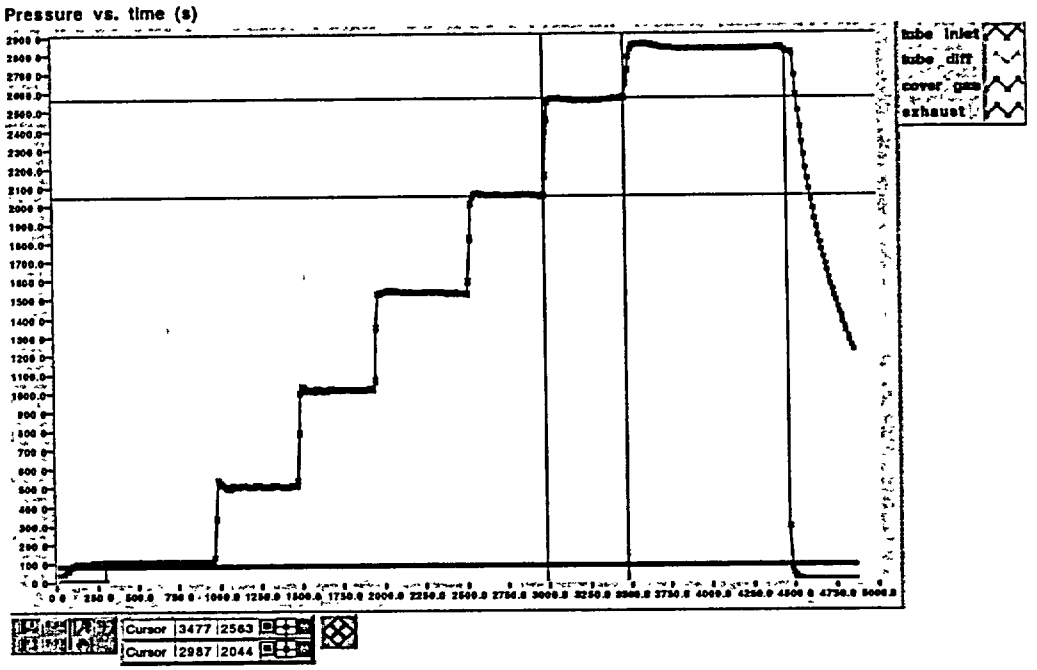

Figure 19. Tube pressure difference vs. time for test of tube with 0.794-mm (1/32-in.)-diameter hole (T6EOTWX.031D).

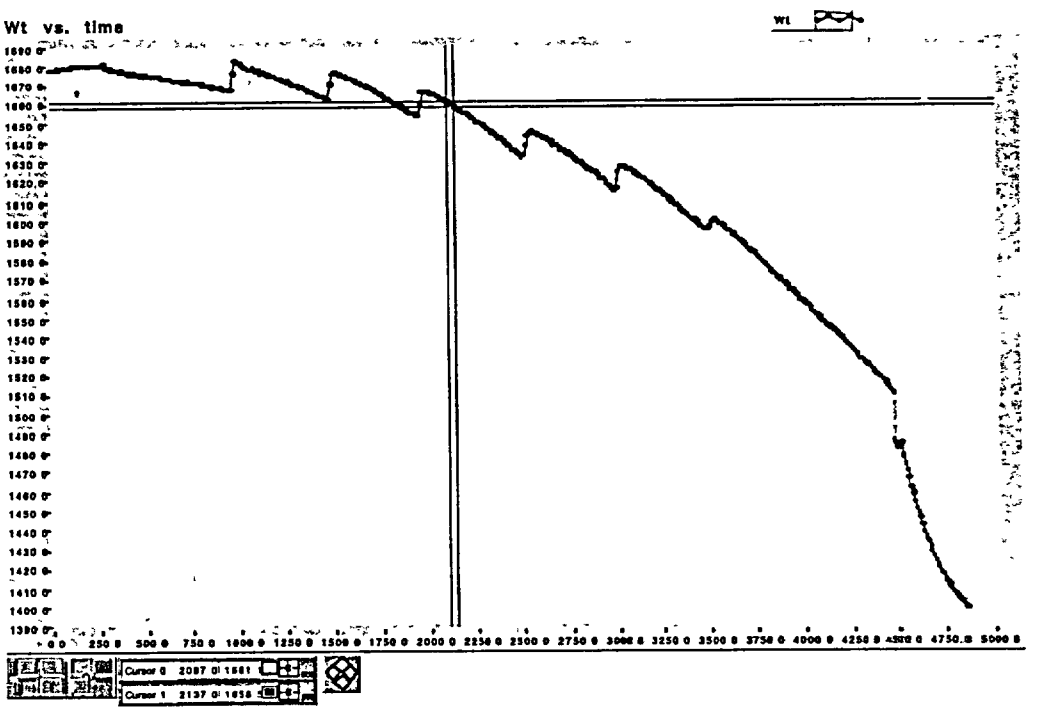

Figure 20. Blowdown vessel weight vs. time during test of tube with 0.794-mm (1/32-in.)-diameter hole (T6EOTWX.031D).

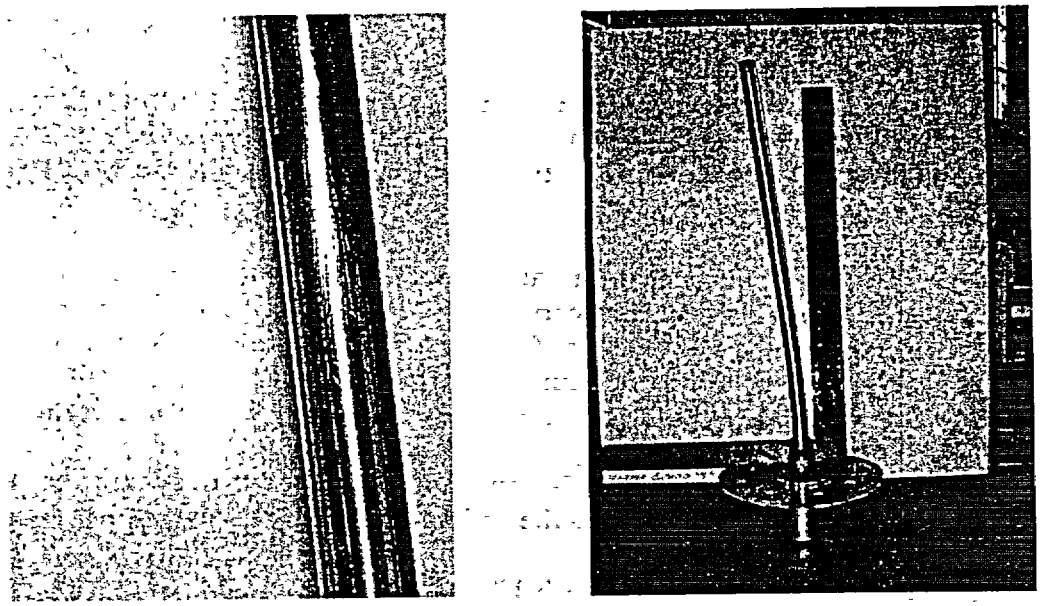

(a) (b)

Figure 21. Two views of tube T5EOTWX.250D having 6.35-mm (1/4-in.)-diameter circular hole after testing, showing bending produced by thrust from water jet.

37.7 L/min (9.95 gpm) for this same 3.175-mm (1/8-in.)-diameter hole under the same pressure differential for room-temperature water, in good agreement with the experimental value of 37.1 L/min (9.8 gpm).

For the 0.79,- 3.18-, and 6.35-mm ($1/32$-, $1/8$-, and $1/4$-in.)-diameter orifices tested at a pressure difference of 17.2 MPa (2500 psi) and room temperature, the orifice model predicts flow rates of 3.33, 53.0, and 212 L/min (0.88, 14.0, and 56.0 gpm), respectively, which are again in good agreement with the experimental values.

Additional tests were performed with orifices of 3.18, 1.59, 0.79, and 0.40 mm ($1/8$, 1/16, $1/32$, and $1/64$ in.) diameter at room temperature (21°C or 70°F) and elevated temperature (282°C or 540°F) for pressure differences from 0 to 17.2 MPa (0 to 2500 psi). The ratio of the flow path length (wall thickness of the tube = 1.27 mm [0.05-in.]) to hole diameter for these hole sizes (L/h) is 0.4, 0.8, 1.6, and 3.2, respectively, which can be compared with those estimated for prototype cracks, as shown in Fig. 18. Even the smallest of the orifices is still very open compared to most cracks.

For the elevated-temperature tests, the internal tube pressurization was held at 17.2 MPa (2500 psi), and the back pressure on the outside of the tube was varied from zero to a few MPa (several hundred psi) to see if the flow was choked. For all four orifice sizes, changes in the back pressure produced changes in hole flow rate, indicating no choking. The orifice flow model predicts the flow rates to within 8% of the experimental values in all the tests. It appears that in the elevated-temperature tests the water does not flash to steam until after it exits the orifice.

4.1.1 Summary of Results

A series of pressure and leak-rate tests was conducted on 22.2-mm (7/8-in.)-diameter Alloy 600 steam generator tubes having EDM sharp-edged, circular throughwall holes. These tests were conducted at room and elevated temperature using the Pressure and Leak-Rate Test Facility. The following conclusions were reached:

1. The observed flow rates for both the room- and elevated-temperature tests could be predicted quite accurately using a standard correlation for incompressible flow through a sharp-edged circular orifice and an assumed orifice discharge coefficient value of 0.6. The flow rate increased with increasing temperature, and this temperature dependence was accommodated by the correlation through the variation of fluid density with temperature.

2. No flow choking was observed in the elevated-temperature tests, and it appears that the water does not flash to steam until after it exits the orifice.

3. The jet velocities through the specimens with 3.175-mm (1/8-in.)-diameter circular holes were great enough to generate sufficient lateral thrust to bend the specimens ≈10°. No bending was observed in specimens with smaller holes.

4.2 Axial EDM Notches

Tests on axial EDM notches were conducted both in the Argonne High-Temperature Pressure and Leak-Rate Test Facility (Section 4.2.1) and the Room-Temperature High-Pressure Test Facility (Section 4.2.2). The tests conducted in the Pressure and Leak-Rate Test Facility did not use bladders, but some of the tests in the High-pressure Test Facility did require bladders/foils. The influence of the various parameters that affect testing with bladders/foils was explored.

4.2.1 Pressure and Leak-Rate Test Facility: Exploratory Axial Notch Testing

4.2.1.1 Single-Axial Notches

A series of tests on tubes with single 38.1-, 25.4-, 12.7-, and 8.9-mm (1.5-, 1.0-, 0.5-, and 0.35-in.)-long axial EDM notches of various depths was performed at room and elevated temperatures in the Pressure and Leak-Rate Test Facility. All flaws were nominally 0.20 mm (0.0075 in.) wide and were tested without bladders at a quasi-steady pressurization rate.

Three tubes (T3EA80X1.5, T4EA80X1.5, and T7EA80X1.5) with geometrically identical axial OD EDM notches, 38.1-mm (1.5 in.)-long, 0.20-mm (0.0075-in.)-wide, and 80% TW, were tested at room temperature. Two of these tubes had the same as-received heat treatment, and the remaining tube was sensitized (solution heat treated at 1100°C for 10 min and aged at 600°C for 48 h) before testing.

The behavior of the three tubes was quite similar, and test details are therefore presented only for tube T4EA80X1.5. For this tube, the pressure difference across the tube wall was increased in a series of pressure steps starting at 0.69 MPa (100 psi) in increments of 1.38 MPa (200 psi) up to 10.3 MPa (1500 psi), then in increments of 0.69 MPa (100 psi) up to 13.8 MPa (2000 psi), and finally in increments of 0.34 MPa (50 psi). At ≈17.22 MPa (2497 psi), the flow

through the flaw abruptly increased from zero to a sustained leak rate of ≈1470 L/min (388 gpm) in less than 1 s. The ANL ligament failure correlation[3] predicted a failure pressure of 17.24 MPa (2500 psi) for this flaw. The facility automatically shut down because of low water inventory in the blowdown vessel. The facility was originally designed to sustain a leak rate of at least 760 L/min (200 gpm), and this design limit was exceeded in this test. Upon removal from the test module, the tube was found to have been bent by the jet thrust, and the crack had opened up to a large hole. Figure 22a shows a photograph of the flaw opening after testing, and Figure 22b shows a side view of the flaw.

Table 2 summarizes the failure pressures, flow rates, and posttest rupture geometries for tests T3EA80X1.5, T4EA80X1.5, and T7EA80X1.5. The rupture geometries were obtained by analyses of digital photographs of the failures that project the actual three-dimensional geometry onto a plane. The data for failure pressures, leak rates, and rupture geometry for the two tubes with the same heat treatment (T4EA80X1.5 and T7EA80X1.5) closely agree. The sensitized tube (T3EA80X1.5) exhibited a reduced failure pressure, an increased flow area, and a larger opening. This heat treatment, which was used in the initial stages of this program to increase susceptibility to SCC, clearly weakens tubes. The failure behavior is consistent with the lower flow stress observed for this heat treatment.[2]

Figures 23 and 24 show the results of a room-temperature test on an EDM TW 25-mm (1-in.)-long axial notch (tube T14EATWX1). The internal pressure was increased in four steps (0.69, 6.9, 10.3, and 13.8 MPa [100, 1000, 1500, and 2000 psi]), at which point the test was stopped, and the tube was removed to measure the flow area prior to higher-pressure testing, in which unstable tearing was anticipated. The projected flaw area was 52 mm^2 (0.081 $in.^2$). Based on this opening area, the orifice flow model predicted a flow rate of 312 L/min (82.5 gpm), in good agreement with the experimentally observed flow rate of 302 L/min (79.8 gpm).

The tube was reinstalled in the facility and pressurized to higher levels in a series of 0.69 MPa (100 psi) increments. At ≈15.9 MPa (2300 psi), the flow rate increased abruptly and the pressure dropped momentarily before stabilizing at 12.8 MPa (1859 psi), at which point a flow rate of 1.098 L/min (290.0 gpm) was observed. Unstable tearing presumably associated with the sudden increase in flow rate at 15.9 MPa (2300 psi) is visible at each end of the notch in Fig. 24. Figure 25 is a side view of the flaw bulge. From Fig. 24, the flow area is 170 mm^2 (0.264 $in.^2$), the length is 21.8 mm (0.86 in.), and the maximum flaw width is 11.7 mm (0.46 in.).

Based on the measured opening area, the orifice flow model predicts a flow rate of 984 L/min (260 gpm), which is lower than the observed value of 1,098 L/min (290.0 gpm). It is believed that this underprediction (in contrast to the accurate prediction for the first stage of the test) is primarily the result of the large amount of bulging associated with the flaw (Fig. 25). Because of this bulging, the projected area underestimates the actual flow area. From Fig. 25, the curved arc length of the flaw between the ends of the notch was measured as 24.3 mm (0.958 in.). This length, when divided by the projected length of 21.8 mm (0.86 in.), yields a ratio of 1.114. Applying this correction factor to the flaw opening area gives a three-dimensional area of 190 mm^2 (0.294 $in.^2$), from which the orifice flow model predicts a flow rate of 1,096 L/min (289.5 gpm), in good agreement with experiment.

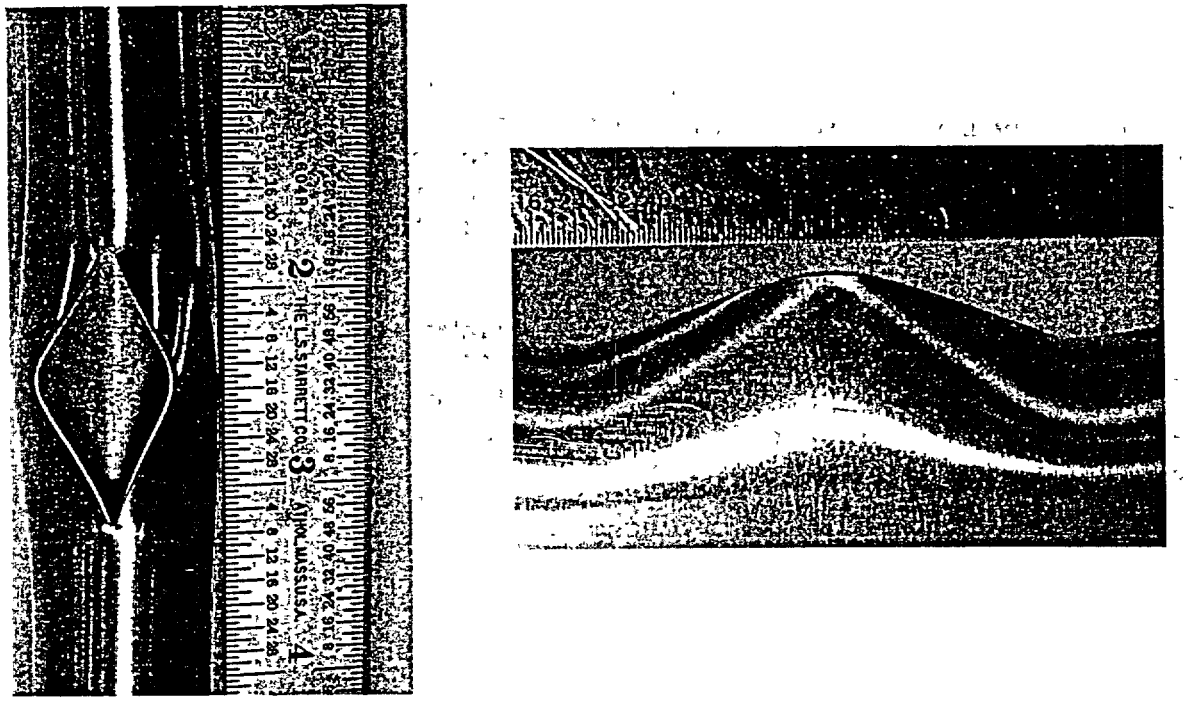

(a) (b)

Figure 22. (a) Photograph of specimen containing 38.1-mm (1.5-in.)-long 80% TW axial EDM notch after failure (test T4EA80X1.5). Side view of tube shown in (b).

Table 2. Results from pressure and leak-rate tests on tubes with 38.1-mm (1.5-in.)-long 80% TW axial EDM flaws. Tube T3EA80X1.5 was subjected to a sensitization heat treatment before testing, and the remaining two tubes were tested in as-received mill-annealed condition.

Tube ID	Failure Pressure, MPa [psi]	Flow Rate, L/min [gpm]	Opening Area, cm^2 [$in.^2$]	Overall Length, cm/ [in.]	Maximum Width, cm/[in.]
T3EA80X1.5	13.8 [2000]	1605 [424]	8.31 [0.507]	3.30 [1.30]	1.83 [0.72]
T4EA80X1.5	17.2 [2497]	1469 [388]	7.41 [0.452]	3.35 [1.32]	1.60 [0.63]
T7EA80X1.5	16.5 [2398]	1453 [384]	7.24 0.442]	3.38 [1.33]	1.57 [0.62]

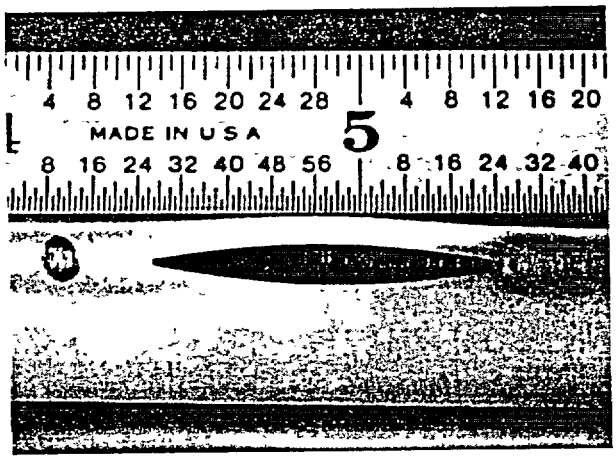

Figure 23.
Opening of 25.4-mm (1-in.)-long axial 100% TW EDM notch (tube T14EATWX1) after test was interrupted at 13.8 MPa (2000 psi) to measure flaw area.

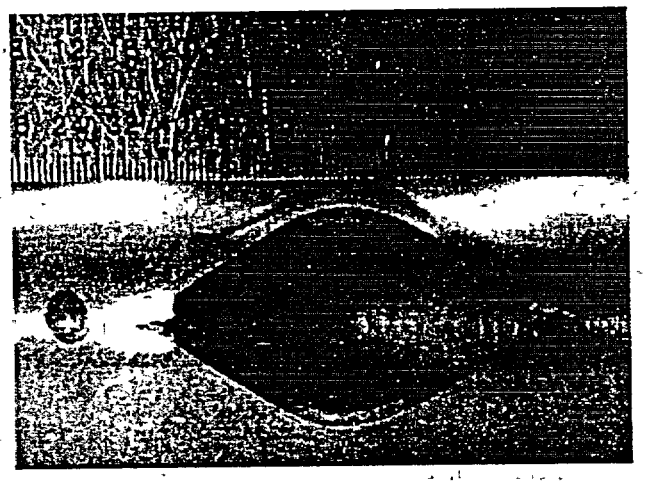

Figure 24.
Opening of 25.4-mm (1-in.)-long axial 100% TW EDM notch in tube shown in Fig. 23 (tube T14EATWX1) after continuing test to 15.9 MPa (2300 psi)

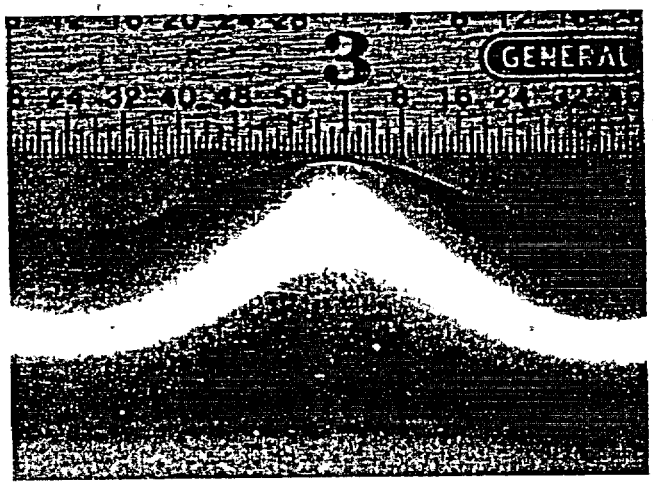

Figure 25.
Side view of tube specimen shown in Fig. 24. Note three-dimensional bulging at failure site.

A test was also performed on a 90% TW axial ODSCC EDM flaw of length 8.9 mm (0.35 in.), width of 0.19 mm (0.0075-in.), and a uniform 90% TW depth (Specimen T13EA90X.35). The tube was first tested at room temperature, with the pressure increasing in 0.69 MPa (100 psi) increments up to 19.3 MPa (2800 psi). No flaw opening or tube leakage occurred, and the test was terminated at this pressure when the facility overpressurization relief valve began to leak. Upon removal and inspection, the tube showed virtually no crack widening or bulging of the tube wall.

The tube was reinstalled and tested at 282°C (540°F) a nd increasing pressure up to 19.3 MPa (2800 psi). Again the tube did not leak, and posttest inspection revealed no change in the flaw width or tube bulging. The observed >19.3 MPa (2800 psi) ligament failure pressure is consistent with the ANL ligament failure correlation, which predicts a failure pressure of 22 MPa (3200 psi) at room temperature and 20 MPa (2900 psi) at 282°C (540°F).[2]

4.2.1.2 Multiple Axial Notches

Initial testing of EDM flawed tubes having two aligned axial notches is presented in this section. More extensive testing of multiple flaws is reported in Sections 4.2.2.2 and 4.3.

We tested two identical specimens with two aligned axial TW notches 6.35-mm (0.25-in.) long, separated by a 0.25-mm (0.01-in.)-long full-wall-thickness ligament. The first specimen (T24EATWX.5 LIG) was tested at room temperature and pressures up to 17.2 MPa (2500 psi). Figure 26 is a posttest photograph of the flaw; little structural distortion is evident, and the width of the flaw next to the ligament increased by only 50-75 μm (0.002-0.003 in.). At pressures of 14.5 and 17.7 MPa (2100 and 2500 psi), the flow rate was 14.8 and 18.5 L/min (3.9 and 4.9 gpm), respectively. Structural models for multiple cracks are being developed.[3]

The second specimen (T25EATWX.5 LIG) was tested at 282°C (540°F). The ligament between the two notches failed at 15.5 MPa (2250 psi), and there was an abrupt increase in flow rate as the two notches joined. The resulting leak rate corresponded to that expected for a 12.7-mm (0.5-in.)-long notch. The posttest appearance of tube T25EATWX.5 LIG after testing at pressures up to 17.9 MPa (2600 psi) is shown in Fig. 27. Ligament failure and an increase in width of the flaw are apparent.

At 14.5 MPa (2100 psi) (ligament intact) and 17.2 MPa (2500 psi) (ligament torn), the flow rates for tube T25EATWX.5 LIG were 17.0 and 32.2 L/min (4.5 and 8.5 gpm), respectively. At the maximum test pressure of 17.9 MPa (2600 psi), the flow rate was 35.6 L/min (9.4 gpm).

4.2.2 High-Pressure Facility: Axial Notch Tests

A total of 42 flawed specimens of several designs were fabricated and tested. These notches were all 0.19 mm (0.0075 in.) wide and had one of four axial lengths: 6.35, 12.7, 19.1, and 25.4 mm (0.25, 0.5, 0.75, and 1.0 in.). Flaws depths explored were 60, 80, 90, and 100% throughwall.

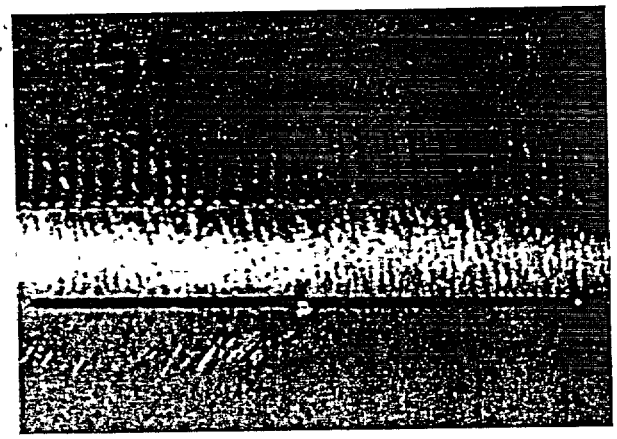

Figure 26.
Posttest photograph of tube T24EATWX.5 LIG tested at room temperature and up to 17.2 MPa (2500 psi). Little flaw distortion and intact ligament are visible.

4.2.2.1 Influence of Bladders/Foils and Pressurization Rate

Bladder Effects

Tests were run on specimens (12.7-mm [0.5-in.] and 19.1-mm [0.75-in.]-long, 80 and 100% TW flaws) without a bladder, with a bladder, and with a bladder plus backup foil to help understand the effects of bladders and foils on failure pressures. These tests are summarized in Table 3. The posttest appearance of specimen OM120, which was tested without a bladder, is shown in Fig. 28. The throughwall ligament failed at a pressure of 26.9 MPa (3900 psi), which is in good agreement with the predicted value of 25.5 MPa (3700 psi). No discernible unstable tearing occurred at the notch ends.

A 2.4-mm ($^3/_{32}$-in.) or 3.2-mm (1/8-in.)-thick hard Tygon bladder was used for the tests with a bladder. Figures 29 and 30 show photographs of how the bladder, which has an outer diameter (OD) slightly smaller than the tube inner diameter (ID) is sealed in the tube with a bored tapered Teflon plug to prevent water penetration between the bladder and the tube ID.

Tests with bladders were performed for specimens with 80% TW flaws of 12.7-mm (0.5-in.) (OM121) and 19.1-mm (0.75-in.) (OM123) lengths, respectively. Posttest photographs of the specimens are shown in Figs. 31 and 32. The tests were conducted at a nominal pressurization rate of 13.8 MPa/s (2000 psi/s). Clearly, both flaws experienced significant tearing at both ends of the original notches. The experimental/predicted unstable burst pressures for the 12.7 and 19.1-mm (0.5- and 0.75-in.)-long 80% TW flaws were 29.0/30.3 MPa (4200/4400 psi) and 21.9/22.8 MPa (3180/3300 psi), respectively.

A 12.7-mm (0.5-in.)-long 60% TW flaw, unlike an 80% TW flaw of the same length, will exhibit unstable tearing or bursting simultaneous with the failure of the throughwall ligament. Such flaws can be tested with and without a bladder to assess the effect of bladders on burst data. Figure 33 shows a posttest photograph of tube OM113, which was tested without a bladder. The flaw burst unstably without a bladder at 40.7 MPa (5900 psi), as compared to the predicted burst pressure of 38.6 MPa (5600 psi).

Figure 34 is a posttest photograph of tube OM112 with the same flaw geometry, but after testing with a bladder. The tube failed at 41.4 MPa (6000 psi), which is close to the predicted

Table 3. Summary of room-temperature pressurization tests conducted using High-Pressure Test Facility on tubes with axial EDM notches to determine effect of internal Tygon tube bladder and 0.13-mm (0.005-in.)-thick brass backup foil on failure pressure. All tests with internal bladders were conducted at a pressurization rate of 13.8 MPa/s (2000 psi/s); the remaining tests were conducted at a quasi-steady-state pressurization rate.

Spec. ID	Flaw Geometry		Internal Bladder and Backup Foil	Unstable Burst Pressure	
	Length, mm (in.)	Depth, % TW		Experimental, MPa (psi)	Predicted, MPa (psi)
OM120	12.7 (0.5)	80	None	26.9[a] (3900)	25.5[a] (3700)
OM121	12.7 (0.5)	80	2.4-mm (3/32-in.)-thick bladder, no foil	29.0 (4200)	30.3 (4400)
OM123	19.1 (0.75)	80	2.4-mm (3/32-in.)-thick bladder, no foil	21.9 (3180)	22.8 (3300)
OM113	12.7 (0.5)	60	None	40.7 (5900)	38.6 (5600)
OM112	12.7 (0.5)	60	2.4-mm (3/32-in.)-thick bladder, no foil	41.4 (6000)	38.6 (5600)
OM102	12.7 (0.5)	100	2.4-mm (3/32-in.)-thick bladder, no foil	29.6 (4300)	30.3 (4400)
OM101	12.7 (0.5)	100	3.2-mm (1/8-in.)-thick bladder, no foil	29.6 (4296)	30.3 (4400)
OM133	12.7 (0.5)	100	3.2-mm (1/8-in.)-thick bladder plus foil extending 6.35 mm (0.25 in.) beyond notch	30.0 (4350)	30.3 (4400)
OM134	12.7 (0.5)	100	3.2-mm (1/8-in.)-thick bladder plus foil extending circumferentially 90° to either side of notch	30.7 (4450)	30.3 (4400)

[a]Pressure for failure of throughwall ligament; tube not tested to unstable burst.

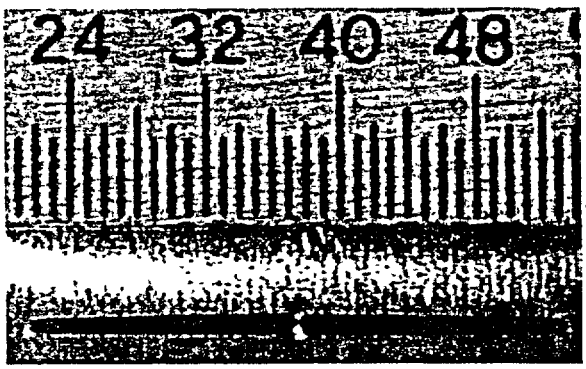

Figure 27.
Posttest photograph of tube T25EATWX.5 LIG tested at 282°C (540°F) and up to 17.9 MPa (2600 psi). Appreciable flaw notch widening and the failed ligament are visible.

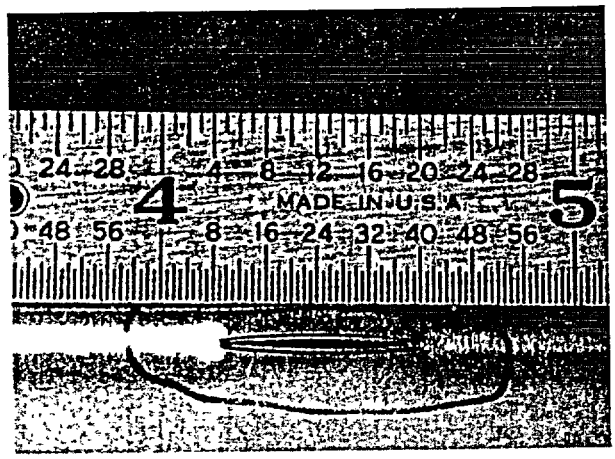

Figure 28.
Posttest appearance of specimen OM120 (12.7-mm [0.5-in.]-long 80% TW axial EDM notch), tested without bladder.

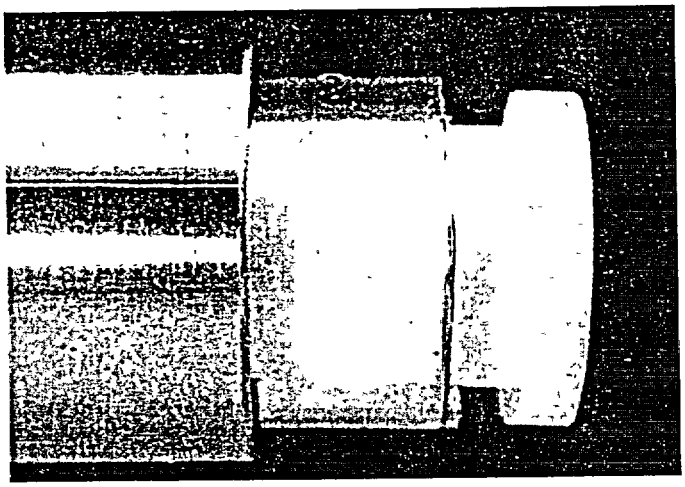

Figure 29.
Side view of tube with bladder and bored plug seal being installed.

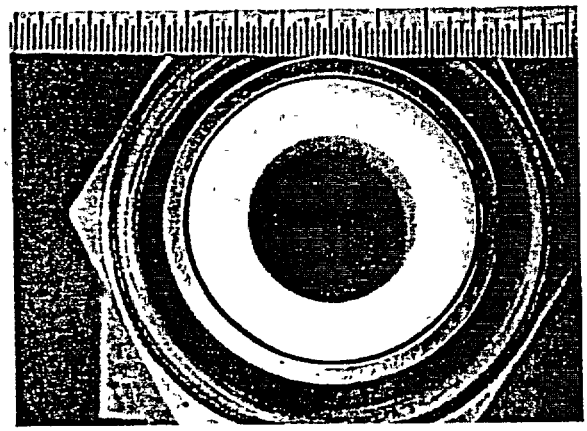

Figure 30.
End view of tube with bladder and plug installed.

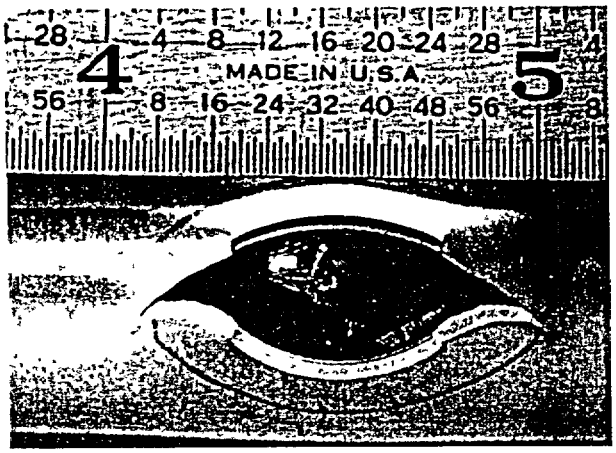

Figure 31.
Posttest appearance of specimen OM121 (12.7-mm [0.5-in.]-long 80% TW axial EDM notch), tested with bladder at a pressurization rate of 13.8 MPa/s (2000 psi/s). Flaw burst occurred at 29.0 MPa (4200 psi), as compared to the predicted failure pressure of 30.3 MPa (4400 psi).

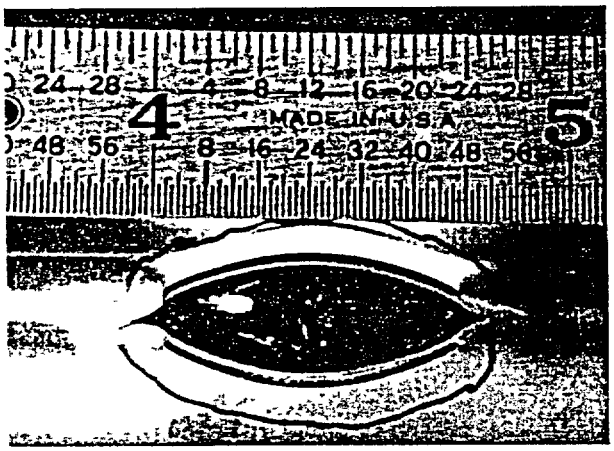

Figure 32.
Posttest appearance of specimen OM123 (19.1-mm [0.75-in.]-long 80% TW axial EDM notch), tested with bladder at a pressurization rate of 13.8 MPa/s (2000 psi/s) Flaw burst occurred at 21.9 MPa (3180 psi), as compared to the predicted failure pressure of 22.8 MPa (3300 psi).

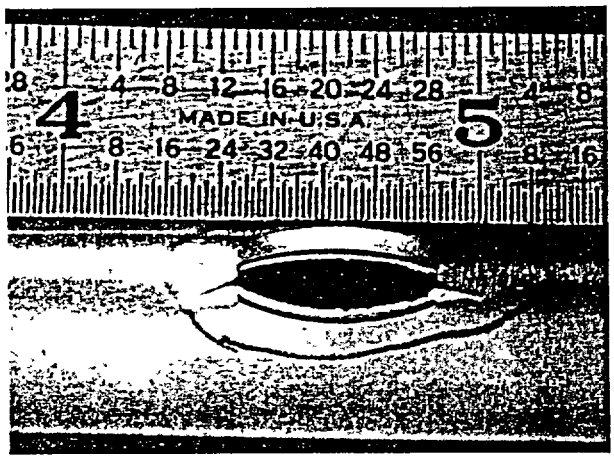

Figure 33.
Tube OM113 with a 12.7-mm (0.5-in.)-long 60% TW EDM axial OD notch, tested without a bladder.

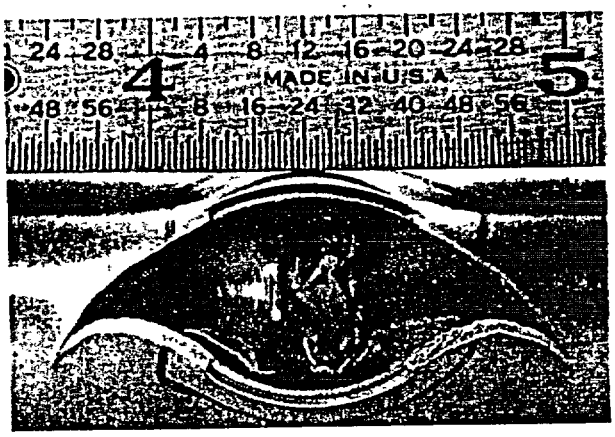

Figure 34.
Tube OM112 with a 12.7-mm (0.5-in.)-long 60% TW EDM axial OD notch, tested with a bladder.

value of 38.6 MPa (5600 psi) and to the failure pressure observed in the test without a bladder. Use of the bladder caused significantly more unstable tearing of the notch ends than in Tube OM113 (Fig. 33).

Tests were also performed on tubes with 12.7-mm (0.5-in.)-long 100% TW EDM axial notches. Such flaws cannot be unstably burst in the High-Pressure Test Facility without the use of a bladder. This flaw geometry was tested with two different bladders. Tube OM102 was tested with a 2.4-mm ($3/32$-in.)-thick bladder, and tube OM101 was tested with a 3.2-mm ($1/8$-in.)-thick bladder. A posttest photograph of the test with the thinner bladder is shown in Fig. 35. The bladder was extruded through the flaw opening. The tube burst at 29.6 MPa (4300 psi), close to the predicted value of 30.3 MPa (4400 psi), but only a very slight amount of unstable tearing occurred.

Figure 36 shows the posttest appearance of tube OM101, which was tested with the thicker bladder. The thicker bladder did not extrude through the flaw, in contrast to tube OM102, and significantly more flaw bulging and unstable tearing took place at the notch ends. Tube OM101 burst at 29.6 MPa (4296 psi), which is good agreement with the predicted value of 30.3 MPa (4400 psi), despite the more extensive tearing with the thicker bladder. Thus, the proper use of bladders produces a unique value for the unstable burst pressure for a given flaw geometry, independent of the extent of tearing. However, it is readily apparent that the resulting leak areas can be drastically different. The question therefore arises concerning the correct area to be used at unstable burst for the purposes of predicting the leak flow rate. We believe that this area can only be reliably determined through a detailed simulation of flaw structure and fluid dynamic interactions during burst, not through testing using bladders.

Foil Effects

Backup foils are sometimes used to prevent premature bladder extrusion through throughwall flaws and the resulting excessive water leakage that would prevent pressurization to a sufficient level to burst a tube. To evaluate the influence of foil backups, two tubes with identical flaw geometries (axial notch, 12.7-mm [0.5-in.] long and 100% TW) were tested at a pressurization rate of 13.8 MPa/s (2000 psi/s) with 3.2-mm (1/8-in.)-thick bladders and two different designs of 0.13-mm (0.005-in.)-thick brass foil backups. Specimen OM133 had a foil that extended 6.35 mm (0.25 in.) beyond the defining dimensions of the axial notch, in conformance with EPRI guidelines. Specimen OM134 had a larger foil that extended

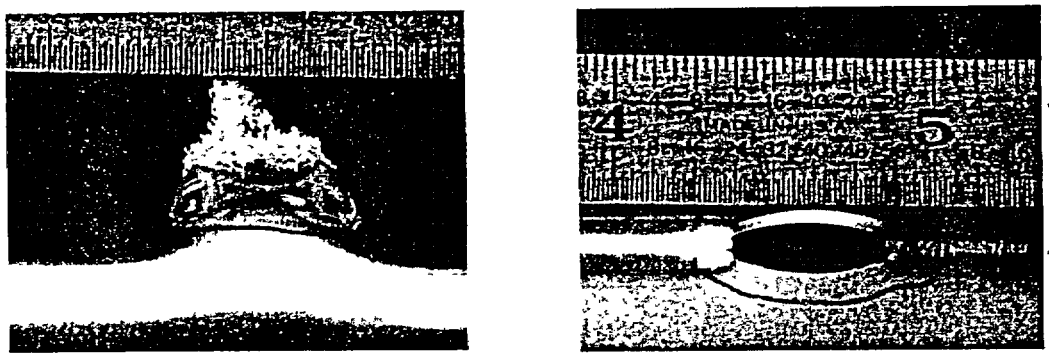

Figure 35. Side (left) and top (right) views of Tube OM102 with a 12.7-mm (0.5-in.)-long 100% TW EDM axial notch. Specimen was tested with a 2.4-mm (3/32-in.)-thick hard bladder at a pressurization rate of 13.8 MPa/s (2000 psi/s).

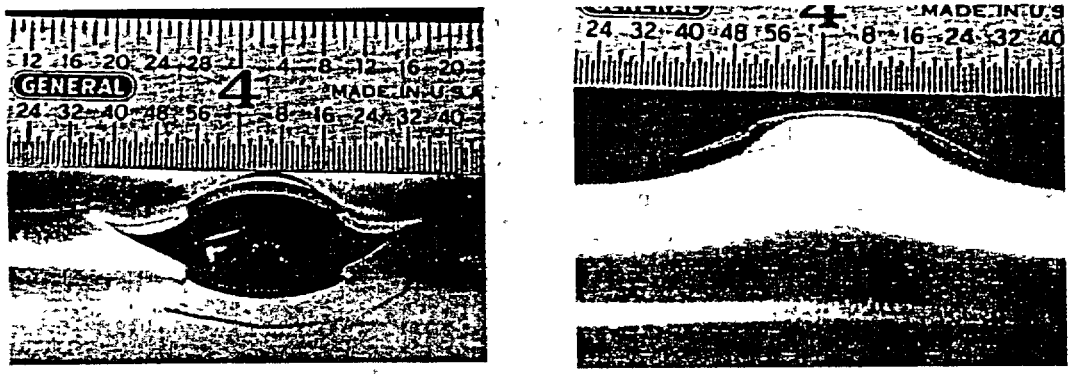

Figure 36. Top (left) and side (right) views of tube OM101 with a 12.7-mm (0.5-in.)-long 100% TW EDM axial OD notch. Specimen was tested with a 3.2-mm (1/8-in.)-thick bladder at a pressurization rate of 13 8 MPa/s (2000 psi/s).

circumferentially 90° to either side of the notch and 12.7 mm (0.5 in.) beyond the ends of the notch. The use of a larger size foil can be advantageous when dealing with large SCC flaws that cover a large tube area and have additional secondary cracking that makes a precise determination of flaw extent by pretest NDE or dye penetrant uncertain. In both cases, the internal tube surface was lubricated with a multipurpose spray lubricant to reduce friction between the foil and the tube.

Figures 37 and 38 show post-test photographs of the failed tubes with bladders and foil still in place for tests OM133 (small foil) and OM134 (large foil), respectively. Both flaws exhibit more unstable tearing than test OM101, which used only a bladder (see Fig. 36). However, most important, the burst pressures of 30.0 MPa (4350 psi) for Specimen OM133 and 30.7 MPa (4450 psi) for Specimen OM134 are close to the observed failure pressure of 29.6 MPa (4295 psi) for Specimen OM101 tested without the foil. For the tube with the smaller foil (Fig. 37), the foil has unsymmetrically slipped partially through the flaw opening. In the tube with the larger foil (Fig. 38), the foil has torn axially and symmetrically along the entire flaw-opening

length, suggesting that this larger foil does not slip as easily through the opening flaw upon failure. Even though these tests show that the foil coverage area has not influenced the failure pressure, this behavior could change if larger foils were used or tubes that fail at considerably lower pressures were tested, in which case the greater extent of foil might produce local strengthening and erroneous flaw opening pressure data. Likewise, thicker foils or foils made of stronger material such as stainless steel could also produce unreliable data.

Pressurization Rate and Short Flaws

Tube failure tests were also conducted on nine tubes with the same short-length (6.35 mm [0.25 in.] long) EDM OD axial notches having depths of 60, 80, and 90% TW. The tests were conducted with and without bladders and foil backups at various pressurization rates. Also, at the end of this section, results from testing three identical 19.1-mm (0.75-in.)-long axial notches at different pressurization rates are presented that supplement these data. Prior to these tests, the shortest flaw tested was 8.89 mm (0.35 in.) long and 90% TW. This short flaw could not be opened in the 20.7 MPa (3000 psi) Pressure and Leak-Rate Test Facility at either room or elevated temperature. In addition, it was considerably stronger than predicted by structural analysis, in contrast to the generally good agreement observed for longer flaws.

The results from the nine tests are summarized in Table 4, and post-test photographs of the flaws are shown in Figs. 39–47. The 60% TW flaws (Specimens OM118 and OM119) were tested at high pressurization rates without and with a bladder, respectively, and the flaws opened within 2.1 MPa (300 psi) of each other. These flaws were predicted to burst unstably at 45.4 MPa (6600 psi) before tearing, but the actual failure pressures were somewhat higher. In addition, Specimen OM118 (Fig. 39) exhibited no unstable tearing, but OM119 tested with a bladder (Fig. 40) exhibited significant tearing many times longer than the original flaw length. This effect of the bladder on flaw opening area is in agreement with the observations for Specimens OM113 and OM112 described above.

Specimens OM116 and OM117 with 80% TW flaws were tested at low and high pressurization rates without and with bladders, respectively. Specimen OM116 exhibited no unstable burst and opened at 37.7 MPa (5475 psi), whereas OM117 tested with a bladder exhibited unstable burst at 43.1 MPa (6252 psi). This flaw geometry was predicted to tear at 37.2 MPa (5400 psi) and to go unstable at 45.5 MPa (6600 psi). Specimen OM116, which could not be pressurized sufficiently rapidly to induce unstable burst because of the absence of a bladder, tore near the predicted value. Specimen OM117 tested with a bladder went unstable at a pressure ≈2.4 MPa (350 psi) lower than the predicted value for unstable burst. Again, as shown in Figs. 41 and 42, the flaws exhibit greatly different opening areas.

Three of the five 90% TW flaws (Specimens OM138, OM139, and OM140) were tested without bladders at progressively increasing pressurization rates of quasi-steady-state, 5.2, and 22.1 MPa/s (750 and 3200 psi/s), respectively. None of these flaws exhibited unstable burst. This flaw geometry was predicted to first tear at 27.6 MPa (4000 psi) and then to go unstable at 45.5 MPa (6600 psi). The specimens actually tore open at pressures of 30.0, 28.3, and 33.8 MPa (4350, 4100, and 4900 psi), respectively. Thus, the results for the tests conducted at the two lower pressurization rates were in good agreement with the predicted

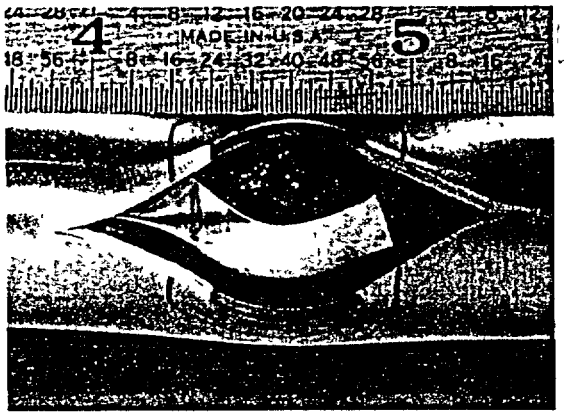

Figure 37.
Specimen OM133 with 12.7-mm (0.5-in.)-long 100% TW OD axial EDM notch tested with 3.2-mm (1/8-in.)-thick hard bladder and small backup foil at a pressurization rate of 13.8 MPa/s (2000 psi/s). Failure pressure was 30.0 MPa (4350 psi).

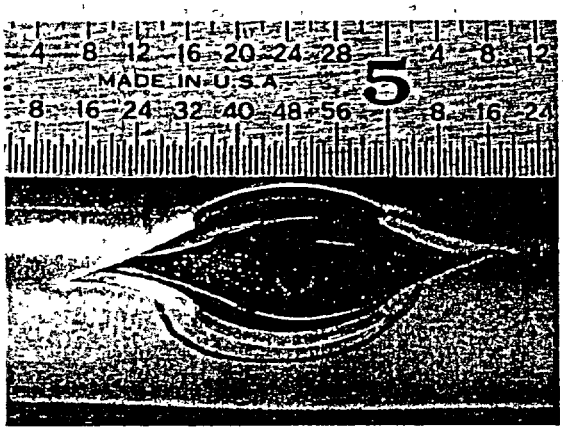

Figure 38.
Specimen OM134 with 12.7-mm (0.5-in.)-long 100% TW OD axial EDM notch tested with 3.2-mm (1/8-in.)-thick hard bladder and large backup foil at a pressurization rate of 13.8 MPa/s (2000 psi/s). Failure pressure was 30.7 MPa (4450 psi).

values, but the specimen tested at the highest pressurization rate tore open at 6.2 MPa (900 psi) above the predicted value. This dependence of flaw-opening pressure on pressurization rate has also been observed in testing of 19.1-mm (0.75-in.)-long axial notches as described at the end of this section. For all three specimens, the leak rates upon flaw opening were below the facility maximum of nominally 45 L/min (12.8 gpm), and the flaws were therefore pressurized to higher levels of 42.7, 43.8, and 44.8 MPa (6200, 6356, and 6492 psi), respectively. At this point, the flow rates reached the facility maximum, and further pressurization to unstable burst (≈45.5 MPa or 6600 psi) could not be achieved. The posttest appearances of these three specimens are shown in Figs. 43–45.

This same flaw geometry was tested with a bladder (Specimen OM141) and a bladder/foil combination (Specimen OM142). Both of these specimens went unstable and exhibited greatly increased flaw opening areas (Figs. 46 and 47). Both of these flaws first tore open near the predicted value of 27.6 MPa (4000 psi) and were then pressurized to higher levels. Specimen OM141, tested with only a bladder, exhibited unstable burst at 45.0 MPa (6520 psi), which is very near the predicted value of 45.5 MPa (6600 psi). However, Specimen OM142, which used a foil backup, burst at 41.5 MPa (6026 psi). The reason for this behavior is not clear.

To supplement the preceding data from a short flaw on the influence of pressurization rate, three identical 19.1-mm (0.75-in.)-long, 80% TW axial notches (OM107, OM122, and OM109) were tested under three pressurization scenarios. A slow quasi-steady-state

Table 4. Test results for flawed tubes containing 6.35-mm (0.25-in.)-long EDM OD axial notches.

Specimen ID	Flaw Depth, % TW	Pressurization Rate, MPa/s (psi/s)	Initial Flaw Tearing		Unstable Burst		Predicted Ligament Tear/Burst Press., MPa (psi)
			Pressure, MPa (psi)	Leak Rate, L/min (gpm)	Pressure, MPa (psi)	Leak Rate, L/min (gpm)	
OM118	60	13.6 (1970)	49.6 (7200)	46.9 (12.8)	d	d	48.3 (7000)/ 45.5 (6600)
OM119[a]	60	20.7 (3000)	47.6[a] (6900)[a]	>49[a] (13)[a]	47.6[a,b] (6900)[a,b]	>49[a,b] (>13)[a,b]	48.3 (7000)/ 45.5 (6600)
OM116	80	Quasi-steady	37.7 (5475)	12.5 (3.31)	d	d	37.2 (5400)/ 45.5 (6600)
OM117[a]	80	21.4 (3110)	43.1[a] (6252)[a]	>49[a] (13)[a]	43.1[a,b] (6252)[a,b]	>49[a,b] (>13)[a,b]	37.2 (5400)/ 45.5 (6600)
OM138	90	Quasi-steady	30.0 (4350)	4.2 (1.1)	42.7[c] (6200)[c]	45.0[c] (11.9)[c]	27.6 (4000)/ 45.5 (6600)
OM139	90	5.2 (750)	28.3 (4100)	2.8 (0.75)	43.8[c] (6356)[c]	45.4[c] (12.0)[c]	27.6 (4000)/ 45.5 (6600)
OM140	90	22.1 (3200)	33.8 (4900)	-	44.8[c] (6492)[c]	45.4[c] (12.0)[c]	27.6 (4000)/ 45.5 (6600)
OM141[b]	90	4.9 (705)	30.3[d] (4400)[d]	4.5[d] (1.2)[d]	45.0[b,d] (6520)[b,d]	48.4[b,d] (12.8)[b,d]	27.6 (4000)/ 45.5 (6600)
OM142[c]	90	6.3 (916)	27.6[e] (4008)[e]	4.9[e] (1.3)[e]	41.5[b,e] (6026)[b,e]	48.4[b,e] (12.8)[b,e]	27.6 (4000)/ 45.5 (6600)

[a]Tested with 2.38-mm (3/32-in.)-thick bladder.
[b]Unstable burst.
[c]No unstable burst.
[d]Tested with 3.18-mm (1/8-in.)-thick bladder.
[e]Tested with 3.18-mm (1/8-in.)-thick bladder with foil backing.

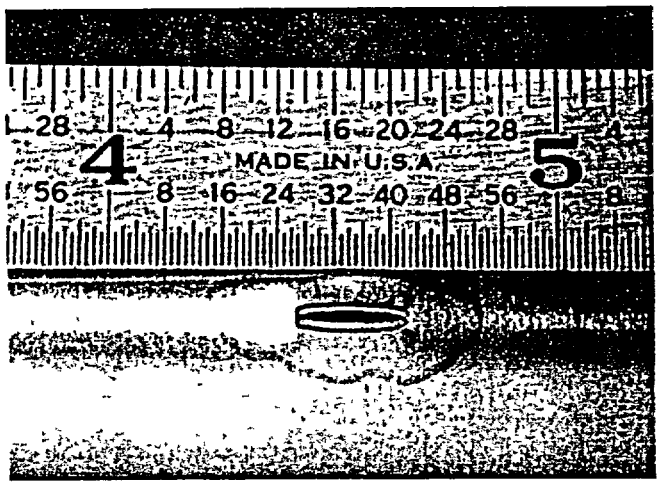

Figure 39.
Macroscopic appearance of Specimen OM118 after pressure testing. Initial flaw tearing occurred at 49.6 MPa (7200 psi). Specimen was tested without an internal bladder.

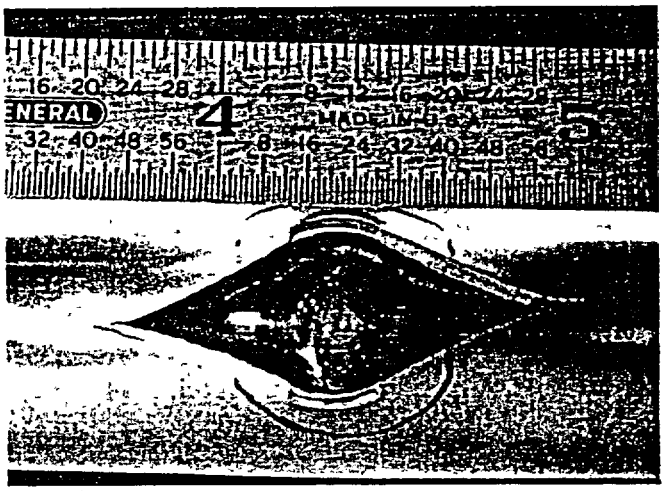

Figure 40.
Macroscopic appearance of Specimen OM119 after pressure testing. Flaw tearing and unstable burst occurred at 47.6 MPa (6900 psi). Specimen was tested with an internal bladder.

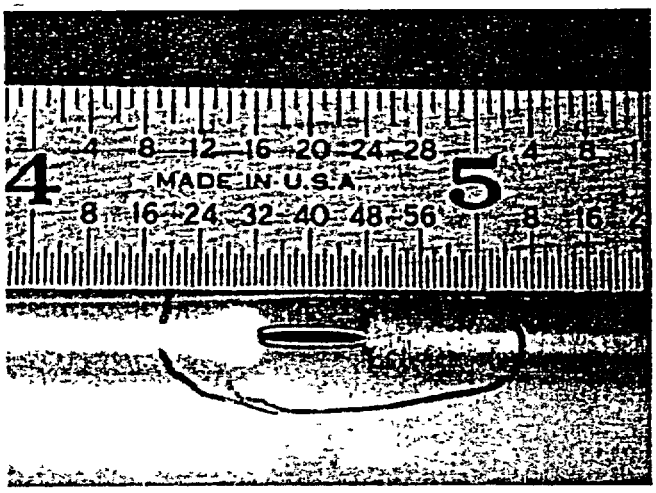

Figure 41.
Macroscopic appearance of Specimen OM116 after pressure testing. Initial flaw tearing occurred at 37.7 MPa (5475 psi). Specimen was tested without an internal bladder.

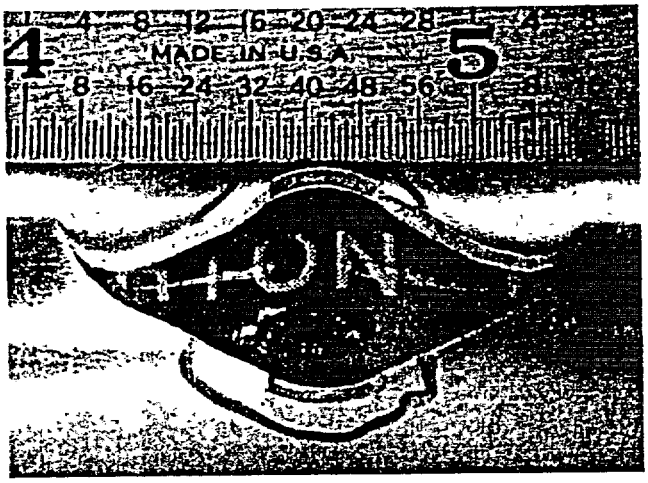

Figure 42.
Macroscopic appearance of Specimen OM117 after pressure testing. Flaw tearing and unstable burst occurred at 43.1 MPa (6252 psi). Specimen was tested with an internal bladder.

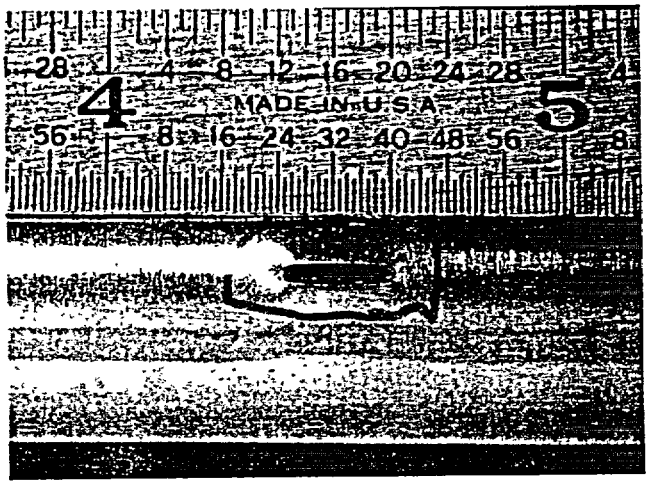

Figure 43.
Macroscopic appearance of Specimen OM138 after pressure testing. Initial flaw tearing occurred at 30.0 MPa (4350 psi), and additional deformation but no unstable burst occurred at maximum pressure of 42.7 MPa (6200 psi).

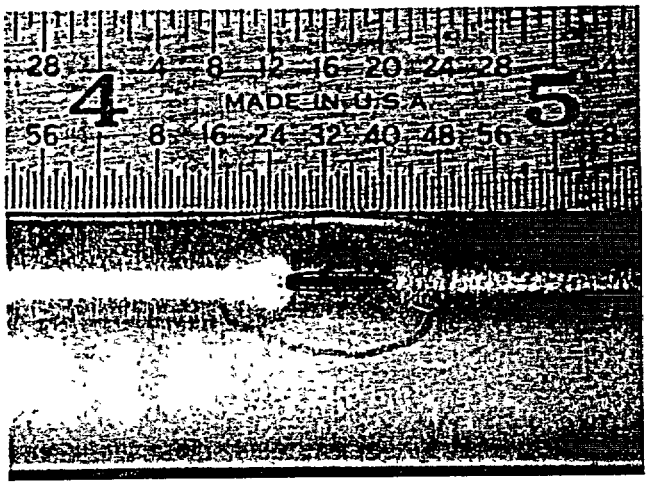

Figure 44.
Macroscopic appearance of Specimen OM139 after pressure testing. Initial flaw tearing occurred at 28.3 MPa (4100 psi), and additional deformation but no unstable burst occurred at maximum pressure of 43.8 MPa (6356 psi).

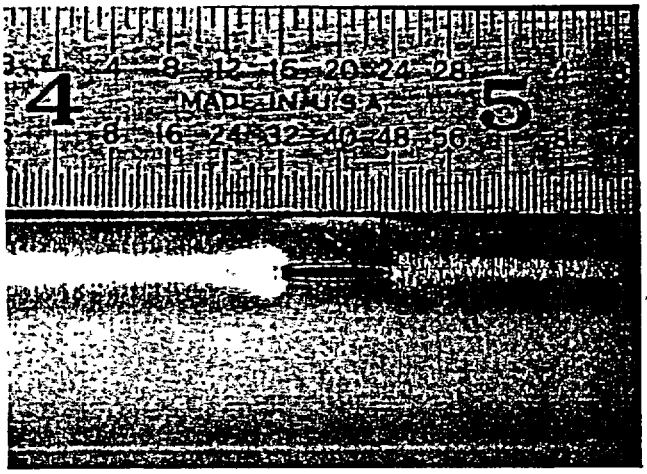

Figure 45.
Macroscopic appearance of Specimen OM140 after pressure testing. Initial flaw tearing occurred at 33.8 MPa (4900 psi), and additional deformation but no unstable burst occurred at maximum pressure of 44.8 MPa (6492 psi).

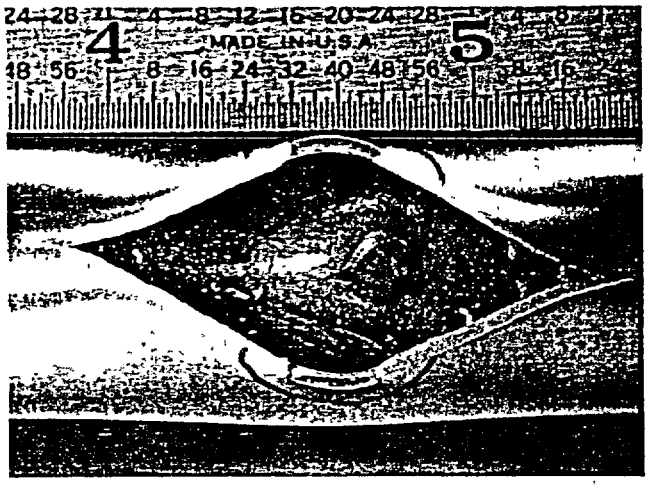

Figure 46.
Macroscopic appearance of Specimen OM141 after pressure testing. Initial flaw tearing occurred at 30.3 MPa (4400 psi), and unstable burst occurred at 45.0 MPa (6520 psi). Specimen was tested with an internal bladder.

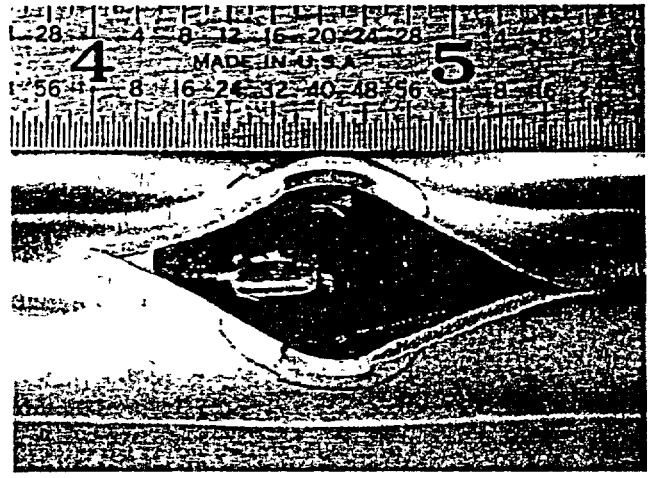

Figure 47.
Macroscopic appearance of Specimen OM142 after pressure testing. Initial flaw tearing occurred at 27.6 MPa (4008 psi), and unstable burst occurred at 41.5 MPa (6026 psi). Specimen was tested with an internal bladder with foil backing.

pressurization rate resulted in ligament tearing at 21.4 MPa (3100 psi), pressurization at 13.8 MPa/s (2000 psi/s) produced ligament tear at 24.2 MPa (3510 psi), and pressurization at 48.3 MPa/s (7000 psi/s) produced ligament tear at 26.4 MPa (3830 psi). The predicted ligament tearing pressure for this flaw geometry is 20.7 MPa (3000 psi), which is in good agreement with the quasi-steady pressurization rate (Test OM107).

Figures 48–50 are posttest photographs of the flaw openings. All three initially identical flaws exhibited ligament tearing but no discernible unstable tearing at the notch ends. In addition to the increase in ligament tear pressure with pressurization rate, the flaws exhibit a slight increase in maximum notch opening width with increasing pressurization rate. This behavior is similar to that for the 6.35-mm (0.25-in.)-long axial notches presented above.

4.2.2.2 Nonuniform Flaw Depth / Interacting Flaws

This section presents results from testing single axial flaws of nonuniform depth and flaws consisting of two interacting axial notches separated by ligaments. The results on interacting notches supplement those already presented in Section 4.2.1.2. Additional results from testing more complex multiple interacting laser-cut flaws are presented in Section 4.3.

Nonuniform Flaw Depth

Results are next presented from tests on three specimens, T29, T30, and T31, with OD axial EDM notches having nonuniform depths along the axial direction. This is in contrast to the above tests, which were all on specimens that had uniform depth flaws. All three notches were nominally 25.4-mm (1-in.) long and 0.19-mm (0.0075-in.) wide. This flaw geometry was tested to further evaluate an ANL equivalent notch analysis that was used to successfully predict flaw opening pressures in a series of five tests on SCC flaws (see Section 5.1). For Specimens T30 and T31, the flaws were 0.635-mm (0.025-in.) deep at each end of the 25.4-mm (1-in.)-long notches and then deepened linearly to 1.14 mm (0.045 in.) at the midpoint of the notches. The flaw in Specimen T31 also had a 0.13-mm (0.005-in.)-diameter TW hole at the deepest midpoint of the notch. This hole was introduced to simulate TW pinholes that have been detected in testing with nonuniform depth SCC flaws. The flaw in Specimen T29 was 1.04 mm (0.041-in.) deep at the ends and deepened linearly to 1.17 mm (0.046 in.) at the midpoint of the notch. It contained no TW hole. All three flaws were tested without bladders or foils at a quasi-steady pressurization rate in which the pressure was increased in 0.69 MPa (100 psi) increments, with a 5-s hold time between increases.

Figures 51 and 52 show the posttest appearance of Specimens T30 and T31, respectively. No unstable tearing into the ends of the notches occurred for either tube. Specimen T30 exhibited abrupt ligament tearing at 18.3 MPa (2650 psi) and T31 at 22.1 MPa (3200 psi), but the tearing did not extend into the notch ends for either flaw. However, Specimen T31, which had the 0.13-mm (0.005-in.)-diameter throughwall hole at the center of the flaw, exhibited greater ligament tearing, a wider crack opening, and a higher opening pressure. The reason for this behavior is being analyzed.

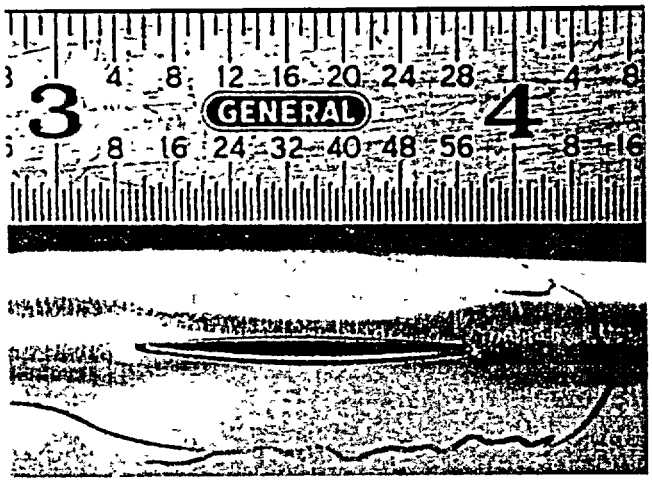

Figure 48.
Posttest appearance of specimen OM107 (19.1-mm [0.75-in.]-long 80% TW axial EDM notch). Speciemn was tested without bladder at a quasi-steady-state pressurization rate. Ligament tearing occurred at 21.4 MPa (3100 psi).

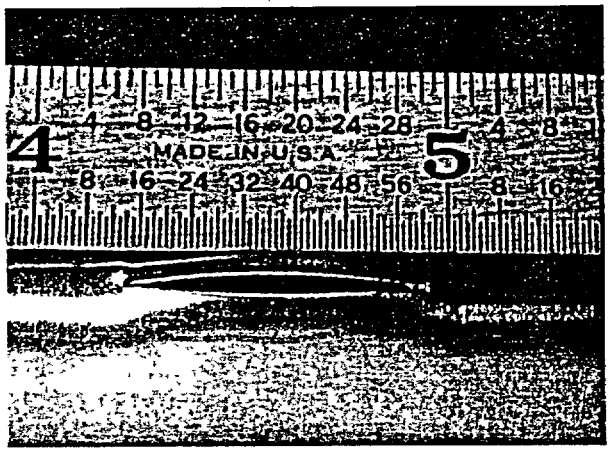

Figure 49.
Posttest appearance of specimen OM122 (19.1-mm [0.75-in.]-long 80% TW axial EDM notch). Specimen was tested without bladder at a pressurization rate of 13.8 MPa/s (2000 psi/s). Ligament tearing occurred at 24.2 MPa (3510 psi).

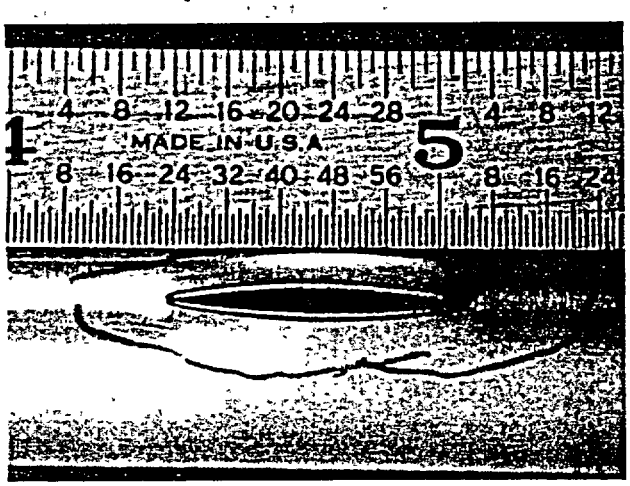

Figure 50.
Posttest appearance of specimen OM109 (19.1-mm [0.75-in.]-long 80% TW axial EDM notch). Specimen was tested without bladder at a pressurization rate of 48.3 MPa/s (7000 psi/s). Ligament tearing occurred at 26.4 MPa (3830 psi).

The flaw in Specimen T29 opened gradually and began leaking at 8.3 MPa (1200 psi), then opened significantly at 9.7 MPa (1400 psi), with the flow rate exceeding 47.3 L/min (12.5 gpm). This is considerably lower than the opening pressure for the shallower flaws in Specimens T30 and T31. These data are also being analyzed by structural analysis.

Interacting Axial Flaws

A nine-tube set of 22.2-mm (7/8-in.)-diameter Alloy 600 tubes containing pairs of 6.35 or 12.7-mm (0.25- or 0.5-in.)-long axial EDM notches was tested in the Room-Temperature High-Pressure Test Facility. The flaws were either 70% TW (for tube OM153) or 80% (remaining eight tubes) separated by various sizes (0.25, 1.25, and 2.5 mm [0.010, 0.050, and 0.100 in.]) of full-wall-thickness ligaments having initial 0.19-mm (0.0075-in.) width. The flaws were either in axial alignment or shifted circumferentially parallel to each other to give the required ligament size. The objective of these tests was to determine how close two notches can be and still act as independent notches or, conversely, how small a ligament must be before it provides no strengthening effect (i.e., the two flaws behave as one larger flaw).

Table 5 summarizes the flaw geometries tested and their behaviors under pressurization. Data are presented on the pressure at first flaw opening and unstable burst, if obtained. Figures 53–64 show posttest photographs of the flaws. For the three specimens that underwent a second-phase burst test, photographs (Figs. 62–64) are also presented for this phase of testing. The flaws were first tested without bladders using quasi-steady pressurization in which the pressure was increased in 0.69 MPa (100 psi) increments with a 5-s hold at each pressure plateau. The testing was stopped when the flaw first opened, as indicated by the abrupt onset of flow. None of the flaws experienced unstable tearing at the end of the quasi-steady pressurization testing (Figs. 53–61). All but three of the flaws exhibited simultaneous tearing of the notch bottoms and the separating ligament in the first phase of testing. Specimens OM152, OM159, and OM162 opened at the bottom of the notch, with the separating ligament remaining intact (see Figs. 56, 58, and 61). Thus, these flaws exhibited sequential tearing of notch bottoms and ligaments at different pressures.

All the flaws consisting of two 12.7-mm (0.5-in.)-long notches leaked the maximum 48.8 L/min (12.9 gpm) capacity of the facility upon opening. Hence, pressurization could not be sustained after the flaws opened. In contrast, the 6.35-mm (0.25-in.)-long flaws when opened in Phase 1 testing were capable of sustained pressurization because the flow rates were less than the facility maximum. The sustained flow rate and pressure for these flaws are presented in Table 6. The flaw openings associated with these flows are shown in Figs. 57–61.

In a second phase of testing, Specimens OM152, OM159, and OM162 were retested with a bladder and a 13.8 MPa/s (2000 psi/s) pressurization rate to obtain information on unstable burst pressure. Figures 62–64 show the burst flaw openings, and a comparison of these figures with those from the Phase 1 testing (Figs. 56, 58, and 61) reveals that the flow openings areas are dramatically larger after unstable burst.

The data in Table 5 on pressure at first leak or abrupt flaw opening furnish some insight on how pairs of equal-sized part-TW axial notches separated by a full-wall-thickness ligament interact. First, relative to whether there is a difference between ligament effects for axial aligned and circumferentially shifted notches with ligaments of the same size, we see by

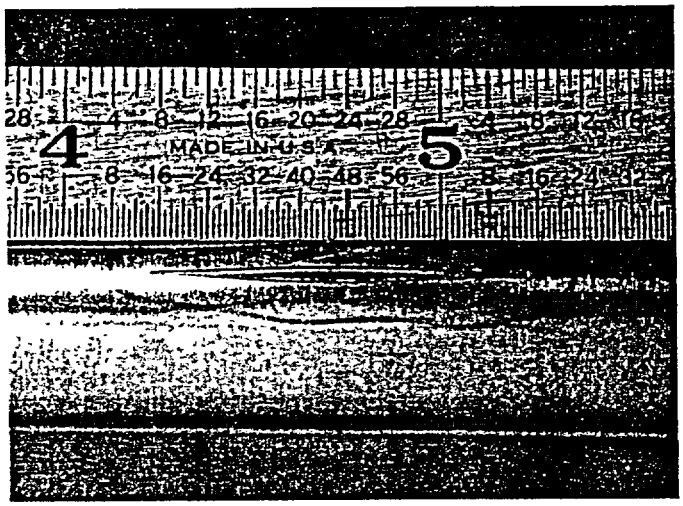

Figure 51.
Specimen T30 with nonuniform 25.4-mm (1-in.)-long OD axial EDM notch tested without bladder at quasi-steady-state pressurization rate. Failure pressure was 18.3 MPa (2650 psi).

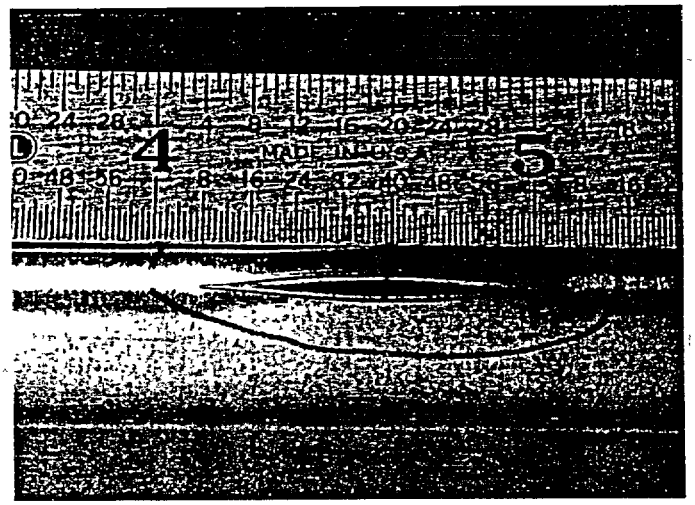

Figure 52.
Specimen T31 with nonuniform 25.4-mm (1-in.)-long OD axial EDM notch tested without bladder at quasi-steady-state pressurization rate. Flaw was identical to that in Specimen T30 (Fig. 51), except that it also had a 0.13-mm (0.005-in.)-diameter throughwall hole at its center. Failure pressure was 2.1 MPa (3200 psi).

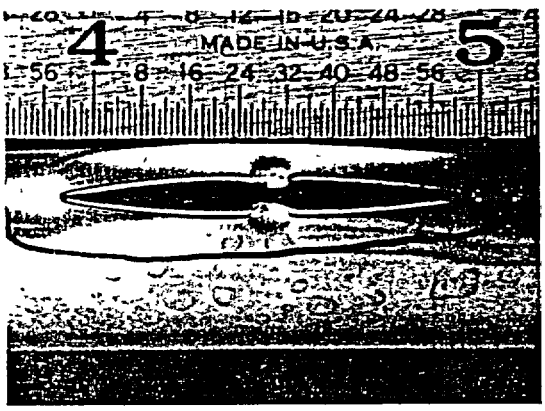

Fig. 53 Specimen OM149 after Phase 1 testing, with two aligned 12.7-mm (0.5-in.)-long axial notches, 2.54-mm (0.100-in.) ligament, and 80% TW.

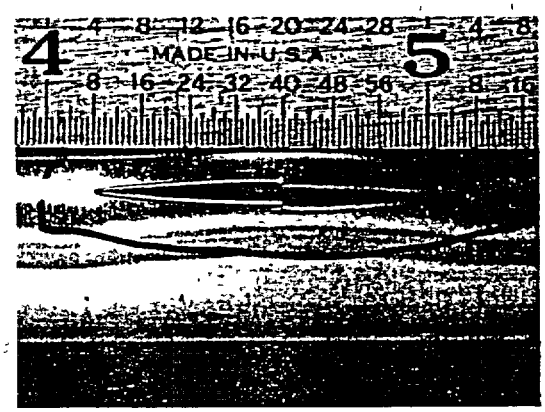

Fig. 54. Specimen OM150 after Phase 1 testing, with two shifted, 12.7-mm (0.5-in.)-long axial notches, 0.25-mm (0.010-in.) ligament, and 80% TW.

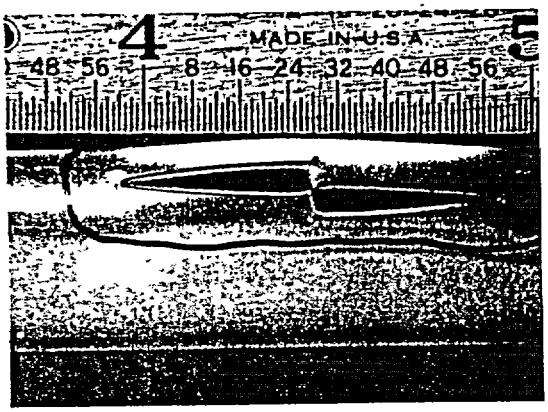

Fig. 55. Specimen OM151 after Phase 1 testing, with two shifted, 12.7-mm (0.5 in.)-long axial notches 1.27-mm (0.050-in.) ligament, and 80% TW..

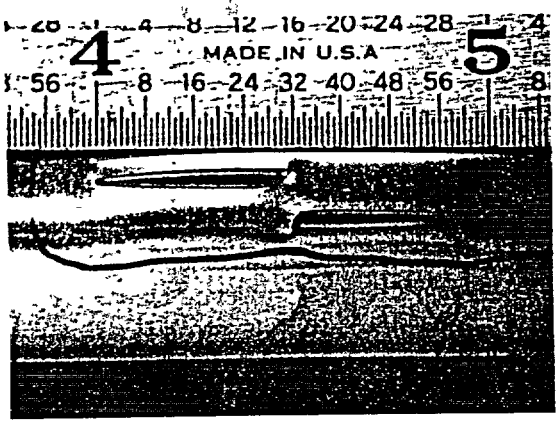

Fig 56. Specimen OM152 after Phase 1 testing, with two shifted, 12.7-mm (0.5 in.)-long axial notches, 2.54-mm (0.100-in.) ligament, and 80% TW.

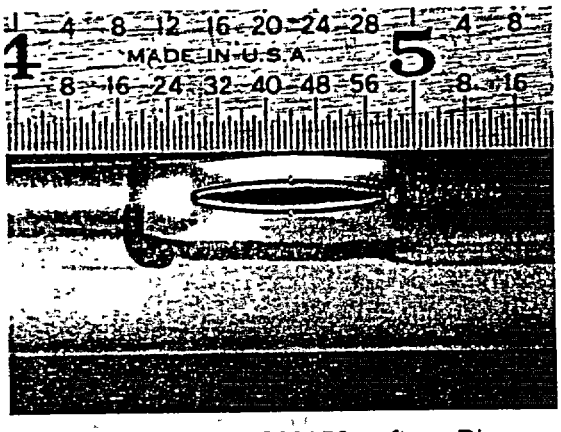

Fig 57. Specimen OM153 after Phase 1 testing, with two aligned, 6.35-mm (0.25-in.)-long axial notches, 0.25-mm (0.010-in) ligament, and 70% TW.

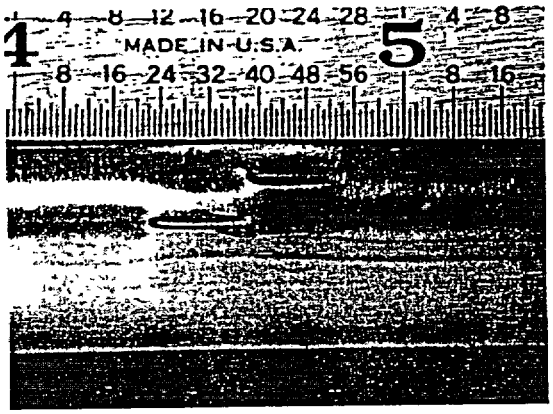

Fig 58. Specimen OM159 after Phase 1 testing, with two shifted, 6.35-mm (0.25-in.)-long axial notches, 2.54-mm (0 100-in) ligament, and 80% TW.

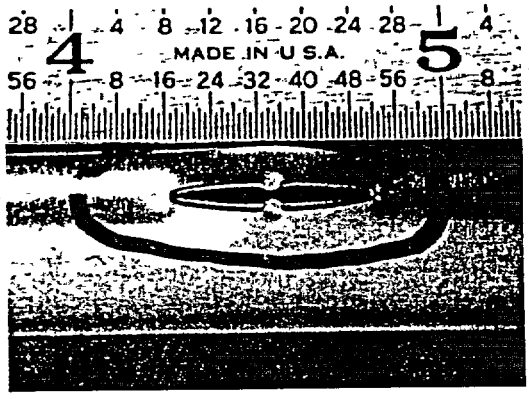

Fig 59. Specimen OM160 after Phase 1 testing, with two aligned, 6.35-mm (0 25-in.)-long axial notches, 1.27-mm (0 050-in) ligament, and 80% TW.

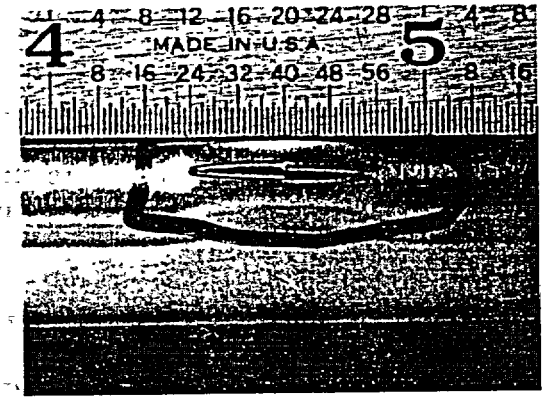

Fig 60. Specimen OM161 after Phase 1 testing, with two shifted, 6.35-mm (0 25-in)-long axial notches, 0.25-mm (0 010-in.) ligament, and 80% TW.

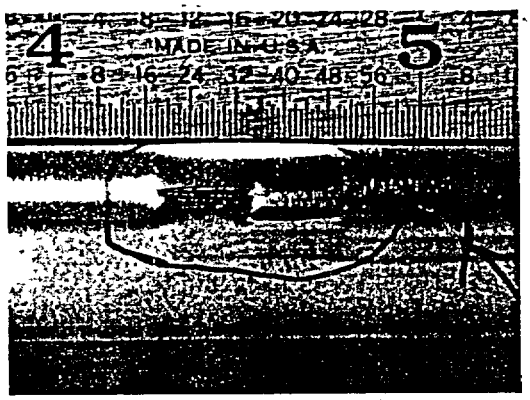

Fig. 61. Specimen OM162 after Phase 1 testing, with two shifted, 6.35-mm (0.25-in.)-long axial notches, 1.27-mm (0.050-in.) ligament, and 80% TW.

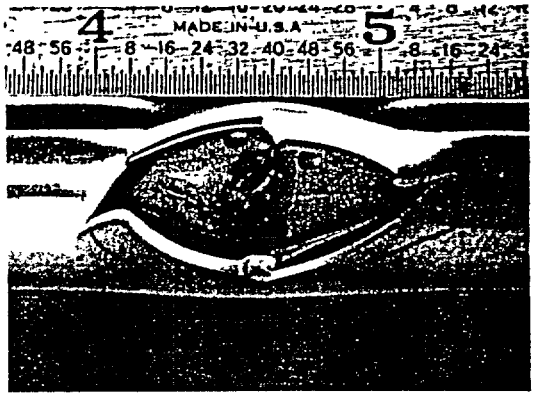

Fig. 62. Specimen OM152 after Phase 1 testing, with two shifted, 12.7-mm (0.50-in.)-long axial notches, 2.54-mm (0.100-in.) ligament, and 80% TW.

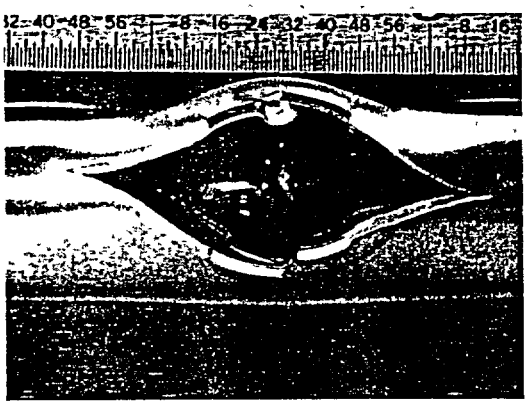

Fig. 63. Specimen OM159 after Phase 1 testing, with two shifted, 6.35-mm (0.25-in.)-long axial notches 2.54-mm (0.100-in.) ligament and 80% TW.

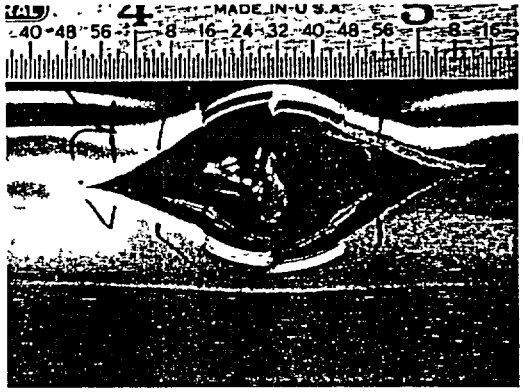

Fig. 64. Specimen OM162 after Phase 1 testing, with two shifted, 6.35-mm (0 25-in.)-long axial notches, 1.27-mm (0.050-in.) ligament, and 80% TW.

comparing pressure data for Specimens OM149 (27.0 MPa) and OM152 (23.5 MPa) that, for 12.7-mm-long flaws with 2.5-mm ligaments, the aligned flaws are stronger. Similarly, for paired 6.35-mm-long notches with 0.25-mm ligaments, i.e., Specimens OM153 (34.8 MPa) and OM161 (28.3 MPa), the aligned flaws are stronger. The same behavior is also seen for paired 6.35-mm-long notches with 1.25-mm ligaments, i.e., Specimens OM160 (32.3 MPa) and OM162 (31.4 MPa).

Secondly, the data provide insight as to how close two axial notches can be and still behave independently by comparing the opening pressures as a function of separating ligament size for the paired 6.35- and 12.7-mm (0.25- and 0.5-in.)-long notches. Table 7 shows data for six tests from Table 5 selected to indicate this behavior. As can be seen, the opening pressure for each flaw length increases to a value that is increasingly less sensitive to increasing ligament size. This finding implies that the flaws are interacting less. Furthermore, the limiting pressure for each flaw length is approaching the predicted opening pressures for single

Table 5. Pressures at first flaw opening and unstable burst for a nine-tube set of 22.2-mm (7/8-in.)-diameter Alloy 600 tubes containing pairs of 6.35- or 12.7-mm (0.25- or 0.5-in.)-long axial EDM notches of 70 and 80% TW separated by various size full-wall-thickness ligaments.

Specimen No.	Flaw Geometry			Pressure at First Leak, MPa (psi)	Pressure at Unstable Burst, MPa (psi)
	Notch Length, mm (in.)	Ligament Length, mm (in.)	Flaw Depth, % TW		
OM149	12.7 (0.5)	2.5 (0.10)	80	27.0[a] (3920)	-
OM150	12.7 (0.5)	0.25 (0.01)	80	19.0[a] (2760)	-
OM151	12.7 (0.5)	1.25 (0.05)	80	23.0[a] (3340)	-
OM152	12.7 (0.5)	2.5 (0.10)	80	23.5[a,b,c] (3405)	18.9 (2744)
OM153	6.35 (0.25)	0.25 (0.01)	70	34.8[a] (5048)	-
OM159	6.35 (0.25)	2.5 (0.10)	80	34.8[a,b,c] (5050)	38.3 (5550)
OM160	6.35 (0.25)	1.25 (0.05)	80	32.3[a] (4675)	-
OM161	6.35 (0.25)	0.25 (0.01)	80	28.3[a] (4100)	-
OM162	6.35 (0.25)	1.25 (0.05)	80	31.4[a,b,c] (4560)	32.5 (4710)

[a]No unstable tearing at this pressure.
[b]Only bottom of notches tore open; no ligament tearing.
[c]Flaw was retested with bladder and 13.8 MPa/s pressurization rate to cause unstable tearing.

Table 6. Sustained pressure and leak rate during Phase 1 testing after flaw opening of two paired 6.35-mm (0.25-in.)-long axial notches.

Specimen No.	Flaw Geometry			Sustained Pressure, MPa (psi)	Sustained Leak Rate, L/min (gpm)
	Notch Length, mm (in.)	Ligament Length, mm (in.)	Flaw Depth, % TW		
OM153	6.35 (0.25)	0.25 (0.01)	70	5.4 (780)	47.69 (12.60)
OM159	6.35 (0.25)	2.5 (0.10)	80	33.2 (4820)	26.08 (6.89)
OM160	6.35 (0.25)	1.25 (0.05)	80	3.9 (560)	48.45 (12.80)
OM161	6.35 (0.25)	0.25 (0.01)	80	13.8 (2000)	46.29 (12.23)
OM162	6.35 (0.25)	1.25 (0.05)	80	29.0 (4200)	32.89 (8.69)

Table 7. Opening pressures of six flaws as a function of separating ligament size for paired 6.35- and 12.7-mm (0.25- and 0.50-in.)-long interacting circumferentially shifted axial notches, all 80% TW.

Specimen No.	Individual Notch Length, mm (in.)		Ligament Size, mm (in.)		Opening Pressure, MPa (psi)	
OM161	6.35	(0.25)	0.25	(0.01)	28.3	(4100)
OM162	6.35	(0.25)	1.27	(0.05)	31.4	(4560)
OM159	6.35	(0.25)	2.54	(0.10)	34.8	(5050)
OM150	12.7	(0.50)	0.25	(0.01)	19.0	(2760)
OM151	12.7	(0.50)	1.27	(0.05)	23.0	(3340)
OM152	12.7	(0.50)	2.5	(0.10)	23.5	(3405)

flaws of 6.35- and 12.7-mm length, which are 34.5 and 20.7 MPa (5000 and 3000 psi), respectively.

4.2.2.3 Pressurization of Flaws to Obtain Specified Openings

The Paul Sherrer Institute (PSI) of Switzerland requested that ANL produce axial-fish-mouth flaw openings of specified sizes in Type 304 stainless steel (SS) tubes for subsequent testing at the Institute. Although only three fish-mouth specimens were needed, PSI provided 10 tubes to permit experimentation in developing the appropriate production technique. Each of the tubes had an OD of 18.8 mm (0.741 in.) and an ID of 16.6 mm (0.655 in.) and contained 100% TW EDM notches of three different lengths and of initial 0.20-mm (0.0075-in.) width. Four of these ten tubes had a notch length of 20 mm (0.8 in.), three had a length of 33 mm (1.3 in.), and three had a length of 48 mm (1.9 in.). ANL was to expand these flaw openings to maximum widths of 10, 5.6, and 4.4 mm (0.4, 0.22, and 0.17 in.), respectively, by internal pressurization.

The Room-Temperature High-Pressure Test Facility was selected for the production of these tubes. Models previously developed to predict the crack opening and failure behaviors of Alloy 600 steam generator tubes were used to calculate the pressures needed to achieve the desired crack openings, as well as the pressures at which the flaws would undergo unstable burst. Yield and tensile strength values provided by PSI were used to calculate the flow stress of the Type 304 SS needed for the models. Initial calculations indicated that the production of the desired 10-mm (0.4-in.) notch opening in the specimens with the 20-mm (0.8-in.)-long notch would be the most difficult, since the calculated pressure for the desired crack opening was predicted to be essentially identical to the unstable burst pressure.

A preliminary pressurization test to unstable burst was then conducted on one of the tubes with a 20-mm (0.8-in.)-long notch. Based on the results of this test, the flow stress value was adjusted, and new values were calculated for the crack opening and burst pressures. The results of these calculations are shown in Fig. 65. As indicated in the figure, the calculated

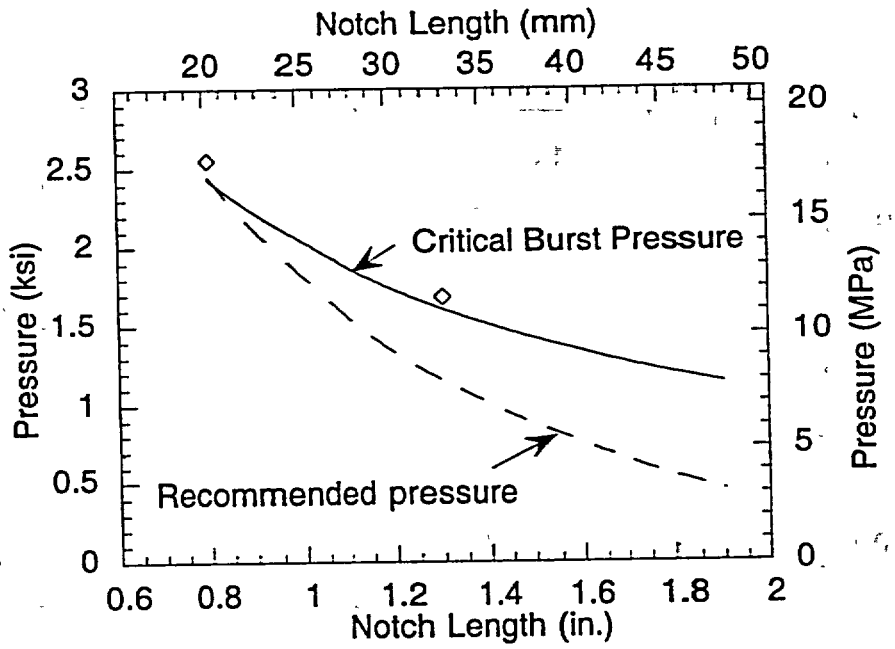

Fig. 65. Calculated recommended pressures and unstable burst pressures for the PSI tubes. Symbols denote tests in which unstable tearing or burst occurred.

internal pressure of 16.9 MPa (2.45 ksi) to achieve the desired flaw opening is actually slightly greater than the calculated critical burst pressure of 16.8 MPa (2.43 ksi) for the tubes containing the 20-mm (0.8-in.)-long notch, a result suggested by the preliminary calculations described above. For the longer flaw lengths of 33 and 48 mm (1.3 and 1.9 in.), the internal pressures required for the desired flaw openings were calculated to be 7.9 and 3.1 MPa (1.15 and 0.45 ksi), respectively, as compared to the calculated unstable burst pressures of 11.0 and 7.9 MPa (1.60 and 1.14 ksi).

The pressurization tests were carried out using internal bladders to prevent excessive leakage through the flaw and reinforcing circumferential brass foils, typically extending 270° around the circumference, to prevent extrusion of the bladder through the flaw opening during pressurization. The foils added significant stiffness to the cracks, particularly at low pressures. The loading started with pressurization at a nominal rate of 4.1 MPa/s (600 psi/s) up to ≈1.4 MPa (200 psi) less than that predicted for the desired flaw opening, followed by a hold time of 30-s at this pressure, during which the flaw opening was visually monitored. The pressure was then increased in increments of 70-140 kPa (10 to 20 psi) with interspersed 30 s hold times until the desired flaw opening was obtained. The flaw opening was commonly observed to gradually increase during the hold periods.

Figure 66 shows that the calculated curves for crack opening displacements (CODs) were in reasonable agreement with test data for the 20.3- and 33.0-mm (0.8- and 1.3-in.)-long notches. The COD for the 48.3-mm (1.9-in.)-long notch was significantly overestimated. However, since the COD vs. pressure curves are fairly steep for all three notches, the final pressures recommended were quite close to the actual pressures applied during the tests. The failure pressures for a couple of tests that were inadvertently pressurized to failure are in good

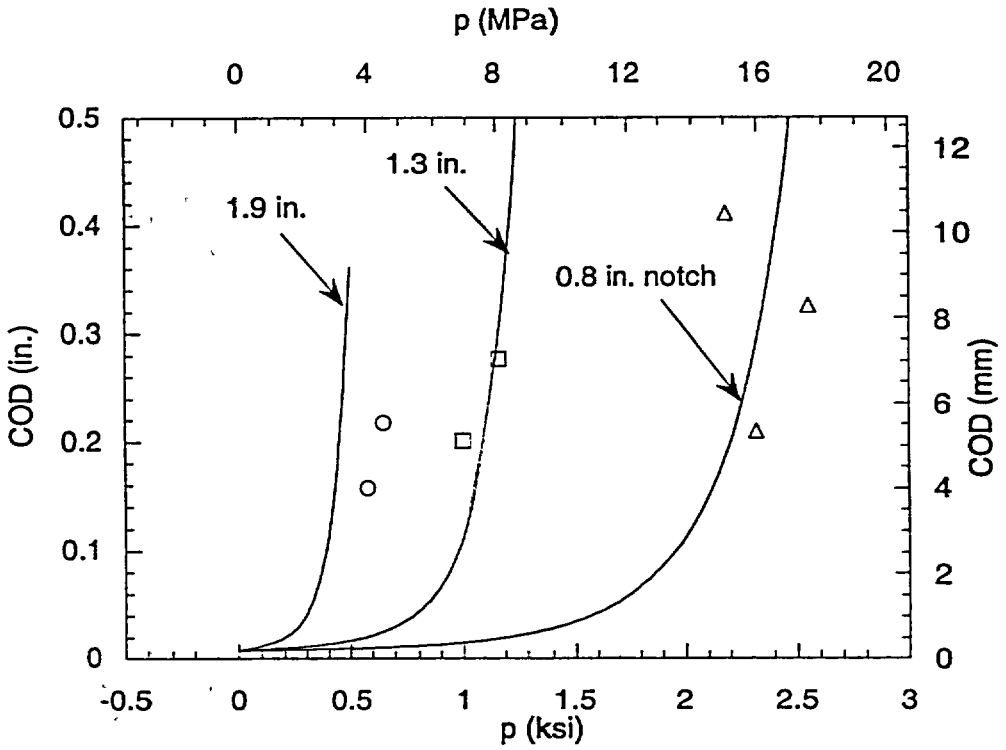

Fig. 66. Calculated variations of crack opening displacements with pressure. Symbols denote measured COD values after the tests.

agreement with predictions (Fig. 65). Overall, the target values for notch width were met within reasonable limits (Table 8). Figures 67-69 show post-test photographs of the opened flaws for each of the three notch lengths.

4.2.3 Summary of Results

A series of pressure and leak-rate tests was conducted on 22.2-mm (7/8-in.)-diameter Alloy 600 steam generator tubes having axial EDM notches of various lengths and depths. These tests were conducted at room temperature in the High-Pressure Test Facility and at room and elevated temperatures in the Pressure and Leak-Rate Test Facility. In addition, a series of pressurization experiments using the High-Pressure Test Facility was performed on Type 304 SS tubes with throughwall axial EDM notches of three different lengths to produce flaw openings of prescribed sizes. Internal bladders and foils were used in some of the specimens with throughwall notches tested in the room-temperature High-Pressure Test Facility to avoid leak rates in excess of the flow capacity of the facility. Foils and bladders were not required for specimens tested in the Pressure and Leak-Rate Test Facility because of its much higher flow capacity.

The results of these tests may be summarized as follows:

Table 8. Flaw opening widths and internal pressures for PSI tubes.

Test No.	Notch Length, mm (in.)	Crack Opening Displacement, mm (in.)		Internal Pressure,[a] MPa (ksi)		Remarks
		Target	Actual	Calculated	Actual	
1	20 (0.8)	-	-	16.8[b] (2.43)	17.6 (2.55)	Intentionally pressurized to unstable burst
2	20 (0.8)	10.0 (0.4)	8.3 (0.326)	16.9 (2.45)	17.6 (2.55)	Slight tearing
3	20 (0.8)	10.0 (0.4)	5.3 (0.210)	16.9 (2.45)	16.0 (2.32)	
4	20 (0.8)	10.0 (0.4)	10.4 (0.411)	16.9 (2.45)	15.0 2.18	Slight tearing
5	33 (1.3)	5.6 (0.22)	-	7.9 (1.15)	11.6[c] (1.68)	Inadvertently tested to large unstable tearing
6	33 (1.3)	5.6 (0.22)	7.0 (0.277)	7.9 (1.15)	8.1 (1.17)	
7	33 (1.3)	5.6 (0.22)	5.1 (0.201)	7.9 (1.15)	6.9 (1.00)	
8	48 (1.9)	4.4 (0.17)	5.5 (0.218)	3.1 (0.45)	4.5 (0.65)	
9	48 (1.9)	4.4 (0.17)	4.0 (0.158)	3.1 (0.45)	4.0 (0.58)	
10	48 (1.9)	4.4 (0.17)	-	3.1 (0.45)	-	Not tested

[a]Calculated internal pressure to produce target COD and actual internal pressure applied to produce observed COD.

[b]Calculated internal pressure required to produce unstable burst.

[c]Actual internal pressure applied to produce inadvertent unstable burst.

1. Flow rates through as-machined 0.19-mm (0.0075-in.)-wide notches or notches widely opened after testing could again be accurately predicted by using the orifice correlation equation with an orifice coefficient of 0.6. For specimens in which bulging occurs in the region of failure, accurate predictions require that this bulging be taken into account when calculating the opening area.

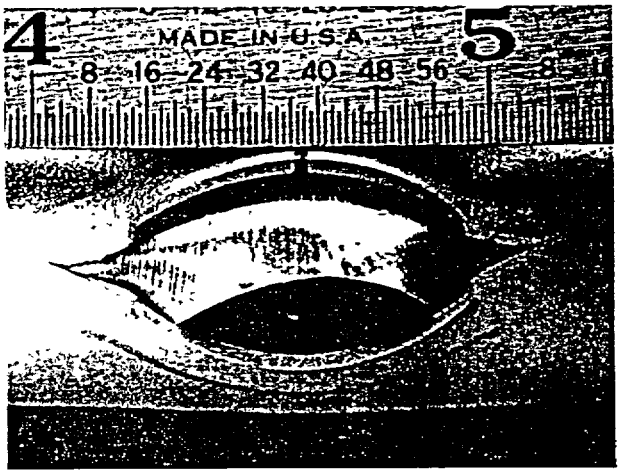

Figure 67. Post-test photo of tube from Test 4 with a 20-mm (0.8-in.)-long notch.

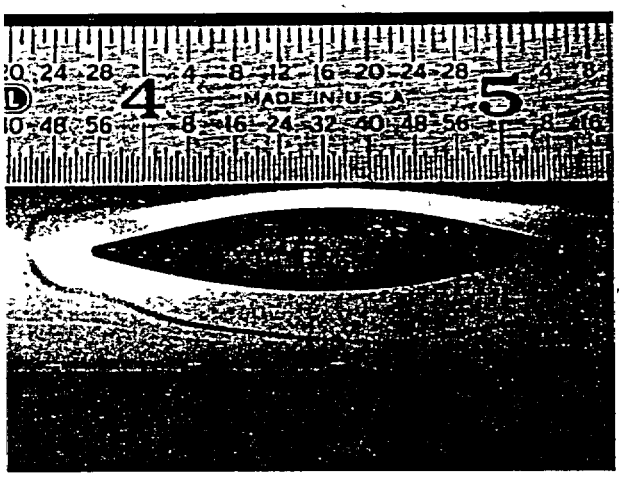

Figure 68. Post-test photo of tube from Test 7 with a 33-mm (1.3-in.)-long notch.

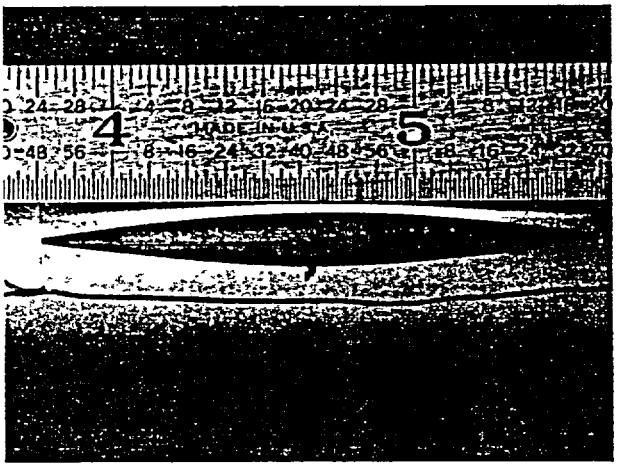

Figure 69. Post-test photo of tube from Test 9 with a 48-mm (1.9-in.)-long notch.

1.

2. The sudden opening of notches of length ≥25 mm (1 in.) with flow rates of several liters per minute could again create sufficient lateral thrust to bend tubes supported at one end.

3. The internal pressures at which ligament tearing and catastrophic failure (burst) occur can be predicted reasonably well for single, axial, part-throughwall notches with lengths ≥12.7 mm (0.5 in.) using a ligament-tearing model previously developed at ANL.[1] However, accurate knowledge of the flaw profile and the material flow stress is required to successfully apply the model. The model tends to underpredict the tearing and failure pressures for notches 6.35 mm (0.25 in.) in length.

4. The pressure at which initial flaw tearing occurs for tubes with part-throughwall flaws, as well as the unstable burst pressure, generally increases somewhat with increasing pressurization rate. The extent of flaw tearing also tends to increase with increasing pressurization rate. The flaw tearing and burst pressures calculated using the ANL ligament tearing model generally agree most closely with the values experimentally observed under quasi-static pressurization conditions, and testing under these conditions is generally preferred to avoid rate effects.

5. Testing of tubes with throughwall flaws without internal bladders and reinforcing foils is preferred whenever possible. Where this is not possible, the tubes should be tested in two stages: the tube is first pressurized to the point of initial flaw opening without a bladder and then further pressurized to unstable burst with an internal bladder and foil, if necessary. A quasi-static pressurization rate is recommended for the first stage of testing, and a rate of ≤7 MPa/s (1000 psi/s) for the second stage.

6. Where the above-described two-state testing is not possible, a 3.2-mm (1/8-in.)-thick Tygon internal bladder and 0.13-mm (0.005-in.)-thick brass foil yield satisfactory test results. The foil should be lubricated and extend no more than 6.35 mm (0.25 in.) beyond the flaw extremities.

7. Tubes containing multiple interacting flaws typically fail in a complex manner, depending upon the precise flaw geometry, and these failures cannot, in general, be analytically predicted. For the specific case of two aligned part-throughwall notches separated by a full-wall-thickness ligament, the strengthening effect of the ligament decreases with decreasing ligament length, as expected, and at sufficiently short ligament lengths, the composite flaw essentially behaves as a single notch. This behavior can be analytically predicted reasonably well.

8. Ten Type 304 SS tubes with throughwall axial EDM notches of three lengths were successfully internally pressurized using the High-Pressure Test Facility to produce flaw openings of specified sizes. After an initial experiment on one tube to determine the flow stress of the material, the required internal pressures to produce the desired flaw openings in the remaining nine tubes were successfully calculated to within reasonable accuracy.

4.3 Laser-Cut Notches

The information reported in this section resulted from testing complex interacting laser-cut flaws in the room-temperature High-Pressure Test Facility. These data complement results reported in Sections 4.2.1.2 (Pressure and Leak-Rate Test Facility) and 4.2.2.2 (High-Pressure Test Facility) from tests on EDM flaws involving two interacting axial aligned or unaligned flaws with separating ligaments of various sizes.

The present tests were performed on twenty-four 22.2-mm (7/8-in.)-diameter Alloy 600 tubes with a variety of laser-cut OD flaws consisting of simple single axial and circumferential notches, as well as complex OD patterns of axial and circumferential notches separated by various ligament sizes. Ten generic flaw geometries were tested. The laser-cutting technique permits considerably more complex flaws to be fabricated than are possible using EDM. These complex flaws are intended to more closely simulate the flaw patterns actually present in field-degraded tubes. The laser-cut flaws are also considerably tighter than the minimum 0.19-mm (0.0075-in.)-wide notches that can be achieved by EDM, and this flaw tightness may influence tube ligament tearing and unstable burst pressure behaviors.

The 24 laser-cut flaws were tested in two stages. The first stage consisted of pressurizing at a quasi-steady-state rate without the use of internal bladders. The pressurization protocol consisted of starting at an internal pressure of 0.34 MPa (50 psi) and increasing the pressure in 0.69 MPa (100 psi) increments after a 10-s dwell at each pressure plateau. This process continued until ligament tearing occurred, accompanied by an abrupt increase in flow. Data were thus obtained on the pressure at first ligament tearing, as well as the flow rate and sustainable pressure observed upon ligament tearing. Posttest photographs of the flaw opening yield information on flaw area, which is used to validate predictions from structural code analyses and from the Argonne sharp-edge orifice flow model.[1]

The second stage of testing generated unstable burst pressure data by re-testing the flaws that exhibited only stable ligament tearing and opening in the first-stage tests. Excessive leakage through the flaws was prevented by using an internal bladder with a foil backup, if necessary, to prevent bladder wedging in the flaw opening. For tubes with complex flaws, the two-stage testing permitted an evaluation of the ligament tearing sequence that takes place as the flaw opens. It also permitted both the unstable burst and the stable ligament tearing pressures to be determined for flaws that do not immediately go unstable. If the testing had been conducted using only internal bladders and rapid pressurization rates (i.e., no Stage 1 testing), data on stable ligament tearing would not have been obtained.

The results from the 24 Stage 1 tests are summarized in Table 9, and the detailed configurations of the ten laser-notched specimen types tested are shown in Fig. 70. Pre- and posttest photographs of representative flaws of the ten types are shown in Figs. 71-80. The ten generic flaw geometries tested are indicated in the second column in Table 9 and are shown in the pre-test photographs of Figs. 71-80. Table 9 gives the nominal flaw dimensions and the nominal sizes of ligaments separating the multiple notches of the more complex flaws. Table 9 also gives pre-test estimates from EC

Table 9. Results from Stage 1 testing (without bladders and quasi-steady pressurization) of flawed tubes containing OD laser-cut notches. All notches had nominal depths of 80% TW except for Specimens 5528-3-3 and 5469-2-2, which had nominal depths of 40% TW. All tubes leaked water through laser burn pinholes at the ends of the laser-cut notches at 0.34 MPa (50 psi) except Specimen 5528-2-2.

Specimen Number	Flaw Type	Number of Notches	NDE Flaw Depth, % TW	Nominal Flaw Length, mm (in.)	Ligament Width, mm (in.)	Max. Pressure at Ligament Tearing, MPa (psi)	Sust. Pressure after Ligament Tearing, MPa (psi)	Flow Rate after Ligament Tearing, L/min (gpm)
5528-1-1	1	1	75	6.35 (0.25)	NA	36.6 (5310)	36.5 (5300)	18.1 (4.78)
5528-1-2	1	1	74	6.35 (0.25)	NA	37.1 (5380)	37.0 (5360)	13.8 (3.65)
5528-1-3	1	1	76	8.89) (0.35	NA	31.7 (4600)	29.8 (4320)	32.6 (8.6)
5528-1-4	1	1	73	8.89) (0.35	NA	32.4 (4700)	31.2 (4530)	30.5 (8.05)
5528-2-1	1	1	69	12.7 (0.5)	NA	34.5 (5000)	3.5 (500)	48.1 (12.7)
5528-2-2	1	1	61	12.7 (0.5)	NA	38.6[a] (5600)[a]	1.4 (200)	48.4 (12.8)
5516-4-3	2	2	72	12.7 (0.5)	0.25 (0.01)	33.8 (4900)	7.2 (1040)	48.1 (12.7)
5516-4-2	2	2	70	12.7 (0.5)	0.13 (0.005)	33.8 (4900)	6.5 (940)	48.1 (12.7)
5528-3-1	3	6	70	12.7 (0.5)	0.13 (0.005)	29.0 (4200)	10.7 (1550)	48.1 (12.7)
5528-3-2	3	6	73	12.7 (0.5)	0.25 (0.01)	30.0 (4350)	8.5 (1240)	48.1 (12.7)
5528-3-3[b]	3	6	61	12.7 (0.5)	0.25 (0.01)	35.2 (5100)	3.7 (540)	48.4 (12.8)
5528-3-4	4	6	76	12.7 (0.5)	0.13 (0.005)	35.9 (5200)	2.7 (390)	48.4 (12.8)
5469-2-1	4	6	74	12.7 (0.5)	0.25 (0.01)	32.8 (4750)	6.0 (870)	48.4 (12.8)
5469-2-2[b]	4	6	60	12.7 (0.5)	0.25 (0.01)	37.6 (5450)	3.8 (550)	48.4 (12.8)
5469-2-3	5	6	79	12.7 (0.5)	0.25 (0.01)	33.5 (4860)	2.1 (800)	48.4 (12.8)
5469-2-4	5	6	78	12.7 (0.5)	0.51 (0.02)	39.3[a] (5700)[a]	1.0 (150)	48.4 (12.8)

[a]Specimen exhibited unstable tearing without internal bladder.
[b]Laser-cut notches had nominal depths of 40% TW.

Table 9. (Cont'd.)

Specimen Number	Flaw Type	Number of Notches	NDE Flaw Depth, (% TW)	Nominal Flaw Length, mm (in.)	Ligament Width, mm (in.)	Max. Pressure at Ligament Tearing, MPa (psi)	Sust. Pressure after Ligament Tearing, MPa (psi)	Flow Rate after Ligament Tearing, L/min (gpm)
5469-3-1	6	6	80	12.7 (0.5)	0.25 (0.01)	28.3 (4110)	13.3 (1930)	46.9 (12.4)
5531-3-1	6	6	79	12.7 (0.5)	0.51 (0.02)	34.3 (4980)	5.2 (760)	48.4 (12.8)
5469-3-3	7	2	75	c	0.13 (0.005)	51.4 (7450)	0.4 (60)	49.2 (12.99)
5469-3-4	7	2	74	c	0.25 (0.01)	51.7 (7500)	did not fail	did not fail
5469-4-1	8	6	70	c	0.13 (0.005)	39.2 (5680)	0.3 (50)	48.8 (12.9)
5469-4-2	8	6	70	c	0.25 (0.01)	38.3 (5550)	0.3 (50)	48.8 (12.9)
5469-4-3	9	2	69	d	NA	30.8 (4475)	0.7 (100)	48.8 (12.9)
5469-4-4	10	2	72	d	NA	31.3 (4540)	0.7 (100)	48.8 (12.9)

[a]Specimen exhibited unstable tearing without internal bladder.
[b]Laser-cut notches had nominal depths of 40% TW.
[c]Circumferential notch 360°.
[d]Circumferential notch 360°; axial notch 12.7 mm (0.5 in.).

analysis of the maximum flaw depth. All of the laser-cut flaws exhibited pinhole laser burn-through at the ends of each notch. These pinholes were too small to be detected by EC techniques, but they leaked water at 0.34 MPa (50 psi). At a pressure of 6.9 MPa (1000 psi), the leak rate through these pinholes was typically in the range of 0.04-0.4 L/min (0.01-0.1 gpm or 14.4-144 gal per day).

The six Type 1 flaws (Fig. 70) were simple single axial notches of three lengths (6.35, 8.9, and 12.7 mm [0.25, 0.35, 0.5-in.]) and all were nominally 80% TW. Duplicate tests of each of the three flaw lengths were conducted to check on test reproducibility. Figure 71 shows the pre- and posttest flaw photographs for Specimen 5528-2-1, which had a 12.7-mm (0.5-in.)-long axial notch. The posttest photograph shows that the ligament has torn completely, but that no unstable tearing has occurred at the notch ends. As shown in Table 9, the ligament tore open at 34.4 MPa (5000 psi) and that the sustained pressure and flow rate after opening were 3.4 MPa (500 psi) and 48.1 L/min (12.7 gpm), respectively. The observed flow rate was near the maximum facility capacity of 48.8 L/min (12.8 gpm). These data can be used to calculate a flaw

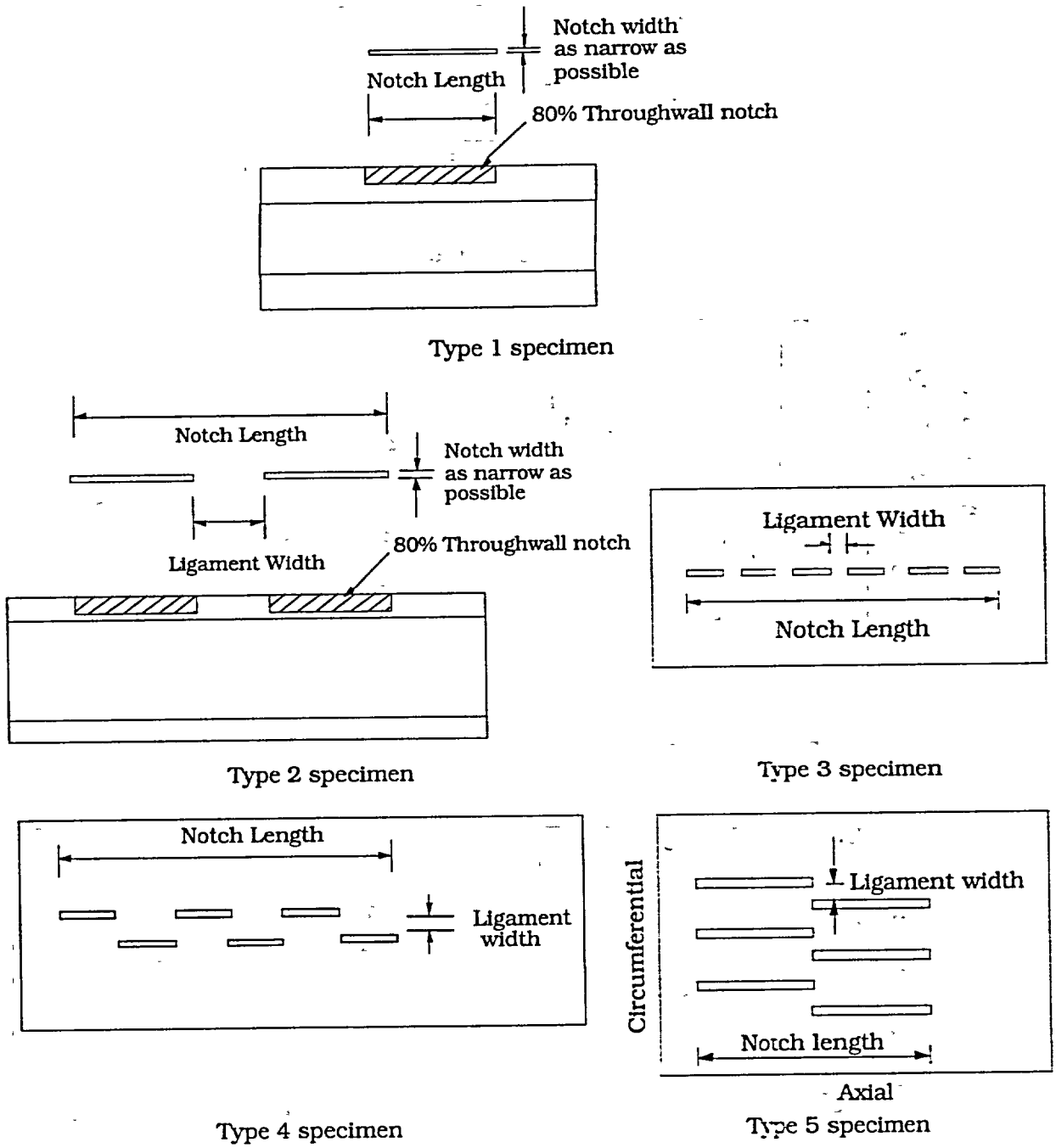

Figure 70. Configurations of notches in various types of laser-cut tube specimens.

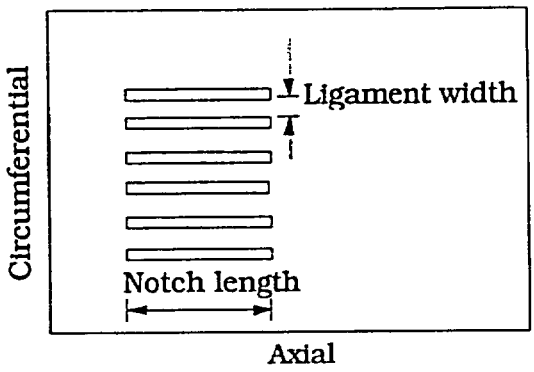

Type 6 specimen

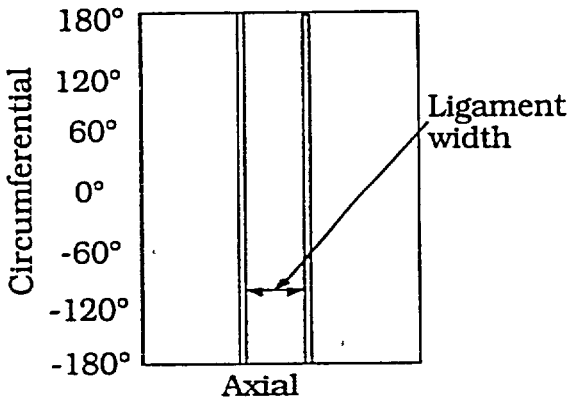

Type 7 specimen

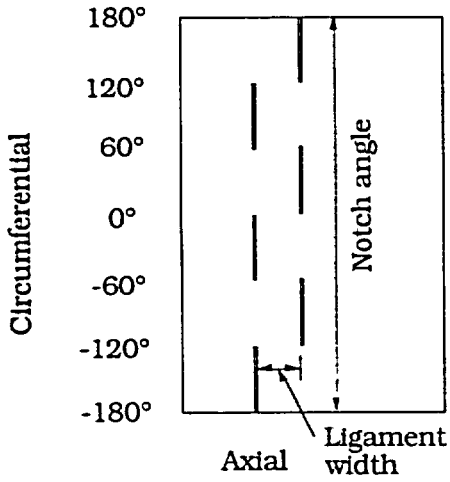

Type 8 specimen

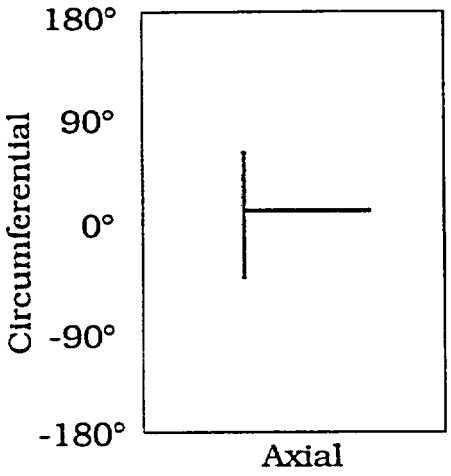

Type 9 specimen

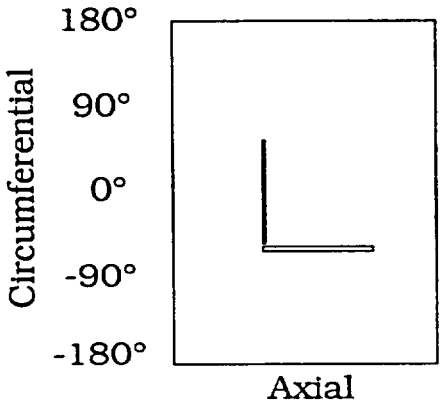

Type 10 specimen

Figure 70. Configurations of notches in various types of laser-cut tube specimens (cont'd.).

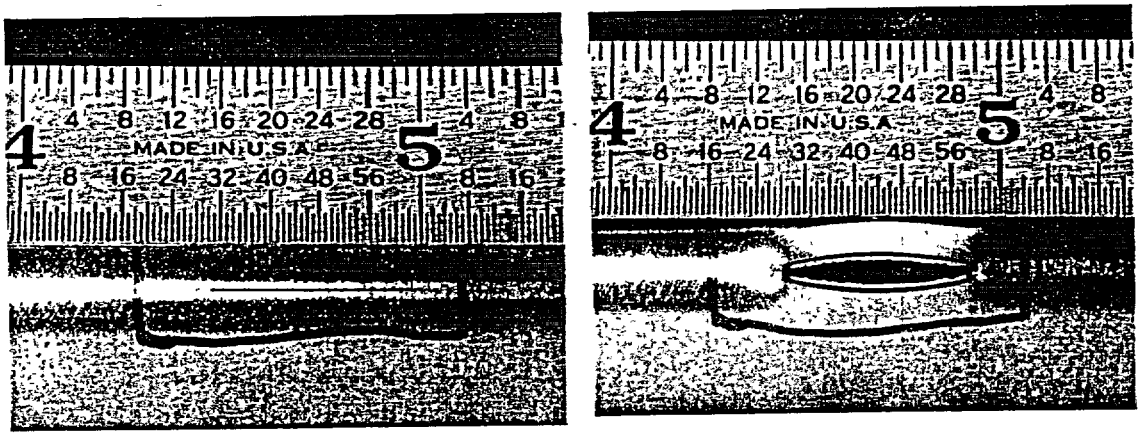

Figure 71. Appearance of Specimen 5528-2-1 with Type 1 flaw before (left) and after (right) Stage 1 testing

opening area, which can then be checked by actual measurement. The duplicate tests indicated reasonable reproducibility of the ligament tear pressure, with the observed variation for the 12.7-mm (0.5-in.)-long flaws believed to be due to differences in actual flaw depth for the two tubes, based on NDE data.

The two Type 2 flaws (Fig. 70) consisted of two aligned axial notches each 6.35 mm (0.25 in.) in length and 80% TW, separated by a complete wall thickness ligament of length 0.25 or 0.13 mm (0.010 or 0.005-in.). Figure 72 shows the pre- and posttest flaw appearances of Specimen 5516-4-3, which had the 0.25-mm (0.010-in.)-long ligament. The posttest photograph indicates no unstable tearing at the notch ends and shows that the ligament between the two notches, as well as the ligaments at the bottom of each notch, have torn. During testing, progressive sequential tearing was not evident; both types of ligaments tore simultaneously at 33.8 MPa (4900 psi).

The three Type 3 flaws (Fig. 70) consisted of six aligned equal-length axial notches separated by complete wall thickness ligaments. The total length of the composite flaw (notches plus ligaments) was 12.7 mm (0.5 in.). For two of the tubes, the flaws were 80% TW, and the interspersed ligaments were 0.13 or 0.25 mm (0.005 or 0.010 in.) in length. For the third tube, the six notches were only 40% TW, and the interspersed ligaments were 0.25-mm (0.010-in.) long. Figure 73 shows the pre- and posttest appearances of Specimen 5528-3-3, which had the 40% TW flaw depth. The posttest photograph indicates no unstable tearing at the notch ends and shows that the ligaments between the notches and the ligaments at the bottom of each notch have torn. Again, all of the ligaments tore simultaneously at the failure pressure of 35.2 MPa (5100 psi). For this type of flaw and the dimensions tested, the length of the ligaments separating the notches had little influence on failure pressure, but the depth of the notches exerted a noticeable influence.

The three Type 4 flaws (Fig. 70) consisted of six nonaligned side-step axial notches of equal length in two axial rows of three aligned flaws, each separated by complete wall thickness ligaments. The overall length of the composite flaw was 12.7 mm (0.5 in.). In two of the three tubes, the individual notches were 80% TW, and the interspersed

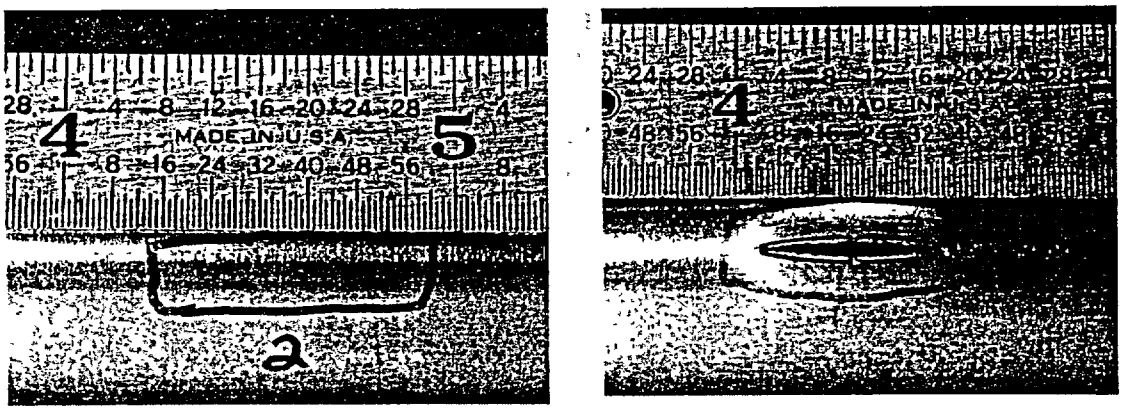

Figure 72. Appearance of Specimen 5516-4-3 with Type 2 flaw before (left) and after (right) Stage 1 testing.

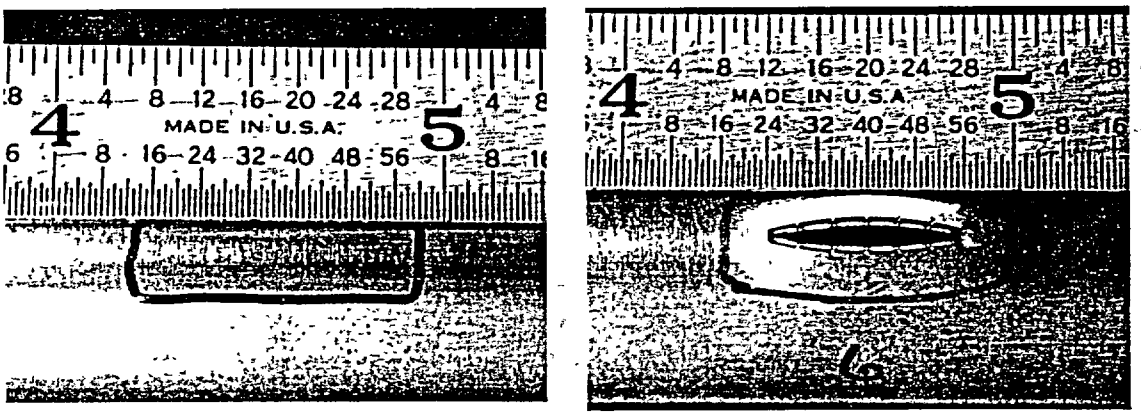

Figure 73. Appearance of Specimen 5528-3-3 with Type 3 flaw before (left) and after (right) Stage 1 testing.

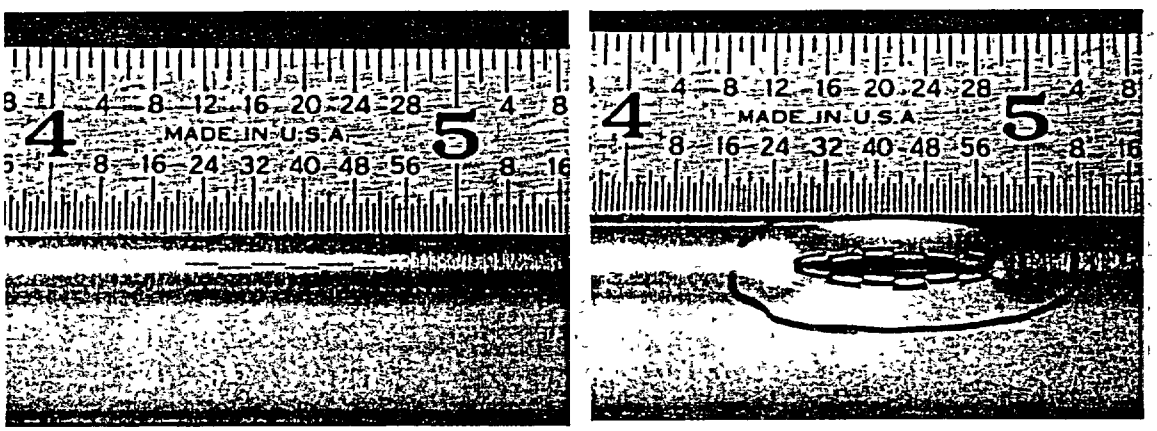

Figure 74. Appearance of Specimen 5469-2-2 with Type 4 flaw before (left) and after (right) Stage 1 testing.

ligaments were 0.13 or 0.25 mm (0.005 or 0.010 in.) in length. In the third tube, the individual notches were only 40% TW, and the interspersed ligaments were 0.25-mm (0.010-in.) long. Figure 74 shows the pre- and posttest flaw appearances of Specimen 5469-2-2, which had the 40% TW flaw depth. The posttest photograph indicates no unstable tearing at the notch ends and shows that the ligaments between the notches and the ligaments at the bottom of each notch have torn. Again, all of the ligaments tore simultaneously at the failure pressure of 37.6 MPa (5450 psi), and the depth of the notches exerted a stronger influence on the failure pressure than did the length of the interspersed ligaments.

The two Type 5 flaws (Fig. 70) were made up of six individual notches of equal length in two parallel offset rows of three notches each. The laser-cut notches in both specimens were 80% TW, and the ligament lengths were either 0.25 or 0.51 mm (0.010 or 0.020 in.). Figure 75 shows the pre- and posttest appearances of Specimen 5469-2-4, which had the 0.51-mm (0.020-in.) ligaments. The posttest photograph shows that ligament tearing occurred along only one of the unaligned axial rows and that, in contrast to the previous tests, unstable tearing also occurred at the flaw ends. This unstable tearing occurred without the use of an internal bladder. No indication of progressive sequential tearing was evident during testing; all ligaments tore simultaneously at 39.3 MPa (5700 psi). The other flaw of this type (Specimen 5469-2-3) with the thinner 0.25-mm ligament between notches did not tear unstably, and it opened at the considerably lower pressure of 33.5 MPa (4860 psi).

The two Type 6 flaws (Fig. 70) consisted of six axial parallel notches of equal 12.7-mm (0.50-in.) length and 80% TW depth with ligament widths of 0.25 or 0.51 mm (0.010 or 0.020 in.) (Table 9). Figure 76 shows the pre- and posttest flaw photographs for Specimen 5531-3-1, which had the 0.51-mm (0.020-in.)-long ligaments. The posttest photograph shows that ligament tearing occurred in only one of the parallel notches and that no unstable tearing occurred at the notch ends. The flaw tore open at 34.3 MPa (4980 psi). The other flaw of this type (Specimen 5469-3-1) with the thinner 0.25-mm (0.010-in.)-long ligament between the notches behaved similarly but opened at the considerably lower pressure of 28.3 MPa (4110 psi).

The two Type 7 flaws (Fig. 70) consisted of two parallel 360° continuous circumferential notches of 80% TW depth separated by ligament widths of 0.13 or 0.25 mm (0.005 and 0.010 in.). Figure 77 shows the pre- and posttest appearances of Specimen 5469-3-3, which had the thinner 0.13-mm (0.005-in.) ligament. The posttest photograph shows that ligament tearing occurred around the entire tube circumference, resulting in complete separation of the tube into two pieces. Failure occurred at 51.4 MPa (7450 psi), which is near the maximum (53.1 MPa [7700 psi]) operating pressure of the facility. The other flaw of this type (Specimen 5469-3-4), but having the thicker 0.25-mm (0.010 in.) ligament, could not be opened at the maximum facility pressure.

The two Type 8 flaws (Fig. 70) consisted of six equal-length circumferential notches of 80% TW depth in two circumferential parallel rows having three notches each, separated by ligament widths of 0.13 or 0.25 mm (0.005 or 0.010 in.). Figure 78 shows the pre- and posttest appearances of Specimen 5469-4-1, which had the thicker 0.25-mm (0.010-in.) ligament. The posttest photograph shows that ligament tearing

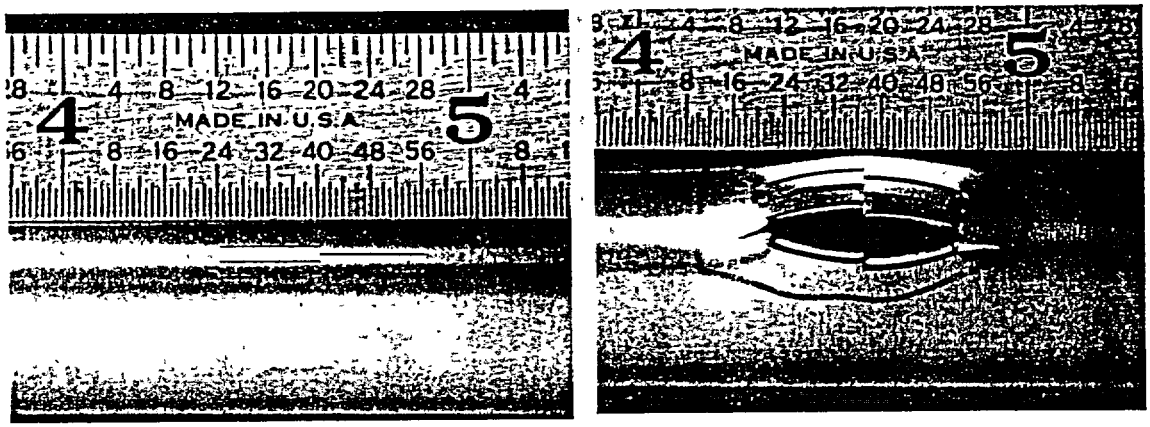

Figure 75. Appearance of Specimen 5469-2-4 with Type 5 flaw before (left) and after (right) Stage 1 testing

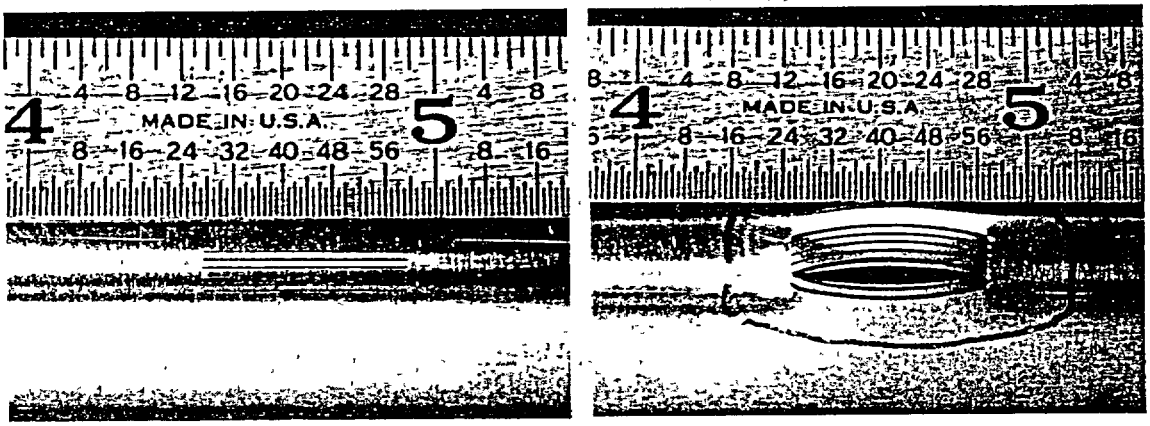

Figure 76. Appearance of Specimen 5531-3-1 with Type 6 flaw before (left) and after (right) Stage 1 testing.

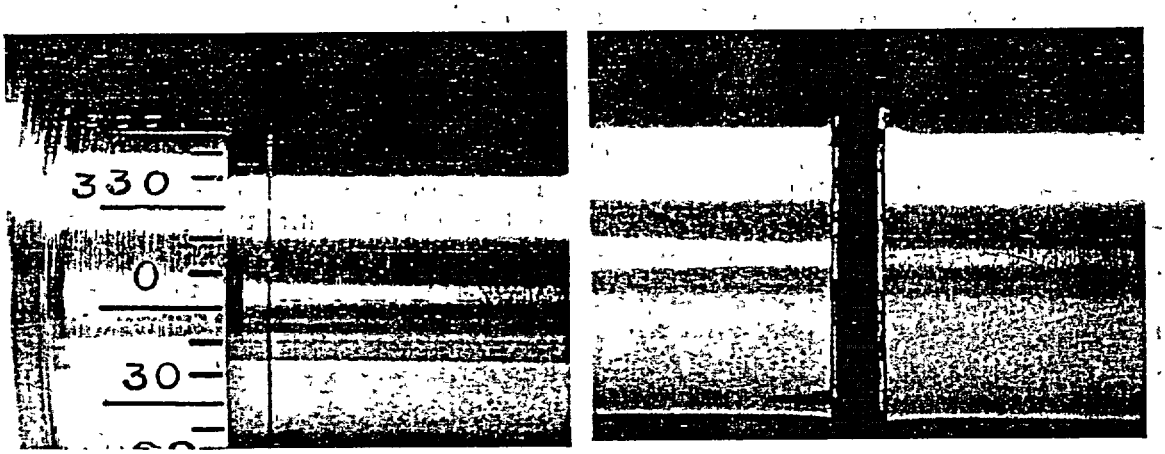

Figure 77 Appearance of Specimen 5469-3-3 with Type 7 flaw before (left) and after (right) Stage 1 testing

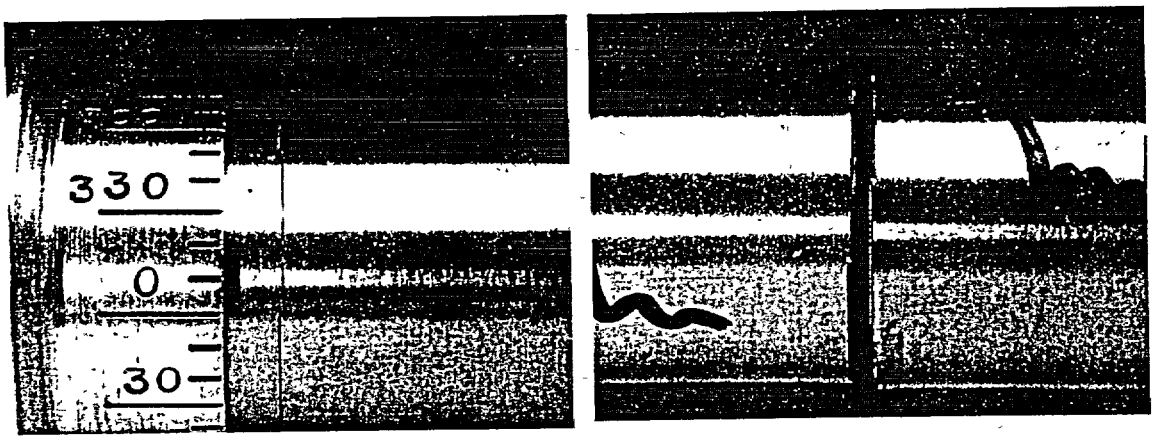

Figure 78 Appearance of Specimen 5469-4-1 with Type 8 flaw before (left) and after (right) Stage 1 testing.

occurred around the entire tube circumference, resulting in complete separation of the tube into two pieces. Failure occurred at 39.2 (5680 psi). The other flaw of this type (Specimen 5469-4-2) with the thinner 0.13-mm (0.005-in.) ligament opened at the slightly lower pressure of 38.3 MPa (5550 psi).

The single Type 9 flaw (Fig. 70) consisted of two intersecting notches, one extending 180° around the circumference and the second perpendicular notch extending 12.7 mm (0.5 in.) in the axial direction. The two notches were 80% TW and formed a tee. Figure 79 shows the pre- and posttest appearances of Specimen 5469-4-3. The posttest photograph shows that ligament tearing occurred primarily along the 12.7-mm (0.5-in.)-long axial notch and only slightly along the circumferential notch. The flaw tore open at 30.9 MPa (4475 psi).

The single Type 10 flaw (Fig. 70) consisted of two intersecting notches similar to those in the Type 9 flaw. However, the notches in the Type 10 flaw were configured to form an ell rather than a tee. Figure 80 shows the pre- and posttest appearances of Specimen 5469-4-4. The posttest photograph shows that ligament tearing again occurred primarily along the 12.7-mm (0.5-in.)-long axial notch and only slightly along the circumferential notch. The flaw tore open at 31.3 MPa (4540 psi), very near the failure pressure for the Type 9 flaw.

Most of the tubes from the 24-tube set were subjected to Stage 2 testing after the above Stage 1 tests. However, several tubes from Stage 1 were not capable of being tested under Stage 2. For example, Specimen 5528-2-2 exhibited unstable tearing in Stage 1 (without an internal bladder); its burst pressure is given in Table 9. Specimens 5528-2-1 and 5528-2-2 were destructively examined after Stage 1 testing to evaluate notch tear characteristics and the true depth of the laser cuts, and they could therefore not be tested in Stage 2. Finally, Specimens 5469-3-3, 5469-4-1, 5469-4-2, 5469-4-3, and 5469-4-4 exhibited such large flaw tear openings from Stage 1 testing that they could not be sealed adequately with a bladder and foil to be unstably burst in Stage 2. As shown in Table 10, the remaining 17 flaws were tested under Stage 2 and exhibited

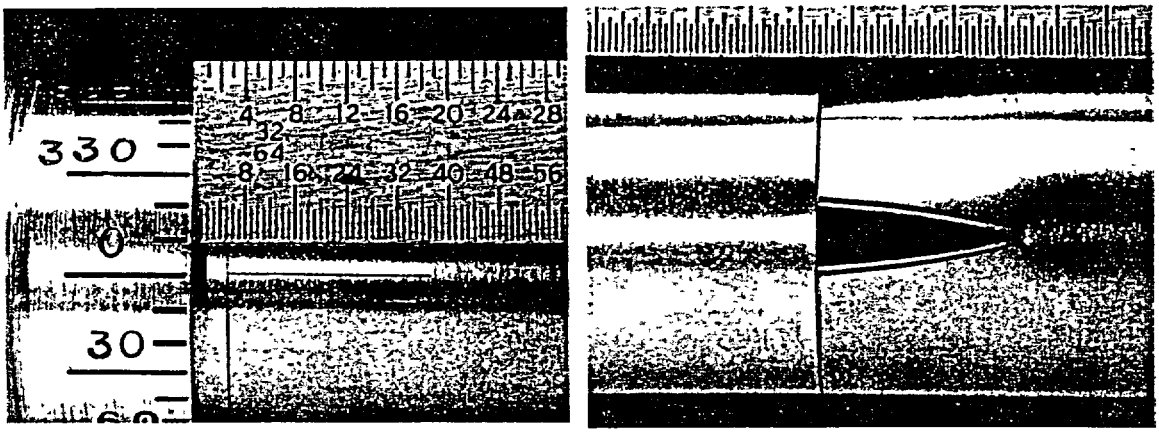

Figure 79. Appearance of Specimen 5469-4-3 with Type 9 flaw before (left) and after (right) Stage 1 testing.

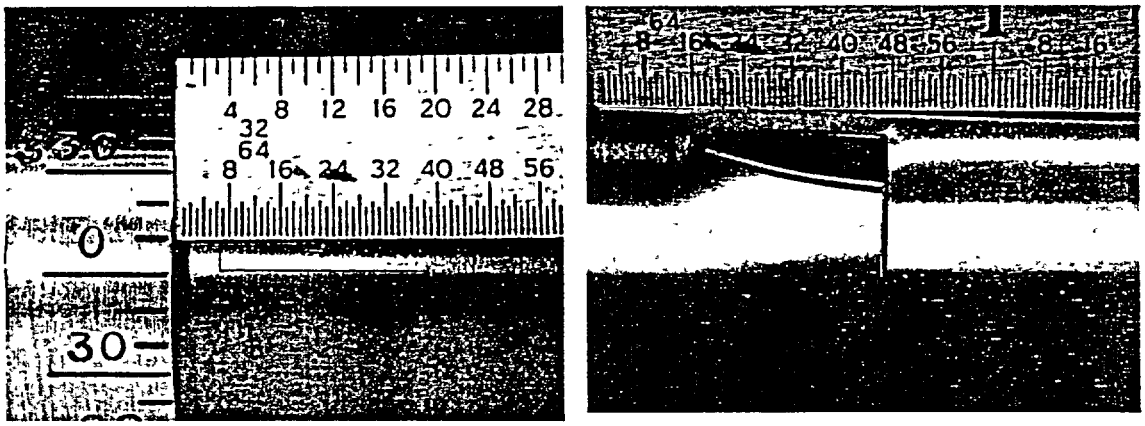

Figure 80. Appearance of Specimen 5469-4-4 with Type 10 flaw before (left) and after (right) Stage 1 testing.

unstable tearing or burst, except for Specimen 5469-3-4, which had a circumferential flaw that could not be opened at the maximum (53.1 MPa [7700 psi]) pressure of the facility. Post-Stage 2 test photographs of the flaws are shown in Figs. 81-85.

Initially, the Stage 2 tests were conducted with only a bladder (3.2-mm [1/8-in.]-thick Tygon tubing) and no foil backup. Seven tubes were tested in this fashion: Specimens 5528-1-1, 5528-1-2, 5528-1-3, 5528-1-4, 5518-3-1, 5516-4-2, and 5516-4-3. However, all flaws after this were tested with a similar bladder and a 0.13-mm (0.005-in.)-thick brass foil backup. Specimens 5516-4-3, 5516-4-2, and 5528-3-1 all had 12.7-mm (0.5-in.)-long notches and exhibited appreciable notch width opening after Stage 1 testing. Their burst pressures were very low during Stage 2 testing, and after testing, the bladders were found to be wedged in the opening, a phenomenon that can result in atypical reduced burst pressures. The reported burst data for these three specimens are thus incorrect, and backup foils were used in the remaining tests. The 6.35- and 8.9-mm (0.25- and 0.35-in.)-long single axial flaws tested with only a bladder

Table 10. Results from Stage 2 testing of flawed tubes containing OD laser-cut notches. All notches had characteristics that existed after Stage 1 testing (from Table 9).

Test Number	Flaw Type	Pressurization Rate, MPa/s (psi/s)	Burst (Yes/No)	Maximum Pressure, MPa (psi)
5528-1-1	1	12.6 (1823)	Y	41.2 (5980)
5528-1-2	1	13.9 (2023)	Y	40.3 (5850)
5528-1-3	1	12.9 (1865)	Y	33.4 (4850)
5528-1-4	1	14.4 (2084)	Y	32.1 (4660)
5528-2-1	1	No Stage 2	-	-
5528-2-2	1	No Stage 2	-	-
5516-4-3	2	12.4 (1802)	Y	26.6 (3865)
5516-4-2	2	13.0 (1929)	Y	27.9 (4040)
5528-3-1	3	12.8 (1850)	Y	26.4 (3825)
5528-3-2[a]	3	13.3 (1928)	Y	30.4 (4409)
5528-3-3[a,b]	3	10.0 (1450)	Y	28.6 (4146)
5528-3-4[a]	4	12.2 (1776)	Y	30.0 (4346)
5469-2-1[a]	4	13.4 (1950)	Y	31.9 (4630)
5469-2-2[a,b]	4	10.3 (1497)	Y	33.4 (4850)
5469-2-3[a]	5	13.3 (1925)	Y	32.2 (4669)
5469-2-4[a]	5	13.3 (1930)	Y	26.8 (3893)
5469-3-1[a]	6	13.5 (1953)	Y	32.2 (4675)
5531-3-1[a]	6	13.2 (1909)	Y	29.0 (4200)
5469-3-3	7	Stage1 opened	-	-
5469-3-4[c]	7	14.2 (2066)	N	53.1 (7700)
5469-4-1	8	Stage1 opened	-	-
5469-4-2	8	Stage1 opened	-	-
5469-4-3	9	Stage1 opened	-	-
5469-4-4	10	Stage1 opened	-	-

[a]Specimen tested in Stage 2 with internal bladder plus foil. All other Stage 2 tests were conducted with an internal bladder only, except for Specimen 5469-3-4, which was tested in Stage 2 with neither a bladder nor a foil.

[b]Specimen exhibited unstable tearing in Stage 1 testing without internal bladder.

[c]Specimen did not open in Stage 1 testing, and therefore was tested in Stage 2 with neither a bladder nor a foil. It did not fail at the maximum system pressure in Stage 2.

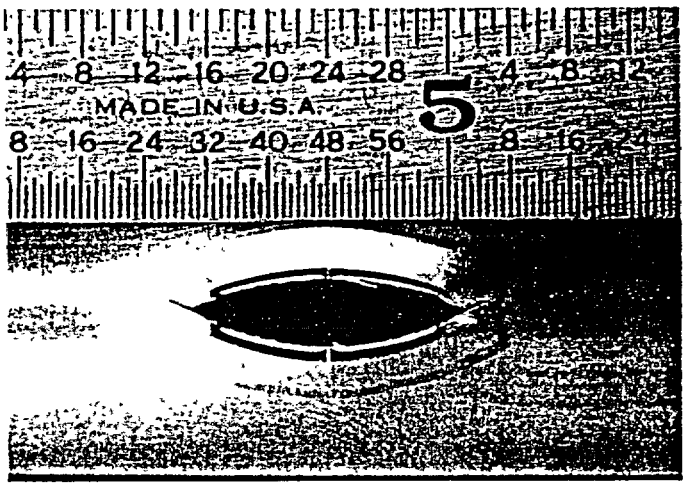

Figure 81. Appearance of Specimen 5516-4-3 with Type 2 flaw after Stage 2 burst testing with bladder.

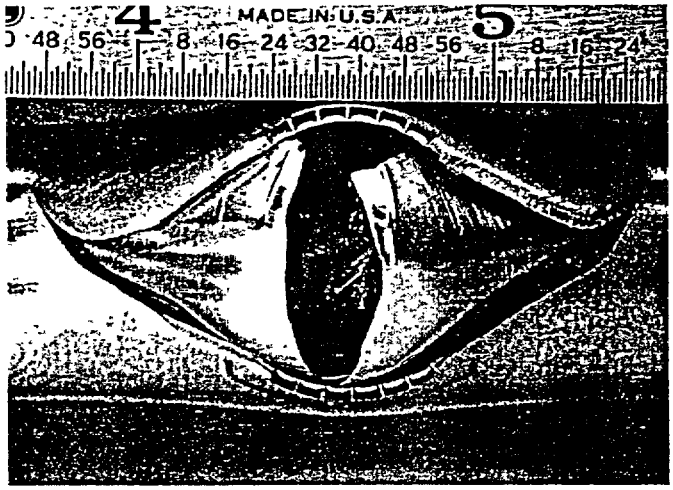

Figure 82. Appearance of Specimen 5528-3-3 with Type 3 flaw after Stage 2 burst testing with bladder and foil.

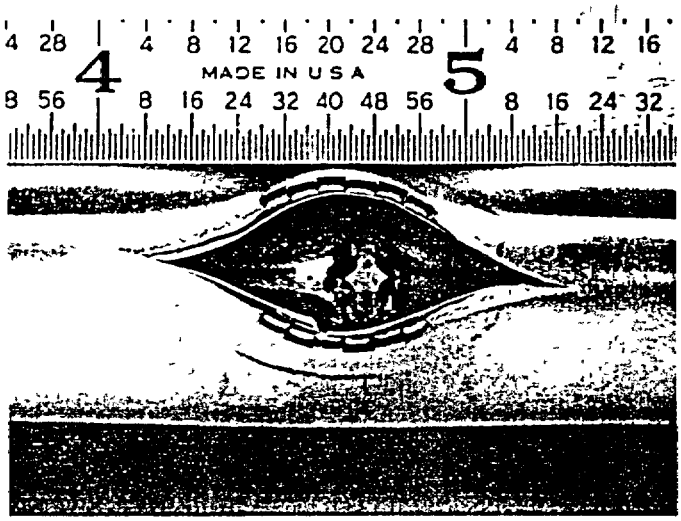

Figure 83. Appearance of Specimen 5469-2-2 with Type 4 flaw after Stage 2 burst testing with bladder and foil.

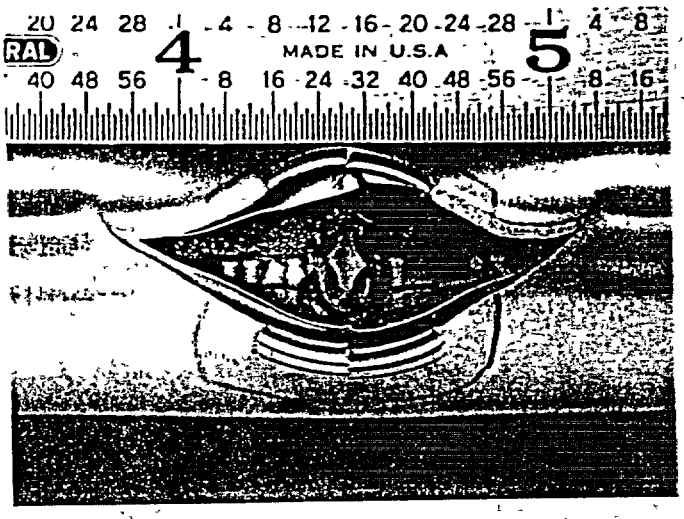

Figure 84. Appearance of Specimen 5469-2-4 with Type 5 flaw after Stage 2 burst testing with bladder and foil.

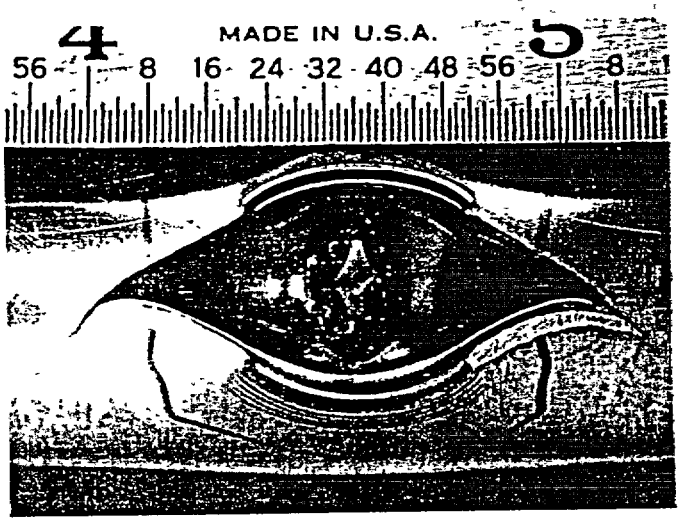

Figure 85. Appearance of Specimen 5531-3-1 with Type 6 flaw after Stage 2 burst testing with bladder and foil.

(Specimens 5528-1-1, 5528-1-2, 5528-1-3, and 5528-1-4) did not exhibit bladder wedging, probably because the flaw openings were much smaller after the Stage 1 tests than for the 12.7-mm (0.5-in.)-long flaws.

4.3.1 Summary of Results

Twenty four tubes with 9 patterns of complex interacting, part-throughwall laser-cut notches (Fig. 70) were pressure tested at room temperature in the High-Pressure Test Facility. In the first stage, the specimens were tested without internal bladders and foils at a quasi-steady-state pressurization rate to the point of ligament tearing. In the second stage, those specimens that did not exhibit unstable tearing in Stage 1 were fitted with an internal bladder (and foil, if necessary) and pressurized to unstable burst. The results of these tests may be summarized as follows:

1. For the six Type 1 flaws, the ligaments tore completely in the Stage 1 tests, and there was no unstable tearing at the notch ends. Under Stage 2 testing, five of the six flaws exhibited unstable burst.

2. No unstable tearing at the notch ends of the two Type 2 flaws was observed after Stage 1 testing, though the ligament between the two notches, as well as those at the bottom of each notch, tore. No indication of progressive sequential tearing was evident; both types of ligaments tore simultaneously. In Stage 2 testing, both flaws burst unstably, but bladder wedging resulted in an artificially low value for the burst pressure.

3. For the three Type 3 flaws, no unstable tearing at the notch ends was observed under Stage 1 testing, and the ligaments between the notches and those at the bottom of each notch tore simultaneously at the failure pressure. The length of the ligaments separating the notches had little influence on the failure pressure, but the depth of the notches exerted a noticeable influence. Significant unstable tearing into the ends of the notch occurred in Stage 2.

4. The three Type 4 flaws exhibited no unstable tearing at the notch ends in Stage 1 testing, and the ligaments between the notches and those at the bottom of each notch again all tore simultaneously at the failure pressure. The depth of the notches exerted a stronger influence on the failure pressure than did the length of the interspersed ligaments. Significant unstable tearing into the notch ends occurred in Stage 2.

5. The two Type 5 flaws exhibited somewhat different behavior in Stage 1 testing, depending upon the ligament thickness. The specimen with the thicker ligament tore along only one of the unaligned axial rows, and unstable tearing also occurred at the notch ends. The specimen with the thinner ligament did not tear unstably in Stage 1 testing, and it opened at a considerably lower pressure. Stage 2 testing of this specimen resulted in significant unstable tearing into the the notch ends.

6. For the Type 6 flaw with the thicker ligaments, ligament tearing occurred in only one of the parallel notches and no unstable tearing occurred at the notch ends. The specimen with the thinner ligaments behaved similarly but opened at a considerably lower pressure. Stage 2 testing again produced significant unstable tearing at the notch ends.

7. For the two Type 7 flaws, Stage 1 testing of the specimen with the thinner ligament resulted in ligament tearing around the entire tube circumference. The specimen with the thicker ligament could not be opened at the maximum facility pressure, either in Stage 1 or Stage 2 testing.

8. The tubes with the Type 8, 9, and 10 flaws all failed unstably in Stage 1 testing and, therefore, did not undergo Stage 2 testing.

4.4 Comparison of Observed and Predicted Failure Pressures for Machined Flaws

4.4.1 EDM Notches

The ligament rupture pressures of a variety of single axial EDM notches have been predicted quite successfully by using the ANL ligament rupture criterion (Fig. 86).[4] A series of specimens with two EDM part-throughwall axial flaws of Type 2 (axial ligament) and Type 4 (circumferential ligament) has also been tested (Section 4.2). The ligament rupture pressures for these specimens were calculated by using the equivalent rectangular crack approach,[2] and an example is shown in Fig. 87a. The two 12.7-mm (0.5-in.)-long 80% TW notches with a 1.27-mm (0.05-in.) axial ligament (solid line) are replaced by an equivalent rectangular crack 25.4-mm (1-in.) long and 75% TW (dashed line). The same approach was used for specimens with two axial notches and a circumferential ligament (Fig. 87b). Figures 88a and 88b show the variation of predicted ligament rupture pressure (solid line) with ligament width for two 6.35-mm (0.25-in.)-long and two 12.7-mm (0.5-in.)-long notches, respectively. Test results denoted by symbols for both types of specimens fall quite close to the predicted lines. The two dashed lines in Fig. 88b denote the upper and lower bounds within which the test results are predicted to lie. When the ligament width is zero, the two notches behave as a single 25.4-mm (1-in.)-long notch. On the other hand, when the ligament width is >5.1 mm (0.2 in.), the two notches behave as two single notches without any interaction. The equivalent rectangular crack approach predicts this behavior.

4.4.2 Laser-cut notches

The depth profiles of the multiple laser-cut notches were measured by pretest multivariate EC analysis as well as by posttest fractography. These specimens were tested at room temperature in the High-Pressure Test Facility, and the results are summarized in Section 4.3 of this report. In all, five types of specimens in addition to single notches (Type 1), were tested: Types 2, 3, 4, 5, and 6, shown in Fig. 70. The overall length of all the notches was 12.7 mm (0.5 in.), with the ligament widths generally varying between 0.13 and 0.25 mm (0.005 and 0.010 in.). The tests were run in two stages. The specimens were first pressurized without an internal bladder until ligament rupture occurred, and the pump could not keep up with the maximum leak rate of 45 L/min (12 gpm). In Stage 2, the same specimens were fitted with an internal bladder and brass foil (when necessary) and pressurized to unstable burst. After crack tip ligament rupture, the axial ligaments between the notches in all specimens except Types 5 and 6 were also ruptured, which caused the multiple notches to coalesce into a single 12.7-mm (0.5-in.)-long throughwall notch. In the Type 5 and 6 specimens, only one of the end notches experienced crack-tip ligament rupture and opened up after Stage 1 testing. The test failure pressures were compared with predicted failure pressures based on both fractography and advanced NDE measurements. In addition, the ligament rupture pressures were calculated by the equivalent rectangular crack approach.[2]

Figure 89 shows the test and predicted ligament rupture pressures calculated using flaw dimensions determined by posttest fractography as well as by pre-test NDE. The test ligament rupture pressures are overestimated in both cases. However, except

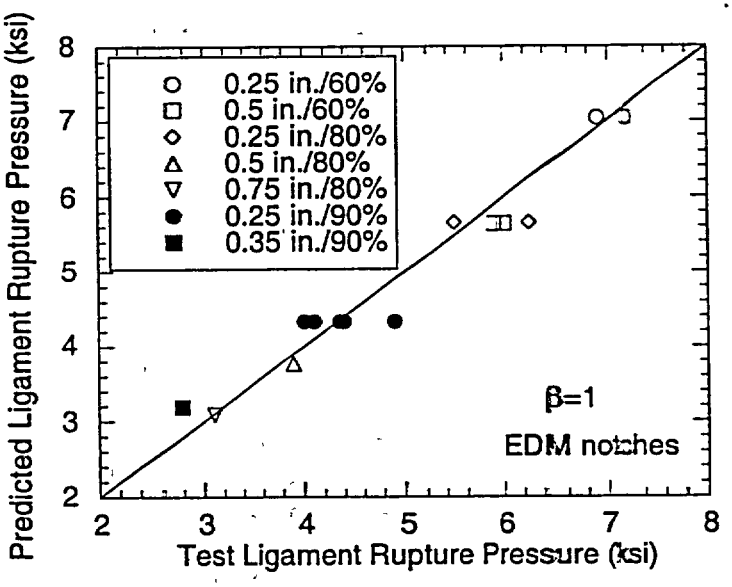

Figure 86.
Predicted vs. observed ligament rupture pressures for specimens with part-throughwall axial EDM notches

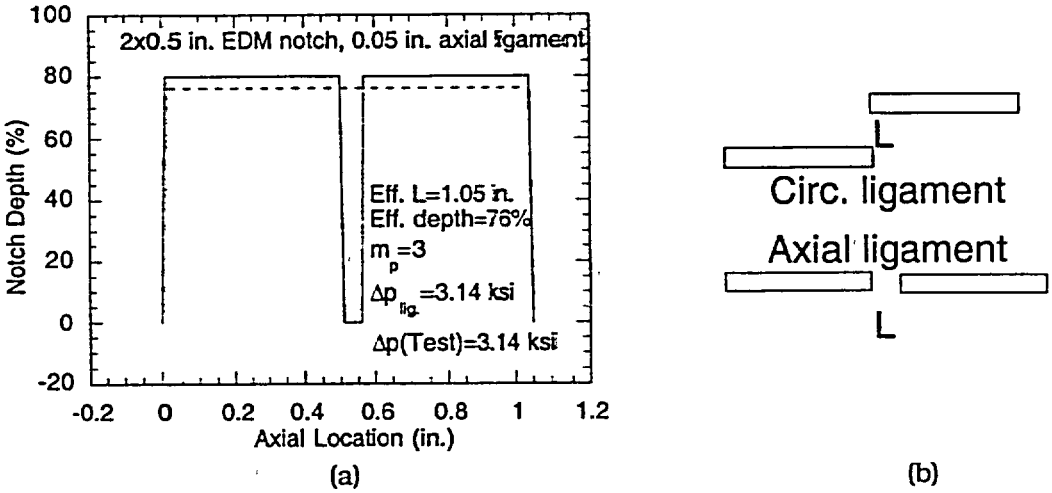

Figure 87. (a) Equivalent rectangular crack approach applied to calculate ligament rupture pressure of a specimen with two axial part-throughwall notches with a 1.27-mm (0.05-in.) axial ligament and (b) comparison of axial ligament (Type 2) with circumferential ligament (Type 4) geometry.

for Type 3 specimens, the predicted ligament rupture pressures using fractography data are reasonably close to the test values. The ligament rupture pressures of Type 3 specimens are overestimated by 20-30%. The predicted ligament rupture pressures using NDE data overestimate the test pressures by ≤35% in all cases. Note that the NDE technique did not detect the presence of the axial ligaments between the notches in any specimen.

To check whether the laser-cutting process itself is responsible for the apparent low ligament rupture pressures, a Type 2 specimen with EDM notches was tested in the High-Pressure Test Facility. A comparison of the EDM notch with a similar laser-cut

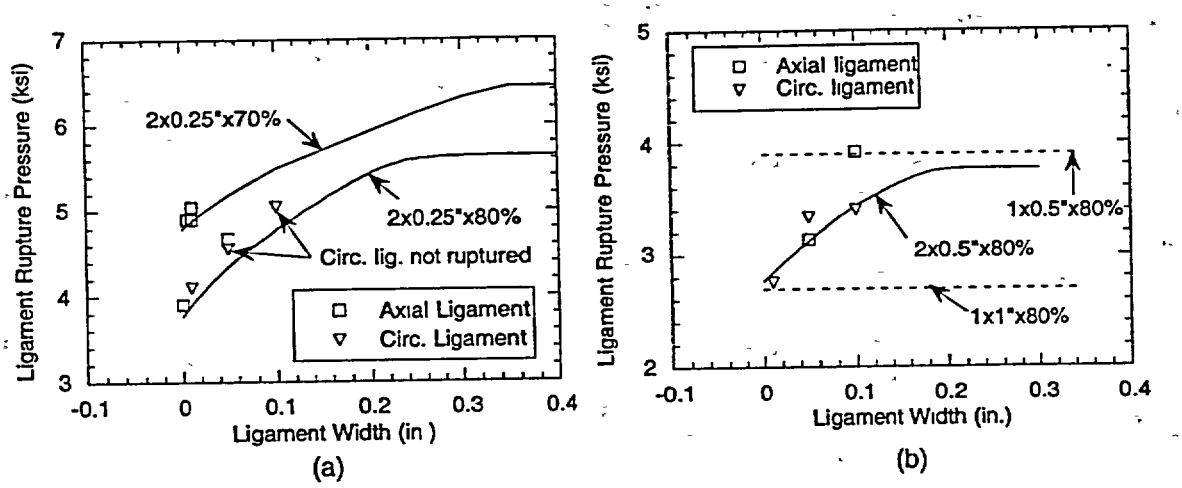

Figure 88. Variation of test and predicted ligament rupture pressure with ligament width for specimens with (a) two 6.35-mm (0.25-in.)-long and (b) two 12.7-mm (0.5-in.)-long part-throughwall axial notches.

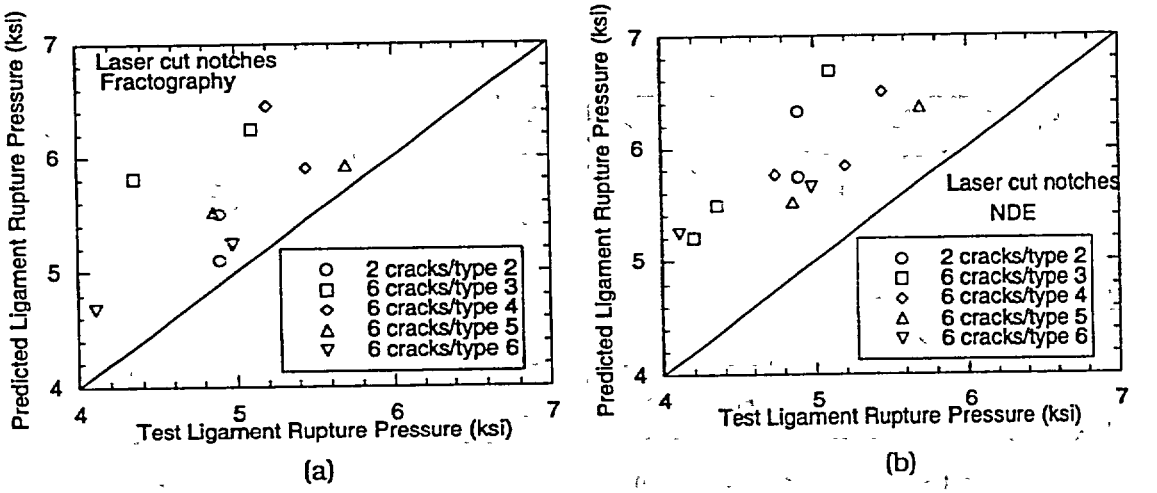

Figure 89. Test ligament rupture pressures and those predicted using depth profiles as measured by (a) posttest fractography and (b) pre-test multivariate EC analysis (right).

notch after Stage 1 testing is shown in Fig. 90. The ligament rupture pressures are quite close to the predicted ligament rupture pressure (35.2 MPa or 5.1 ksi), indicating that the ligament rupture pressure is not significantly affected by the machining technique. The discrepancy between the observed and predicted ligament rupture pressures for the Type 3 laser-cut specimens may be due to multiple (>2) notch effects.

Similar comparisons for the Stage 2 failure pressures (unstable burst) are shown in Fig. 91. In contrast to the ligament rupture pressures, the predicted Stage 2 failure pressures in both cases are close to and scattered evenly about the test failure pressures.

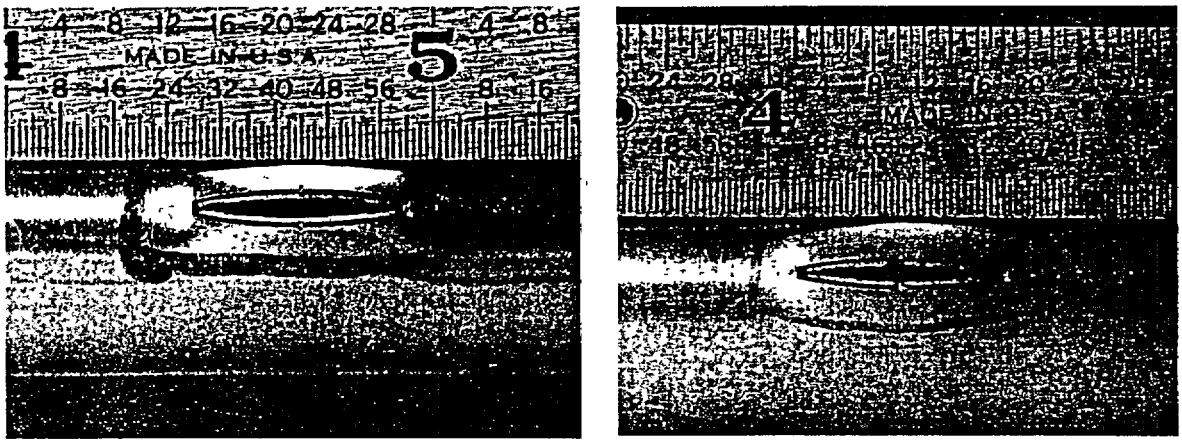

(a) (b)

Figure 90. Type 2 specimens with two 6.35-mm (0.25-in.)-long, 70% TW notches separated by 0.25-mm (0.010-in.)-wide ligaments fabricated by (a) EDM (OM 153) and (b) laser cutting (5516-4-3) after Stage 1 testing. Ligament rupture occurred at 34.8 MPa (5.05 ksi) for the EDM notch and at 33.8 MPa (4.90 ksi) for the laser-cut specimen.

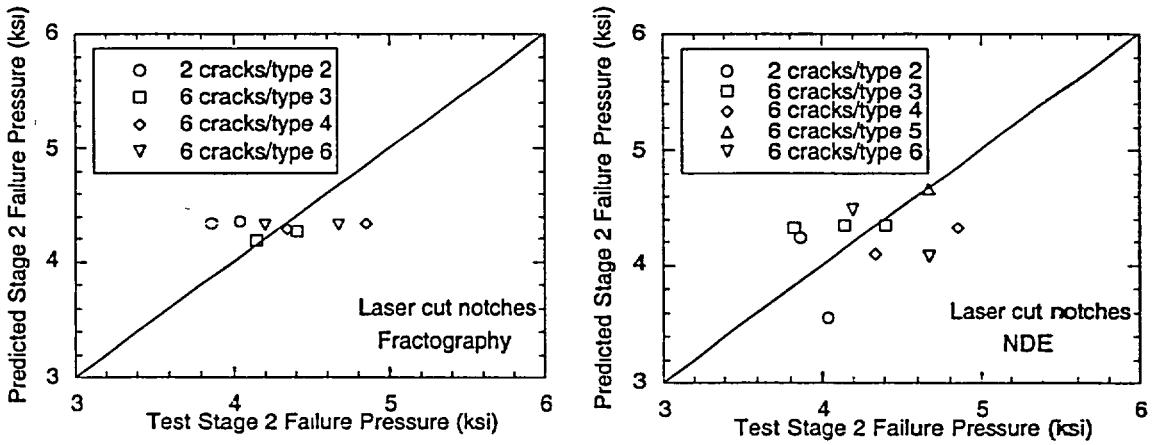

(a) (b)

Figure 91. Comparison of test Stage 2 failure pressures with predicted failure pressures using depth profiles as measured by (a) posttest fractography and (b) pre-test multivariate EC analysis (right).

5 Test Results for SCC Flaws

Experimental results from pressure and leak-rate tests for ANL-produced SCC flaws at room and elevated temperature are presented in this section. The overall goal of these tests is to provide data that would allow relating pretest NDE flaw information to failure behavior and the actual crack morphologies and to improve techniques for predicting failure pressures and leak rates. These tests also yielded information on flaw leak stability under constant temperature and pressure.

In contrast to rectangular machined notches of constant depth, laboratory-grown SCC cracks are irregular in shape and have variable depths along their lengths. They are often comprised of a family of crack segments in different planes rather than a single planar crack. Local variations in crack depth and geometry tend to be smoothed out in EC measurements, since the EC signals are necessarily averaged over a finite volume related to the size of the EC coil. This is evidenced by the fact that many specimens tested to date have shown leakage under a preliminary low-pressure bubble test prior to high-pressure testing, even though EC techniques have failed to detect throughwall segments. Often, these same flaws exhibit no detectable leakage during high-pressure testing until significant pressures are applied.

Currently, no reliable models are available for predicting the ligament failure pressures or the associated leak rates for cracks with such complex geometries. The preliminary analyses of the first data on SCC flaws from the High-Temperature Pressure and Leak-Rate Test Facility described in the next subsection are reported in Ref. 2.

5.1 High-Temperature Pressure and Leak-Rate Test Facility

Test results from five 22.2-mm (7/8-in.)-diameter Alloy 600 tubes with laboratory-produced axial ODSCC of nominal length 12.7 mm (0.5 in.) are described here. Four of the tubes, SGL-177, SGL-195, SGL-104, and SGL-219, were cracked at ANL in an aqueous solution of sodium tetrathionate. The fifth tube (W 2-10) contained an axial ODSCC flaw produced by Westinghouse using a doped steam procedure. All five tubes underwent the same multi-step pretest flaw characterization process.

The tests were designed to gain information on flaw stability under constant temperature and pressure conditions associated with normal SG operation and main steam line break, i.e., T = 282°C (540°F) and p = 8.3 and 17.2 MPa (1200 and 2500 psi), respectively. These pressure plateaus were held for at least 2 h (depending on leak rate and amount of water in the blowdown vessel), with extended duration holds at intermediate pressures if flaw tearing, as indicated by a sudden increase in flow, was observed. Tubes SGL-177 and SGL-195 were tested at room temperature, and tubes SGL-104 and SGL-219 were tested at 282°C (540°F). The Westinghouse tube W 2-10 was tested at both temperatures.

As described in Section 3.1, several techniques were used to characterize the SCC flaws prior to testing: (a) dye-penetrant examination and digital photography with computerized image analysis, (b) bubble testing with low-pressure (0.28 MPa [40 psi]) air in a water bath to identify regions of throughwall penetration, and (c) EC NDE. Finite-element structural calculations were used to estimate crack opening pressures

from the NDE crack-depth profiles. The information on opening pressures was used to guide facility operation during testing.

The four ANL-produced tubes with ODSCC flaws were selected for testing on the basis of having the same nominal axial crack length of 12.7 mm (0.5 in.), as determined by dye-penetrant examination (see Figs. 92-95) as well other similarities. The Westinghouse tube (see Fig. 96) had an axial ODSCC flaw of similar length, 12.4 mm (0.49 in.). Air bubble testing at 276 kPa (40 psi) revealed that the flaw in the latter tube had two locations of throughwall penetration, coinciding with the two largest dye-penetrant indications in Fig. 96. Each penetration exhibited very small intermittent bubble generation, with the one on the right exhibiting a larger bubble size and higher generation frequency than that on the left.

Eddy current examinations indicated that all four ANL-produced SCC flaws had variable crack depths along their lengths, with maximum depths of 75-95%. The Westinghouse tube exhibited a similar crack depth profile. The TW regions identified by bubble testing in both the Westinghouse and the four ANL tubes were not seen by EC techniques because of their tightness and very small axial extents, and the dye-penetrant inspections revealed flaw branching for all of the flaws. The EC bobbin coil (BC) voltages indicated that the five flaws fell into two categories. The EC BC voltage for the Westinghouse tube was 4.5 V, very close to the 4.0 V exhibited by the ANL tube in Test SGL-177. The other three ANL tubes had higher EC voltages, in the range of 6-10 V.

The crack depth profiles for all flaws were used not only to qualitatively prescreen the flaws for similarity, but also to estimate the initial flaw-opening pressure. Calculations of flaw-opening pressures indicated that the Westinghouse tube was most similar to ANL tube SGL-177, although somewhat stronger. Because of this similarity, the initial testing phase for the Westinghouse tube, like the ANL tube, was conducted at room temperature, with follow-on testing at 282°C (540°F).

5.1.1 Room-Temperature Tests

Results are first presented for ANL tubes SGL-177 and SGL-195, tested at room temperature. The two flaws are quite similar in their overall characteristics. The flaw in sample SGL-177 (test T501ACTW177-B), shown in Fig. 92, is nominally 12.2-mm (0.48-in.) long and exhibits "Y" branching at both ends. The flaw in sample SGL-195 (test T500ACTW195-B), shown in Fig. 93, is nominally 13.7-mm (0.54-in.) long and also exhibits "Y" branching at both ends. The bubble-leak test results also revealed similar leakage locations for both flaws; a main leak region located near the center of each crack pattern and a secondary leak region located at a "Y" branch point. It thus appears that both cracks have a non-throughwall ligament between the two regions of throughwall penetration. Time-dependent failure of this ligament (or a portion thereof) could produce changes in leak rate under conditions of constant temperature and pressure.

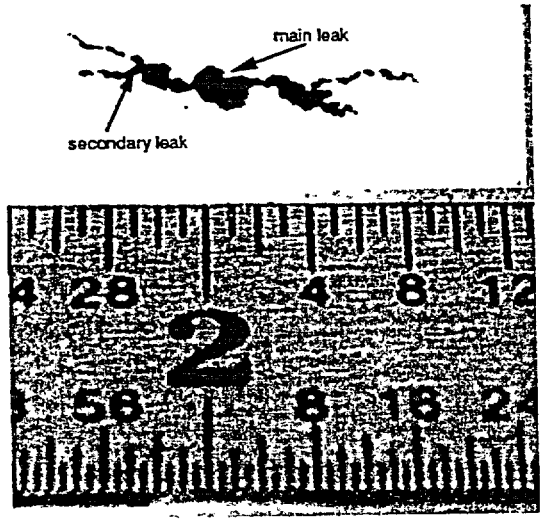

Figure 92.
Pretest image of Specimen SGL-177 with flaw highlighted by dye penetrant and digital image processing. Two regions of TW penetration are indicated by bubble testing.

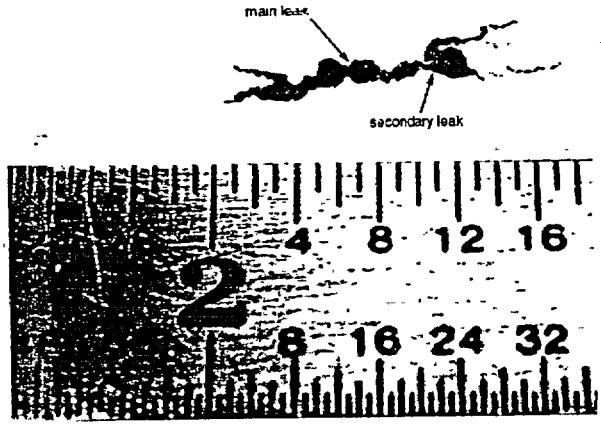

Figure 93.
Pretest image of Specimen SGL-195 with flaw highlighted by dye penetrant and digital image processing. Two regions of TW penetration are indicated by bubble testing.

Figure 94.
Pretest image of Specimen SGL-104 with flaw highlighted by dye penetrant and digital image processing. A single region of TW penetration was indicated by bubble testing.

Figure 95.
Pretest image of Specimen SGL-219 with flaw highlighted by dye penetrant and digital image processing. A single region of throughwall penetration was indicated by bubble testing.

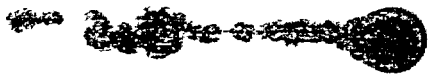

Figure 96.
Pretest dye-penetrant digital image of Westinghouse Tube W2-10 cracked using doped steam.

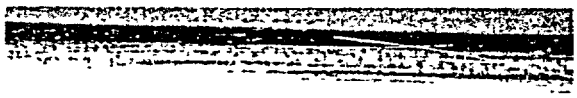

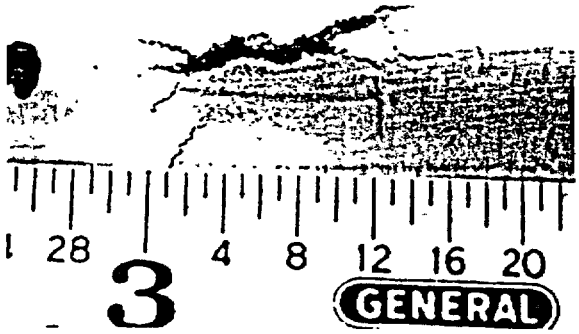

Figure 97.
Photograph of failed region of Specimen SGL-195 after testing.

Specimen SGL-195. This tube was tested by gradually increasing the internal pressure in ≈2.1-MPa (300-psi) increments. Each pressure plateau was held for ≈15-30 min, except that at 8.27 MPa (1200 psi) approximating normal plant operating conditions, which was held for 2 h. Even though the crack showed definite gas leakage at two locations during the pretest gas bubble check, no leakage was detected in water testing during the 2-h hold at 8.27 MPa (1200 psi). As stated previously, the facility can detect leak rates of several hundredths of a liter per minute. The tube continued to show no detectable leakage until the pressure reached the ≈14.7 MPa (2129 psi) plateau, where very slight leakage was observed. As the pressure was increased toward the final target plateau of 17.2 MPa (2500 psi), the tube abruptly started leaking at 29.9 L/min (7.9 gpm) and a pressure of ≈15.1 MPa (2188 psi). When the pressure stabilized at 15.5 MPa (2250 psi), the leak rate had increased to 32.6 L/min (8.6 gpm) and remained at that level for another 15 min. The test was terminated at this point because of low blowdown vessel water inventory.

The tube was removed from the test module and photographed (see Fig. 97). The tube also underwent posttest EC examination. A visual comparison of the posttest photograph (Fig. 97) with the pretest photograph of the dye-penetrant crack image (Fig. 93) showed that the flaw had opened up significantly in width along its entire length, even into the extremities of the Y branches at each end of the main flaw. Additional zones of what appeared to be faint dye streaks in Fig. 93 are seen in Fig. 97 to correspond to several posttest cracks emanating from the main crack pattern. The region around the flaw is raised noticeably, i.e., puckered.

Specimen SGL-177. This tube was tested using the same general procedure as for tube SGL-195, except that the pressure plateaus associated with normal operating (8.27 MPa or 1200 psi) and MSLB conditions (17.2 MPa or 2500 psi) conditions were held for >15 h by running the test facility at fixed pressure overnight under automatic control. As with tube SGL-195, no leak was detected on the approach to the normal tube operating pressure differential or during the >15 h overnight hold at normal operating pressure. Thus, both SCC flawed tubes, even though exhibiting throughwall localized penetration in the low-pressure gas bubble test at locations marked in Figs. 92 and 93, did not leak at detectable rates under normal operating pressure in subsequent water tests.

Following the overnight hold at 8.27 MPa (1200 psi), tube pressure was increased in 1.38-MPa (200-psi) increments toward MSLB conditions. No leakage was detected until the pressure was held for 100 min at 16.9 MPa (2450 psi), at which point a very small leak of less than several hundredths of a liter per minute abruptly developed. Leak initiation was verified by an ultrasonic leak detector that sensed the water jet noise when held on the walls of the test module. After ≈1 h of a steady leak rate at this constant pressure, the rate abruptly increased to ≈0.26 L/min (0.07 gpm). This increase was accompanied by a stronger signal output from the ultrasonic leak detector. The crack was allowed to leak at this fixed pressure level overnight, but no additional increase in flow rate was observed.

After replenishing the blowdown vessel water inventory and recharging the nitrogen cover gas pressurization system, the pressure on the tube was increased to a maximum of 19.3 MPa (2800 psi) in a series of plateaus held for 30 min or less, during

which the leak rate continuously increased. At each increased leak level, increasing leak noise was also measured, though the audible noise would occasionally change frequency and fluctuate randomly. At 19.3 MPa (2800 psi), the leak rate was 1.67 L/min (0.44 gpm). This was considerably less than the 32.6 L/min (8.6 gpm) leak at 15.5 MPa (2250 psi) that abruptly occurred for Specimen SGL-195 under similar conditions. The crack depth profile determined by pretest EC inspection for tube SGL-177 was not as uniformly deep over its length as the profile for tube SGL-195. Similarly, the posttest digital image of the opened flaw in Specimen SGL-177 (Fig. 98) shows less opening than that for Specimen SGL-195 (Fig. 97).

For room-temperature testing of the Westinghouse tube, the pressure was increased from 0 in 1.4-2.1 MPa (200-300 psi) increments, with hold times of 15-30 min at each level until 8.3 MPa (1200 psi) was reached. The pressure was then held at this level for 2 h. Like the four ANL specimens, the Westinghouse tube exhibited no observable water leakage during this portion of the test, even though all of these tubes exhibited localized throughwall penetration during bubble testing at very low pressure. The cracks thus appear to be very tight. Following the 2-h hold at 8.3 MPa (1200 psi), the pressure was increased in a series of steps to 17.2 MPa (2500 psi) over 45 min, with no leakage observed. After a subsequent hold time of 3.25 h at this pressure, a leak rate of ≈0.04 L/min (0.01 gpm) was detected. This pressure was held overnight, and the tube continued to leak, with the leak rate increasing to ≈0.068 L/min (0.018 gpm) by the following morning. In comparison, the ANL Specimen SGL-177 leaked at a rate of ≈0.26 L/min (0.07 gpm) under an extended hold time at 17.2 MPa (2500 psi). The pressure on the Westinghouse tube was then raised to 18.6 MPa (2700 psi) and held at this level for 5.5 h, at which time a leak rate of 0.12 L/min (0.032 gpm) was measured. The room-temperature phase of the test was terminated at this point. The ANL Specimen SGL-177 exhibited a leak rate of 1.7 L/min (0.44 gpm) at 19.3 MPa (2800 psi). Thus, the Westinghouse tube, like the ANL tubes, developed a leak under constant pressure and exhibited an increasing leak rate (though somewhat lower than the ANL tubes) over an extended hold period.

5.1.2 Elevated-Temperature Tests

Argonne tubes SGL-104 and SGL-219 were tested at 282°C (540°F) by using procedures similar to those for the room-temperature tests. The flaws in these tubes had overall axial extents of 10.4 and 14.0 mm (0.41 and 0.55 in.), respectively, as determined by dye-penetrant examinations. These flaws are thus nominally the same size as the flaws present in tubes SGL-177 and SGL-195 tested at room temperature. Like tubes SGL-177 and SGL-195, the flaws in Specimens SGL-104 and SGL-219 exhibited Y-branch cracking at both ends of a central axial crack zone (Figs. 94 and 95). These flaws also had a central region of throughwall penetration, as determined by pretest bubble testing. Unlike Specimens SGL-177 and SGL-195, however, Specimens SGL-104 and SGL-219 did not have a second smaller leak zone at a branch point. Based on EC examination results, the flaws in all four tubes had variable crack depths along their main flaw zones, with maximum depths of 75-95%.

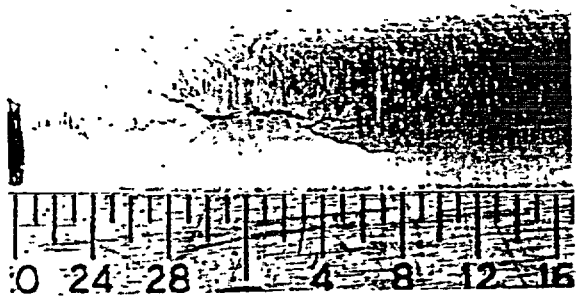

Figure 98.
Photograph of failed region of Specimen SGL-177 after testing.

Specimen SGL-104. This tube again exhibited no detectable leakage at pressures below 8.27 MPa (1200 psi) or during the 2-h hold at that pressure, despite the throughwall penetration indicated by the bubble test. In fact, no detectable leakage occurred until the pressure exceeded 15.9 MPa (2300 psi). During the subsequent pressure ramp to 17.2 MPa (2500 psi), the flaw abruptly opened at 16.2 MPa (2352 psi) and yielded a flow of 21.2 L/min (5.6 gpm). When the pressure stabilized at the final 17.2 MPa (2500 psi) hold plateau, the flow rate held steady at 23.5 L/min (6.2 gpm). The increases in flow rate were all associated with increases in internal pressure for this tube, and no flaw tearing under constant conditions was indicated. The test was terminated after an additional 15 min because of low water inventory in the blowdown vessel.

A comparison of posttest (Fig. 99) and pretest (Fig. 94) photographs of the flawed region of Specimen SGL-104 shows that the flaw opened significantly in width in all regions highlighted by the pretest dye-penetrant examination, similar to that of tube SGL-195. Like Specimen SGL-195, several posttest secondary cracks also emanate from the main crack pattern in Specimen SGL-104 after testing, again corresponding to faint pretest dye-penetrant images. The region around the flaw is again raised noticeably, or puckered, as seen in the side view of Fig. 100.

Specimen SGL-219. As for the other SCC flaws tested, this tube exhibited no detectable leakage at pressures below 8.3 MPa (1200 psi) or during a 2-h hold at 8.3 MPa (1200 psi), although it had also leaked air in the pretest bubble test. Leakage was first detected at a pressure of 13.3 MPa (1930 psi), when the flaw abruptly opened and leaked at 3.7 L/min (0.97 gpm). This pressure was held for 90 min, during which time no change in flow rate was observed. The test was stopped because of low water inventory and was restarted after refilling and reheating the system. The test was resumed at 13.3 MPa (1930 psi), which resulted in the same leak rate as before, and pressure ramping continued. After 10 min at 16.2 MPa (2346 psi), the leak rate increased abruptly to 14.0 L/min (3.7 gpm), indicating ligament tearing. During the subsequent 11 min at this pressure, the leak rate gradually increased to 39.0 L/min

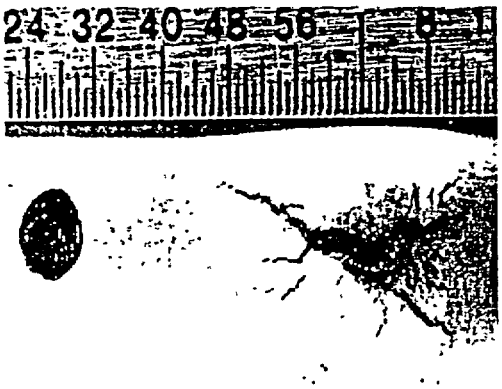

Figure 99. Photograph of failed region of Specimen SGL-104 after testing.

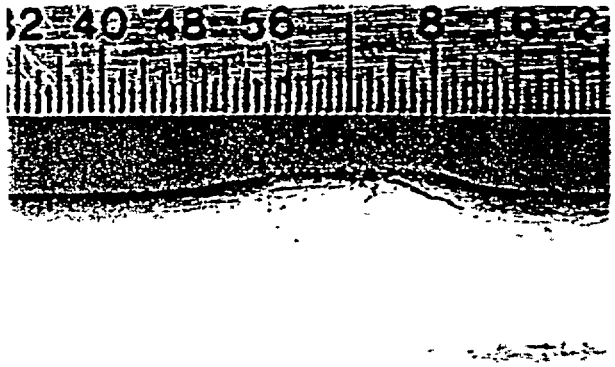

Figure 100. Side view of tube shown in Fig. 99.

(10.3 gpm), suggesting additional ligament tearing under constant conditions. For the next 9 min, the flow remained stable at 39.0 L/min. The test was then terminated because of low water inventory.

Posttest photographic inspection of Specimen SGL-219 (Figs. 101 and 102) and comparison with the pretest photograph (Fig. 95) show that the flaw opened significantly in width along its entire length, even into the extremities of the Y branches on the ends of the main flaw. Again, several posttest secondary cracks emanate from the main crack; these cracks are marginally observable in the pretest flaw image. The region around the flaw is raised noticeably, or puckered.

Specimen W 2-10. Westinghouse Specimen W 2-10, after undergoing room-temperature testing, was pressure tested at elevated temperature. The tube was tested at 282°C (540°F) and 18.6 MPa (2700 psi) to determine the leak rate and to see if the crack would open further. The flow rate was observed to increase from ≈0.30 L/min (0.08 gpm) to 0.72 L/min (0.19 gpm) during a 2-h hold at this pressure. The test was then terminated and the tube was removed. The flaw had opened slightly over its entire axial extent (see pretest photograph of Fig. 96). Like ANL Test SGL-177, no flaw-zone puckering was evident. Westinghouse Specimen W 2-10 thus behaved in a manner qualitatively similar to the ANL tube SGL-177 under leak testing.

Observations from all five SCC flaw tests are presented in Table 11 and can be summarized as follows:

All four ANL SCC flaws and the single Westinghouse SCC flaw were very tight and had regions of TW penetration, as determined by bubble testing, that were not detected in the pretest eddy current exam. However, none of the five flaws

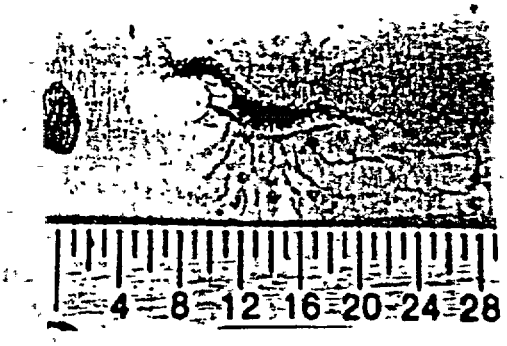

Figure 101. Photograph of failed region of Specimen SGL-219 after testing.

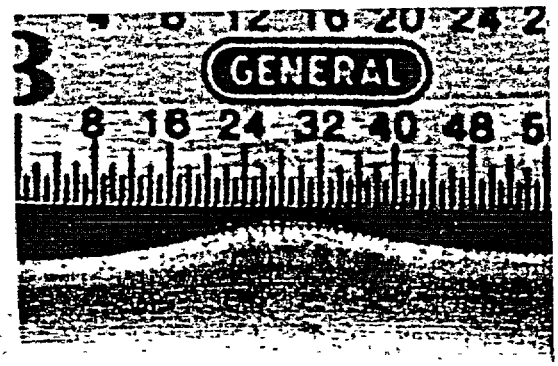

Figure 102. Side view of tube shown in Figure 101.

Table 11. Summary of results from tests on four Argonne tubes and Westinghouse tube with axial ODSCC cracks.

Spec. Number	Overall flaw length, mm	Test Temp., °C	Pretest air leak at 0.28 MPa	Flaw opening pressure (initial/ final), MPa	Tearing pressure, (constant conditions), MPa	Flow rate at (initial/final) opening pressure. L/min
SGL-177	12.2	R.T.[a]	yes	16.9/19.3	16.9	0.04-0.26/ 1.67
SGL-195	13.7	R.T.[a]	yes	14.7/15.5	14.7	<0.04/32.6
SGL-104	10.4	282	yes	16.2/17.2	no tearing	21.2/23.5
SGL-219	14.0	282	yes	13.3/16.2	16.2	3.7/ 14.0-39.0
W 2-10	12.4	R.T.[a]	yes	17.2/18.6	17.2	0.04- 0.068/0.12
W 2-10	12.4	282	yes	18.6	18.6	0.30-0.72

[a]R.T. = room temperature.

exhibited detectable water leakage at pressures below 8.3 MPa (1200 psi), nor was leakage detected during a 2-h (or greater) hold time at this pressure. Detectable leakage did not occur until higher pressures were attained.

2. Posttest inspection showed that flaws in three ANL Specimens (SGL-195, 104, and 219) opened significantly in width along their entire length, even into the extremities of the Y branches on each end of the main flaw. However, ANL Specimen SGL-177 and Westinghouse Specimen W 2-10, for which the nominal EC voltages of 4 V were considerably lower than the values of 6-10 V observed for the other three tubes, did not exhibit Y branching. Additionally, the latter three tubes had several obvious posttest secondary cracks emanating from the main crack, even though these cracks were barely perceptible in pretest characterizations. Furthermore, the region around the flaws was raised noticeably upward, or puckered, suggesting the presence of a weakened region in the vicinity of the cracking. In contrast, Specimens SGL-177 and W 2-10 exhibited very little puckering. Tests previously conducted on 12.7-mm (0.5-in.)-long axial EDM notches over the same pressure range produced significantly less puckering.

3. Specimens in four of the five tests (SGL-195, SGL-177, SGL-219, and W 2-10) exhibited crack tearing under the constant temperature and pressure conditions tested, which caused the leak rate to increase.

4. Specimen flaws in three of the four ANL tests (SGL-195, SGL-104, and SGL-219) suddenly opened to their full extent at pressures less than that associated with MSLB, yielding flow rates of 23 to >38 L/min (6 to >10 gpm). These three tubes had the highest EC voltages (6-10 V). This behavior suggests that once a small ligament tears, there is a strong tendency for other ligaments to tear in a domino fashion (sometimes after a delay under constant pressure) until the crack is completely open over its full extent. Tests SGL-177 and W 2-10, which had the lowest EC voltages (nominally 4 V), had leak rates of only 1.7 L/min (0.44 gpm) and 0.19 L/min (0.72 gpm), respectively, and did not exhibit this behavior.

5.2 Room-Temperature High-Pressure Test Facility

Additional pressure tests were conducted on tubes with laboratory-produced SCC flaws using the room-temperature High-Pressure Test Facility. The room-temperature operation of this facility and its ease of test specimen loading and unloading permit more rapid testing, and higher test pressures can be achieved than in the elevated-temperature Pressure and Leak-Rate Test Facility. In this section, test results are presented from two sets of SCC flawed tubes produced at ANL. The first set consists of 14 tubes, and the second set, 31 tubes.

5.2.1 14-Tube Set

The 14-tube set contains flaws of several types, including OD axial and circumferential cracks and combinations of these types, as well as OD flaws in the roll transition. The tubes underwent extensive pretest characterization, pressure testing, and posttest examination using metallographic and fractographic techniques to

characterize the flaw morphologies, as described in Section 3.1. The overall goal of this series of tests was to relate pretest NDE information to failure behavior and the actual crack morphologies and to improve the techniques for predicting leak and burst pressures. The general test procedures followed were similar to those used for the five SCC flaws tested in the Pressure and Leak-Rate Test Facility described in the previous section, except that no extended holds were used at normal and MSLB pressures. The tubes were tested without bladders using a quasi-steady pressurization rate with 0.69 MPa (100 psi) increments in pressure and a 10-s hold time after each increase.

Table 12 summarizes the results from the 14 tests, all on tubes with OD flaws. Specimens SGL-226 and SGL-363 contained complex flaws with combinations of axial and circumferential cracks, including cracking in the roll transition for Specimen SGL-363. Specimens SGL-413, 425, 480, 493, 494, 719, 728, 730, 731, and 734 contained axial flaws, and Specimens SGL-099 and 158 contained circumferential cracks, based on dye-penetrant determinations. The tabulated maximum depths and the EC voltages represent pretest characterizations using standard EC signal analysis procedures and software.

The information on pressure at first leak comes from visual observation of the flawed tube through observation windows for the first signs of water leakage. For Specimens SGL-158, 413, 425, 480, 493, 728, 731, 226, and 363, first leak occurred in the form of one drop of water issuing from the flaw over a period of several minutes (a much lower leak rate than could have been detected in the Pressure and Leak-Rate Test Facility or from the turbine flow meter in the present facility). The frequency of drop formation increased with increasing pressure, and the leaks often passed through an atomized small droplet spray, followed by a continuous leak stream jet. The tests were terminated when the flaw opened enough that the flow reached the maximum (48.4 L/min [12.8 gpm]) capacity of the pressurizer pump. The tabulated maximum pressure for the tests represents the pressure at which the flow capacity of the facility was reached.

For Specimens SGL-099, 494, 719, and 734, the pressure at first leak and maximum pressure achieved were the same or differed only slightly. These tests were characterized by essentially no leak prior to sudden rapid flaw opening, yielding a leak rate >48.4 L/min (12.8 gpm). All of the flaws tested in this 14-tube series exhibited significant tearing, with varying degrees of secondary cracking. Some tubes also exhibited evidence of unstable tearing without the use of bladders.

Specimen SGL-226 contained an ODSCC flaw that exhibited both axial and circumferential cracking, based on pretest dye-penetrant and NDE examinations. A posttest photograph of the flaw opening (Fig. 103) shows a ≈6.35-mm (0.25-in.)-long axial crack intersected by a ≈25-mm (1-in.)-long circumferential crack. This flaw first began to leak at 12.1 MPa (1750 psi), with a leak rate of approximately one drop every few minutes. By the time the pressure had reached 20.7 MPa (3000 psi), the leak rate had increased to 4.39 L/min (1.16 gpm). The test was terminated at 26.2 MPa (3800 psi), when the flaw suddenly opened and the flow rate exceeded the facility capacity.

Table 12. Summary of results from pressure tests on fourteen SCC flaws

Test No.	Flaw Type	Max. Flaw Depth, %	BC Voltage	Pressure at First Leak, MPa (psi)	Max. Pressure Attained, MPa (psi)
099	OD/Circ	20	3.25	51.0 (7400)	51.0 (7400)
158	OD/Circ	60	4.32	24.8[a,b] (3600)	31.4 (4560)
413	OD/Axial	90	1.57	12.4[b] (1800)	24.6 (3570)
425	OD/Axial	0	2.14	16.5[b] (2400)	30.0 (4350)
480	OD/Axial	0	3.08	6.2[b] (900)	15.2 (2200)
493	OD/Axial	0	3.84	0.6[b] (80)	17.6 (2550)
494	OD/Axial	0	0.54	31.7 (4600)	33.6 (4880)
719	OD/Axial	55	0.83	29.0 (4200)	29.6 (4300)
728	OD/Axial	90	1.97	14.5[b] (2100)	20.7 (3000)
730	OD/Axial	100	1.10	37.9 (5500)	41.7 (6050)
731	OD/Axial	90	3.12	0.3[a,b] (40)	21.4 (3100)
734	OD/Axial	55	1.71	34.5 (5000)	36.5 (5300)
226	OD/Axial/Circ	90	-	12.1[b] (1750)	26.2 (3800)
363	OD/Axial/Circ/ Roll Trans.	90	-	18.6[b] (2700)	24.7 (3580)

[a]Pretest air bubble leak test at 0.28 MPa (40 psi) indicated throughwall pinhole.

[b]First leak occurred as one drop of water issuing from the flaw over a period of several minutes.

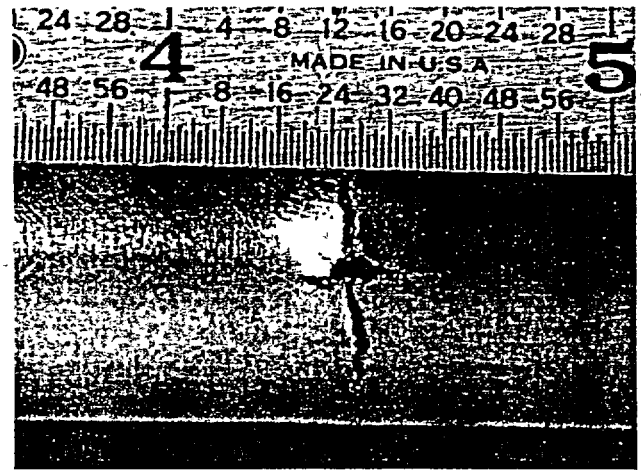

Figure 103.
Posttest appearance of complex ODSCC flaw in Specimen SGL-226 exhibiting both axial and circumferential cracking.

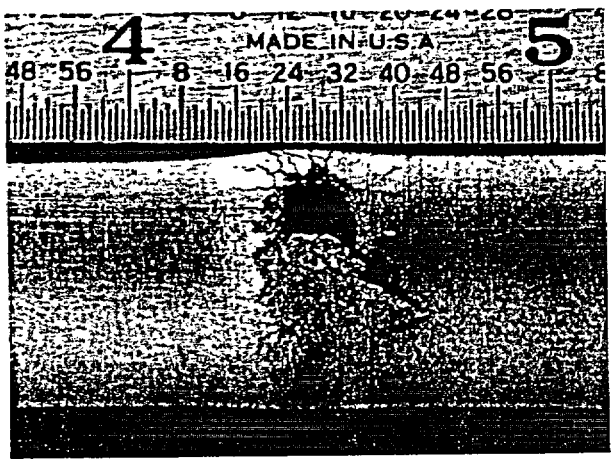

Figure 104.
Posttest appearance of complex ODSCC flaw in Specimen SGL-363 exhibiting a large opening resulting from both axial and circumferential cracking.

Specimen SGL-363 contained an ODSCC flaw at a roll transition that, based on pretest dye-penetrant and NDE examinations, was made up of a complex series of axial/circumferential cracks. Figure 104 shows the posttest photograph of the flaw opening, a large hole with both circumferential and axial ligament tearing and considerable secondary cracking. This flaw began to leak at 18.6 MPa (2700 psi) with a leak rate of approximately one drop every few minutes. The flaw abruptly opened at 24.7 MPa (3580 psi) and the flow rate again exceeded the facility capacity.

5.2.2. Thirty-One-Tube Set

A set of 31 flawed Alloy 600 tubes, all 22.2-mm (7/8-in.) in diameter and from the same heat of material as the 14-tube set, was also tested at room temperature in the High-Pressure Test Facility. These tubes also contained a variety of axial and circumferential OD and ID flaws. All of the tubes received extensive pretest characterization, including EC and dye-penetrant examinations and gas bubble leak testing at 0.28 MPa (40 psi) to check for throughwall pin holes.

Because the primary objective in testing these 31 tubes was to obtain flaw opening and fractography information to compare with pretest EC characterization of the flaw morphologies, the pressure testing of these tubes was performed in a carefully controlled manner to minimize excessive flaw tearing (unstable bursting) and bulging, which could complicate subsequent fractographic examinations. In contrast, the previous 14-tube set was tested to full and sudden flaw opening. The present flaws were tested without bladders using quasi-steady pressurization rates, which consisted of starting at 0.34 MPa (50 psi) and raising the pressure in 0.69 MPa (100 psi) increments with a 10-s dwell at each pressure plateau. In addition, the maximum test pressure was limited to 20.7 MPa (3000 psi) to further reduce chances of excessive flaw distortion. Some flaws that started leaking at low pressure and showed a rapid increase in leak rate for a few successive 0.69 MPa (100 psi) pressure increments were stopped short of the 20.7 MPa (3000 psi) pressure limit. For these tests, the flow was usually less than 7.6 L/min (2 gpm) for the highest pressure achieved. For many tests, no flaw leak was detected at the maximum 20.7 MPa (3000 psi) pressure. Nevertheless, after the tests were stopped at this pressure, meaningful fractographic examinations could be conducted for most flaws.

Table 13. Test results for 31-tube set containing SCC flaws

Test Number	Flaw Type	Leak in Bubble Test?	Pressure at First Leak, MPa (psi)	Maximum Pressure, MPa (psi)
AGL-224	ID/circ	no	No leak	20.7 (3000)
AGL-235	ID/circ	no	No leak	20.7 (3000)
AGL-284	ID/axial	no	No leak	20.7 (3000)
AGL-286	ID/axial	no	No leak	20.7 (3000)
AGL-288	ID/axial	no	No leak	20.7 (3000)
AGL-394	OD/circ	no	18.6 (2700)	20.7 (3000)
AGL-533	OD/axial	no	10.3 (1500)	16.5 (2400)
AGL-535	OD/axial	no	10.3 (1500)	15.9 (2300)
AGL-657	OD/axial	no	0.34 (50)	20.7 (3000)
AGL-686	OD/axial	no	No leak	20.7 (3000)
AGL-824	OD/axial	no	No leak	20.7 (3000)
AGL-825	OD/axial	no	No leak	20.7 (3000)
AGL-828	OD/axial	no	No leak	20.7 (3000)
AGL-835	OD/axial	no	No leak	20.7 (3000)
AGL-838	OD/axial	no	No leak	20.7 (3000)
AGL-855	OD/axial	no	13.8 (2000)	17.9 (2600)
AGL-866	OD/axial	no	10.9 (1580)	18.6 (2700)
AGL-868	OD/axial	no	No leak	20.7 (3000)
AGL-871	OD/axial	no	No leak	20.7 (3000)
AGL-874	OD/axial	yes	13.8 (2000)	19.3 (2800)
AGL-876	OD/axial	no	No leak	20.7 (3000)
AGL-881	OD/axial	yes	9.7 (1400)	20.7 (3000)
AGL-883	OD/axial	yes	3.4 (500)	8.3 (1200)
AGL-893	OD/axial	no	No leak	20.7 (3000)
AGL-894	OD/axial	no	No leak	20.7 (3000)
AGL-897	OD/axial	no	No leak	20.7 (3000)
AGL-908	OD/circ	no	No leak	20.7 (3000)
AGL-909	ID/circ	no	No leak	20.7 (3000)
AGL-916	ID/axial	no	No leak	20.7 (3000)
AGL-918	ID/axial	no	No leak	20.7 (3000)
AGL-923	ID/circ	no	No leak	20.7 (3000)

Table 13 summarizes the results from the tests conducted on the 31-tube set. As indicated in the table, nine tubes had ID flaws, with five being axial and four circumferential. The remaining 22 tubes had OD flaws, with 20 being axial and 2 circumferential. Only 3 of the 31 tubes, AGL-874, 881, and 883, exhibited pretest pinhole leaks in the bubble test. As previously observed, these small pinhole leaks are undetectable by EC examination.

The column labeled "Pressure at First Leak" lists the pressure at which the first indication of a water leak through the flaw was visually observed. In all cases, the first leak flow rate was in the form of successive individual single drops forming over periods ranging from several seconds to fractions of a second. As the pressure was increased above that associated with leak initiation, the leak would change to a fine water droplet mist and then, with increasing pressure, to a continuous water jet. As shown in Table 13, 9 of the 31 flaws exhibited leakage, namely, AGL-394, 533, 535, 657, 855, 866, 874, 881, and 883. The other 22 tubes exhibited no leak at pressure up to 20.7 MPa (3000 psi). Of the 9 leaking tubes, pressure testing of 6 (AGL-533, 535, 855, 866, 874, and 883) was stopped before reaching 20.7 MPa (3000 psi) because the leak rate began to increase rapidly with increasing pressure, and it was felt that the flaws might abruptly open and undergo excessive distortion. Of the 9 leaking tubes, 8 began leaking at pressures below 17.2 MPa (2500 psi) (MSLB pressure), and 5 started leaking at pressures of 10.3 MPa (1500 psi) or less.

Posttest photographs of 7 of the 9 flaws that leaked during testing are shown in Figs. 105-111. The photographs for tests AGL-394 and 657 are not shown because the flaws were too small and tight to be visible.

5.3 Summary of Results

The data base under development is being used to improve techniques for predicting failure pressure and leak rate by evaluating how pretest NDE information relates to failure behavior and the actual crack morphologies. The results reported here indicate that part-throughwall axial cracks with highly profiled ligaments can exhibit increases in leak rate (sometimes with delays) during constant-pressure holds at both room temperature and 282°C (540°F) until the crack is completely open over its full extent. The increasing leak rate is probably a consequence of progressive ligament rupture at the through-thickness crack tip. The above behavior suggests that ligament failure in an SCC flaw may occur progressively (sometimes with delays under constant loading conditions) until the crack is completely open over its full extent. In various flawed specimens with quite different ligament thicknesses, initial leakage occurred abruptly at pressures significantly lower than those predicted. The experimentally observed time-dependent increase of leak rate at both room temperature and 282°C (540°F) highlights the fact that no criterion for predicting time-dependent ligament rupture is currently available.

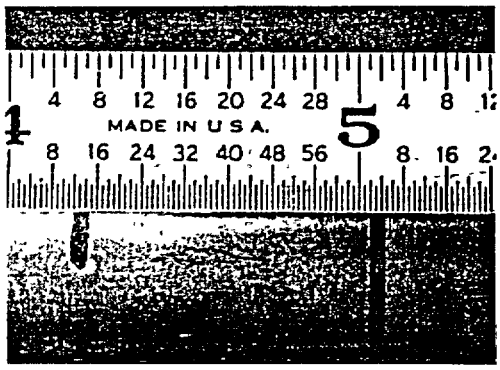

Figure 105. Posttest photograph of Specimen AGL-533.

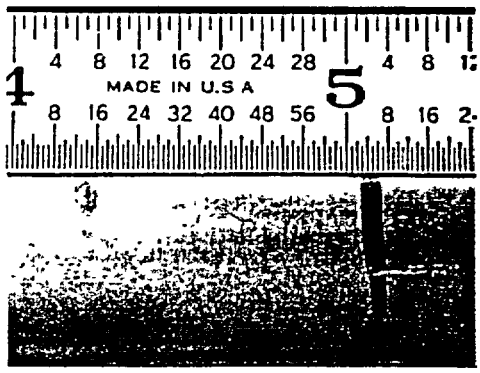

Figure 106. Posttest photograph of Specimen AGL-535.

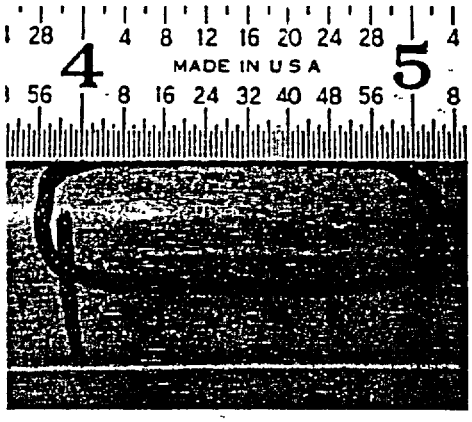

Figure 107. Posttest photograph of Specimen AGL-855.

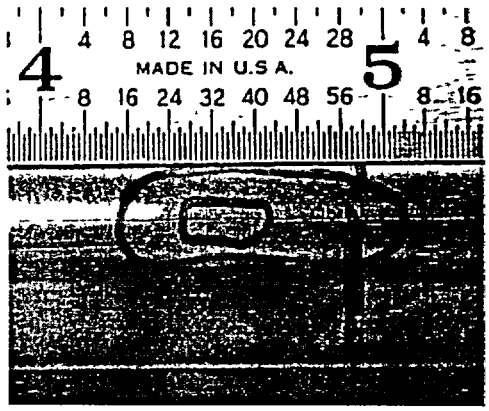

Figure 108. Posttest photograph of Specimen AGL-866.

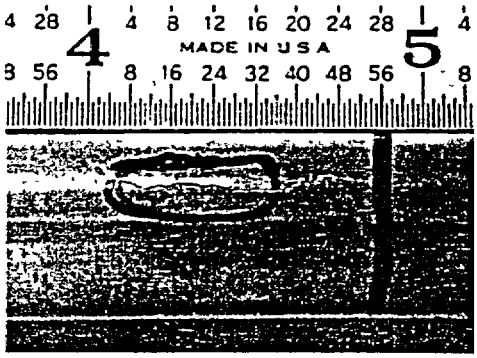

Figure 109 Posttest photograph of Specimen AGL-874.

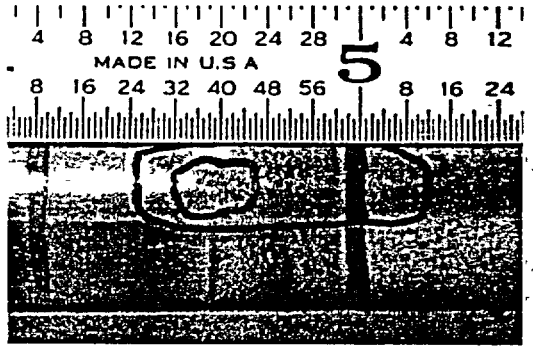

Figure 110. Posttest photograph of Specimen AGL-881

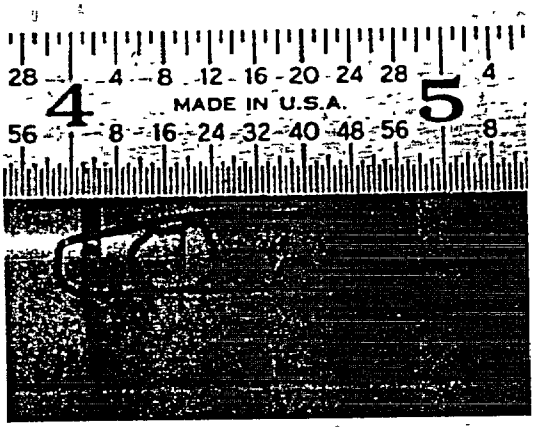

Figure 111. Posttest photograph of Specimen AGL-883.

6 Overview of Test Results

This report describes results from the pressure and leak-rate testing of flawed steam generator tubes. These results may be summarized as follows:

6.1 Tubes withg Circular Holes

1. The observed flow rates for both the room- and elevated-temperature tests could be accurately predicted by using a standard correlation for incompressible flow through a sharp-edged circular orifice and an orifice discharge coefficient of 0.6.

2. No flow choking was observed in the elevated-temperature tests for the hole sizes tested, and it appears that the water does not flash to steam until after it exits the orifice.

3. The jet velocities through the specimens with 3.175-mm (1/8-in.)-diameter circular holes generated sufficient lateral thrust to bend the tubes ≈10°.

6.2 Tubes with EDM Notches

1. The observed flow rates through as-machined and highly opened notches could be accurately predicted by using the same standard correlation as was used for circular holes, again with an orifice discharge coefficient of 0.6.

2. The sudden opening of notches of length ≥25 mm (1 in.) created sufficient lateral thrust to bend tubes supported at one end.

3. The pressures at which ligament tearing and burst occur could be predicted for single axial part-throughwall notches with lengths ≥12.7 mm (0.5 in.) using a model previously developed at ANL. The model tends to underpredict the tearing and failure pressures for notches 6.35 mm (0.25 in.) in length.

4. The pressures required for both flaw tearing and unstable burst, as well as the extent of flaw tearing, generally increase somewhat with increasing pressurization rate. Testing under quasi-steady-state conditions is preferred to minimize this effect.

5. Testing of tubes with throughwall flaws without internal bladders and reinforcing foils is preferred wherever possible. Where this is not feasible, the tubes should be tested in two stages, with the tube pressurized to the point of initial flaw opening without a bladder in the first stage and subsequently pressurized to unstable burst with a bladder in the second stage. Where leak rates require the use of a bladder for the entire test, a 3.2-mm (1/8-in.)-thick Tygon internal bladder and 0.13-mm (0.005-in.)-thick brass foil yield satisfactory results. The foil should be lubricated and extend no more than 6.35 m (0.25 in.) beyond the flaw extremities. In addition, the pressurization rate should be ≤7 MPa/s (1000 psi/s).

6. Tubes containing complex multiple flaws typically fail in a complex manner that cannot be analytically predicted. For the case of two aligned part-throughwall notches separated by a full-wall-thickness ligament, the strengthening effect of the ligament decreases with decreasing ligament length, and the composite flaw behaves essentially as a single notch for sufficiently short ligaments. The behavior of these flaws can be analytically predicted.

7. Ten Type 304 SS tubes with throughwall axial EDM notches of three lengths were internally pressurized to produce flaw openings of specified sizes. The required internal pressures were successfully calculated to within reasonable accuracy.

6.3 Tubes with SCC Flaws

1. Part-throughwall axial cracks with highly profiled ligaments can exhibit increasing leak rates (sometimes with delays) until the crack is completely open over its full extent during constant-pressure hold times at both room temperature and 300°C (572°F). The increasing leakage rate is apparently a consequence of progressive ligament rupture at the through-thickness crack tip. No criterion for predicting time-dependent ligament rupture currently exists.

2. The observed internal pressures at which first leak and unstable rupture occur generally show only a moderate correlation with the maximum flaw depths estimated from pretest EC characterization and with the BC voltages.

3. Throughwall pinhole leaks that exist prior to testing are not generally detected by EC techniques, apparently because they are small relative to the optimum resolution of the probe.

References

1. S. Majumdar, K. Kasza, and J. Franklin, "Pressure and Leak-Rate Tests and Models for Predicting Failure of Flawed Steam Generator Tubes," NUREG/CR-6664, Argonne National Laboratory (1999).

2. S. Majumdar, W. J. Shack, D. R. Diercks, K. Mruk, and J. Franklin, "Failure Behavior of Internally Pressurized Flawed and Unflawed Steam Generator Tubing at High Temperatures—Experiments and Comparison with Model Predictions," NUREG/CR-6575, Argonne National Laboratory (1997).

3. D. R. Diercks, S. Bakhtiari, K. E. Kasza, D. S. Kupperman, J. Y. Park, and W. J. Shack, "Steam Generator Tube Integrity Program Annual Progress Report for the Period Ending September 30, 1999," NUREG/CR-6511, Vol. 8, (2002).

4. C. N. Amos and V. E. Schrock, "Two-phase Critical Flow in Slits," Nuclear Science and Engineering, 88, **3**, pp. 261-74 (1984).

NRC FORM 335 (2-89) NRCM 1102, 3201, 3202

U.S. NUCLEAR REGULATORY COMMISSION

BIBLIOGRAPHIC DATA SHEET

(See instructions on the reverse)

1. REPORT NUMBER (Assigned by NRC, Add Vol., Supp., Rev., and Addendum Numbers, If any)

NUREG/CR-6789

2. TITLE AND SUBTITLE

Results from Pressure and Leak-Rate Testing of Laboratory-Degraded Steam Generator Tubes

3 DATE REPORT PUBLISHED

MONTH	YEAR
November	2002

4 FIN OR GRANT NUMBER

W6487

5 AUTHOR(S)

Ken Kasza, Saurin Majumdar, Jang-Yul Park, Jeff Franklin

6. TYPE OF REPORT

Technical Report

7. PERIOD COVERED *(Inclusive Dates)*

10/00-11/01

8 PERFORMING ORGANIZATION - NAME AND ADDRESS *(If NRC, provide Division, Office or Region, U S Nuclear Regulatory Commission, and mailing address, if contractor, provide name and mailing address.)*

Argonne National Laboratory
9700 S. Cass Avenue
Argonne, IL 60439

9 SPONSORING ORGANIZATION - NAME AND ADDRESS *(If NRC, type "Same as above", if contractor, provide NRC Division, Office or Region, U S Nuclear Regulatory Commission, and mailing address.)*

Division of Engineering Technology
Office of Nuclear Regulatory Research
U.S. Nuclear Regulatory Commission
Washington, D.C. 20555-0001

10 SUPPLEMENTARY NOTES

J. Davis, NRC Project Manager

11. ABSTRACT *(200 words or less)*

This report presents experimental results obtained from the pressure and leak-r ate testing on laborabory-degraded steam generator (SG) tubes. Two tube test facilities were built to carry out the tes ts. One is the High-Temperature, Pressure, and Leak-Rate Test Facility (temperatures up to 343oC [650oF], pressures of up to 2 1 MPa [3000 psi], and pressurized-water flow rates up to 1520 L/min [400 gpm] for conducting tube failure and leak-rate test s under prototypic SG operating conditions. The other is the Room-Temperature, High-Pressure Facility (pressures up to 52 MPa [7,500 psi] and flow rates up to 48.4 L/min [12.8 gpm]) capable of testing at pressures associated with overpressure safety margins. The report includes information on flawed-tube testing portocals for test with or without internal bladders, the v alidity of simple orifice flow models for the prediction of flow rates from flaws, and a large data base containing failure p ressures and leak rates for machined and stress corrosion cracking flaws produced in the laboratory.

12 KEY WORDS/DESCRIPTORS *(List words or phrases that will assist researchers in locating the report.)*

steam generator tubes
leak-rate
stress corrosion cracks
High-Temperature, Pressure and Leak-Rate Test Facility
Room-Temperature, High-Pressure Facility

13 AVAILABILITY STATEMENT

unlimited

14 SECURITY CLASSIFICATION

(This Page) unclassified

(This Report) unclassified

15 NUMBER OF PAGES

16. PRICE

Federal Recycling Program

UNITED STATES
NUCLEAR REGULATORY COMMISSION
WASHINGTON, DC 20555-0001